NBS MONOGRAPH 93

Spot Diagrams for the Prediction of Lens Performance From Design Data

U.S. DEPARTMENT OF COMMERCE
NATIONAL BUREAU OF STANDARDS

THE NATIONAL BUREAU OF STANDARDS

The National Bureau of Standards is a principal focal point in the Federal Government for assuring maximum application of the physical and engineering sciences to the advancement of technology in industry and commerce. Its responsibilities include development and maintenance of the national standards of measurement, and the provisions of means for making measurements consistent with those standards; determination of physical constants and properties of materials; development of methods for testing materials, mechanisms, and structures, and making such tests as may be necessary, particularly for government agencies; cooperation in the establishment of standard practices for incorporation in codes and specifications; advisory service to government agencies on scientific and technical problems; invention and development of devices to serve special needs of the Government; assistance to industry, business, and consumers in the development and acceptance of commercial standards and simplified trade practice recommendations; administration of programs in cooperation with United States business groups and standards organizations for the development of international standards of practice; and maintenance of a clearinghouse for the collection and dissemination of scientific, technical, and engineering information. The scope of the Bureau's activities is suggested in the following listing of its four Institutes and their organizational units.

Institute for Basic Standards. Applied Mathematics. Electricity. Metrology. Mechanics. Heat. Atomic Physics. Physical Chemistry. Laboratory Astrophysics.* Radiation Physics. Radio Standards Laboratory:* Radio Standards Physics; Radio Standards Engineering. Office of Standard Reference Data.

Institute for Materials Research. Analytical Chemistry. Polymers. Metallurgy. Inorganic Materials. Reactor Radiations. Cryogenics.* Materials Evaluation Laboratory. Office of Standard Reference Materials.

Institute for Applied Technology. Building Research. Information Technology. Performance Test Development. Electronic Instrumentation. Textile and Apparel Technology Center. Technical Analysis. Office of Weights and Measures. Office of Engineering Standards. Office of Invention and Innovation. Office of Technical Resources. Clearinghouse for Federal Scientific and Technical Information.**

Central Radio Propagation Laboratory.* Ionospheric Telecommunications. Tropospheric Telecommunications. Space Environment Forecasting. Aeronomy.

---

*Located at Boulder, Colorado, 80301.
**Located at 5285 Port Royal Road, Springfield, Virginia, 22171.

UNITED STATES DEPARTMENT OF COMMERCE • John T. Connor, *Secretary*
NATIONAL BUREAU OF STANDARDS • A. V. Astin, *Director*

Spot Diagrams for the Prediction of Lens Performance From Design Data

Orestes N. Stavroudis and Loyd E. Sutton

National Bureau of Standards Monograph 93

Issued September 7, 1965

For sale by the Superintendent of Documents, U.S. Government Printing Office
Washington, D.C., 20402 - Price 75 cents

Library of Congress Catalog Card Number: 65–60037

Contents

	Page
1. Introduction	1
2. Methods for calculating and displaying spot diagrams	3
3. Interpreting spot diagrams	5
3.1. Direct visual inspection to obtain subjective comparisons	5
3.2. Interpreting supplementary tables and graphs obtained from the numerical data generated by spot diagrams	6
4. References	15
5. Appendix. A compendium of analyses	15

Spot Diagrams for the Prediction of Lens Performance From Design Data

Orestes N. Stavroudis and Loyd E. Sutton

This Monograph presents an outline of the methods used at the National Bureau of Standards to predict the performance of lenses from an analysis of their designs. The technique is based on the use of spot diagrams, which are analogs of star image tests, and makes extensive use of high-speed digital computers. A collection of twenty-one spot diagram analyses is included.

1. Introduction

The U.S. Air Force Reconnaissance Laboratory at Wright Field requested the assistance of the National Bureau of Standards in evaluating designs for aerial camera lenses. The task was to develop a procedure for the determination of the performance of lenses from the design data alone and to apply the procedure to specific lens design submitted by the Air Force. An obvious solution to this problem would be to fabricate prototypes of each design submitted and subject them to physical tests. However the construction of prototypes is expensive and time consuming and the need for an alternate procedure was clearly indicated. At first rays were traced through each system and the geometric aberrations were calculated and plotted. The resulting graphs were forwarded to the Air Force where they were used as aids in selecting the better designs. But this process was slow and tedious and a great deal of skill was required to interpret the results. With the development of the high-speed digital computer it became possible to compute a very large number of rays in a minimum of time, making routine spot diagram analyses possible.

It is intended that this Monograph provide an outline of the methods used to calculate, produce, and interpret spot diagrams at this and other laboratories, as well as provide a compendium of the results of our spot diagram analyses.

A spot diagram is nothing more than a plot of points representing the intersections of rays from a given object point with a focal plane of a lens. The data for such a plot is obtained by calculating the paths of rays through a lens to a plane in image space, using its design specifications as parameters. This procedure is illustrated in figure 1. Spot diagrams provide a representation of the distribution of the light intensity in the image of a luminous point object and therefore are the geometrical optics analogs of star images. Within the framework of geometrical optics, a spot diagram, constructed from a numerical model of a lens, can be interpreted in the same way as a star image made with a real lens. Spot diagrams therefore provide a convenient and economical means of testing lenses prior to their fabrication.

Another experimental analog of a spot diagram is the *photogram* obtained in applying the Hartmann bench test to a lens [1].[1] A diaphragm consisting of a number of small holes drilled in an opaque plate is placed in front of the lens to be tested. Light from an object point is then passed through the diaphragm and lens and is allowed to fall on a photographic plate displaced considerably from the Gaussian image plane. A second exposure is made on the opposite side of the Gaussian focus. Thus, an image of the diaphragm appears on each plate from which the direction and position of the beams on the Gaussian image plane can be calculated. Figure 2 illustrates the experimental setup. Sets of such photograms are made for a number of object points and the results are used to calculate the aberrations of the lens. Photograms (see fig. 3) can be thought of as spot diagrams on planes displaced considerably from the Gaussian focus. The diaphragm plays the role of the grid network on the entrance pupil plane and the lens does the work of the computing machine.

The earliest published report on spot diagrams appeared in 1946 in a paper by Hawkins and Linfoot [2] to describe the performance of several designs of Schmidt cameras. Later, Herzberger [3] reported on a method of calculating spot diagrams that had been in use since 1939. Increasing interest in spot diagrams has been noted in the technical literature since high-speed digital computers became available.

The computational procedures used to make spot diagrams can provide a great deal of auxil-

[1] Figures in brackets indicate the literature references on page 15.

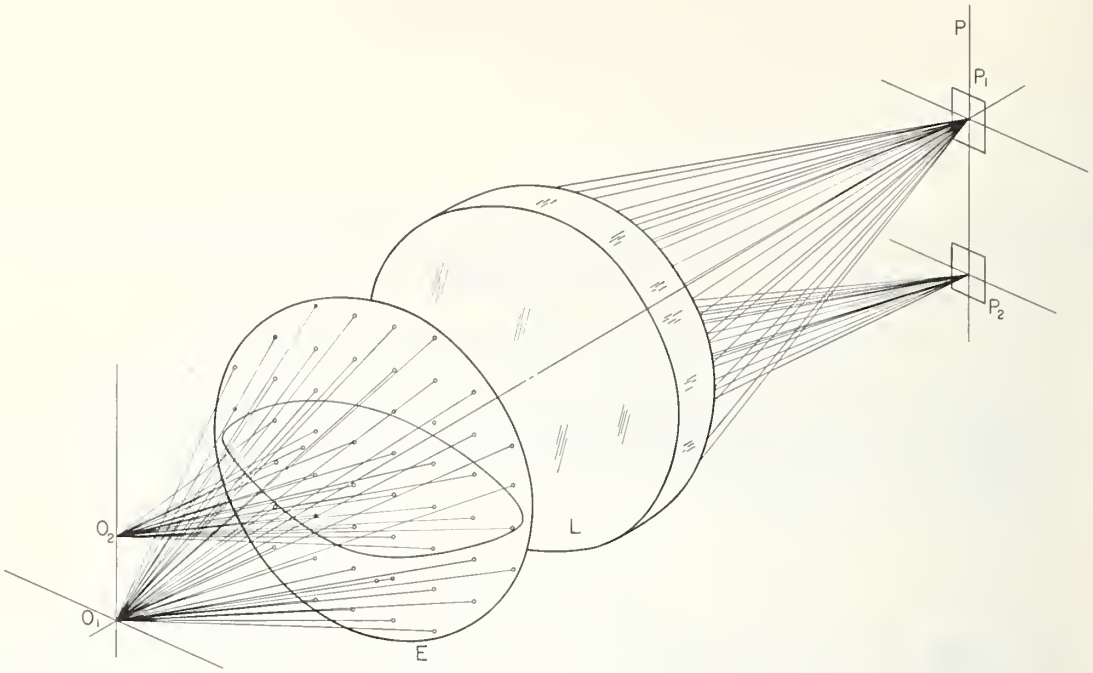

FIGURE 1. *Spot diagram construction.*

O_1 represents an axial object point; O_2, an off-axis object point. E is the entrance pupil plane. L represents the lens. P is the image plane. From each object point a ray is traced to a system of lattice points on the entrance pupil, thence through the lens to the image plane P. The intersection of these rays with the image plane form the spot diagrams. The spot diagrams associated with the object points O_1 and O_2 are situated in the rectangular areas P_1 and P_2 respectively.

Only those rays actually transmitted by the lens are illustrated. Note that more rays from the axial object point are transmitted than rays from the off-axis point, resulting in the narrowing of the entrance pupil aperture.

iary information about a lens. For example, the computer programs developed at the Bureau provide automatically the shape of the vignetted entrance pupil. This shape is given by a plot of points on the entrance pupil plane indicating, for a given object point, the intersections of those rays which are not vignetted by the diaphragm or any of the mounting edges of the lens. This is illustrated in figures 1 and 9. Accurate information of this type is virtually unobtainable by any other means. In addition these programs provide information on distortion and chromatic aberration of a lens.

As a representation of the image of a point object, a spot diagram is subject to certain limitations. First, each ray is represented as contributing an equal amount to the intensity distribution of the image. In reality there is a considerable variation in the flux density associated with rays which travel along different paths through the lens. Each surface is entered at a different angle of incidence, resulting in different proportions of energy transmitted according to the Fresnel formulas [4]. Second, if a point of a spot diagram is superimposed on another they appear as a single point, so that the intensity distribution in the dense portion of a spot diagram is underestimated. Third, no effort is made to take into account the diffraction effects due to the wave nature of light. The conditions under which these defects became important and possible means of overcoming them will be discussed.

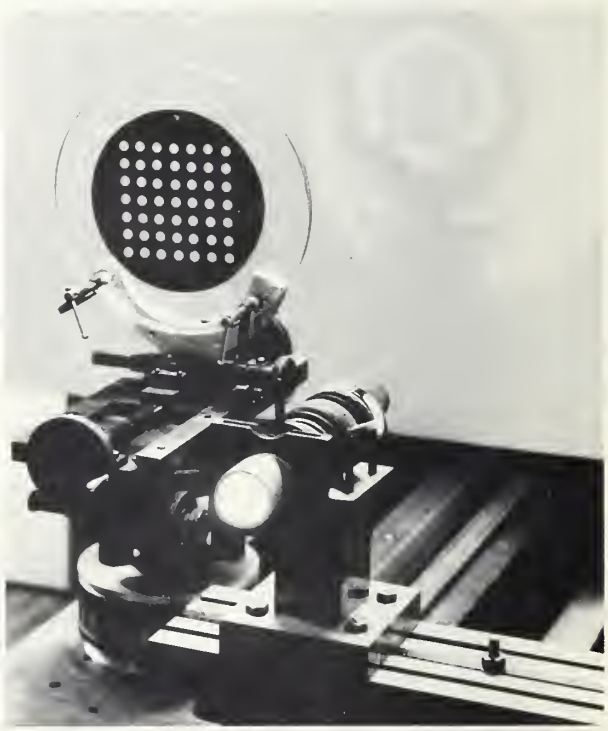

FIGURE 2. *Illustrating the Hartmann bench test.*

A long-focal-length, wide aperture simple lens is shown clamped to the bench. Taped to it is a mask containing a number of small circular apertures. The system is illuminated by collimated light from a parabolic mirror (not shown). The light source is shown in the lower center portion of the picture. The image of the mask is in the background.

2. Methods for Calculating and Displaying Spot Diagrams

Necessary in any program for the routine calculation of spot diagrams is a method for tracing large numbers of rays. At the time high-speed digital computers were first applied to optical problems, it was found necessary to reevaluate the lens analytical procedures then in current use. These procedures, devised primarily for hand computation, were inconvenient and impracticable for machine use. One of the earliest applications of digital computers to ray tracing was given by Grosch in a paper read at a meeting of the Optical Society in 1945 [5]. In 1951 more comprehensive reports were published by Feder [6] and Allen and Stark [7]. Later in the same year, Herzberger [8] published a description of a process for tracing rays by machine.

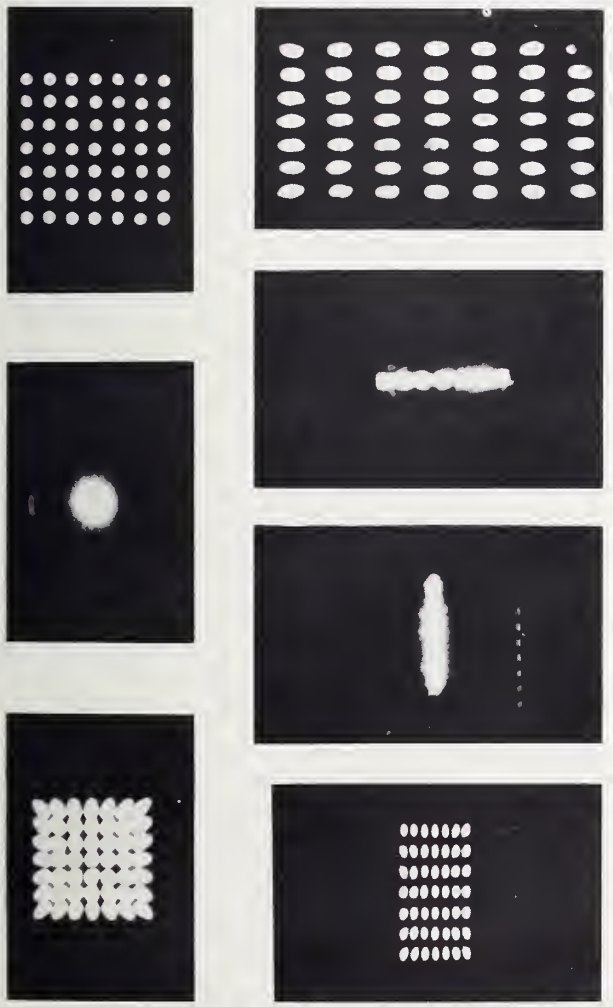

FIGURE 3. *Hartmann photograms from the experimental setup shown in figure 3.*

The three pictures on the left show photograms for an on-axis beam. The center picture is at the focus; the upper and lower pictures are outside and inside the position of best focus. The four pictures on the right show photograms for an off-axis beam. The uppermost picture is outside the plane of best focus, upper center is at the sagittal focus, lower center is at the tangential focus, lowest is inside the tangential focus.

At the National Bureau of Standards Feder's formulas were coded for both the IBM Card Programmed Calculator (CPC) and the Standards Electronic Automatic Computer (SEAC); in fact, this was the code used to test the SEAC on its initial run [9]. The Bureau's first lens analyses in which total aberrations were calculated used these codes.

The first program for the preparation of spot diagrams was based on an interpolation process and made use of the CPC exclusively [10]. A relatively small number of rays were traced through the optical system for each of several obliquities to determine the coordinates of intersection of each ray on a focal plane. A separate code was then used to determine the coefficients of two interpolation polynomials, one for each focal plane coordinate, with entrance pupil coordinates as arguments. Then, using a third computer program, the coordinates of a large number of rays on the focal plane were determined by evaluating the interpolation polynomials. The coordinates of the points of a grid on the entrance pupil were used as arguments.

This program was accurate, fairly rapid, and utilized completely the capacity of the CPC. However, it was subject to several drawbacks. A large amount of preliminary hand calculation was necessary. In particular, it was necessary to determine the shape of the entrance pupil and restrict the coordinates to the interior of this region. This computation could be performed only by examining each of the rays at each surface and at the stop to determine whether or not it was transmitted. The location of the edge of the vignetted region was then estimated and the coordinates of all the points on the grid network lying within this region were punched by hand. In determining the coefficients of the interpolation polynomial, tracing rays outside this region was also necessary to avoid the inaccuracies resulting from extrapolation. Moreover, the results applied only to the one focal plane to which the ray tracing referred.

When SEAC became available for routine optical calculation, an overall program was devised in which the tracing of a single ray was done by a subroutine.

Such a program was written to trace rays of a given obliquity starting from the points of a square grid on the entrance pupil. The rays specified by such a set of starting points were traced in a sequence which proceeded outwards from the meridian plane along horizontal lines, each line being ended by means of certain comparisons, described as follows: The radii of the clear apertures for each surface and for the stop plane were part of the input data of the lens system, so that SEAC could compare these radii with the radial displacements of the rays on each surface, and only those rays clearing the system comprised the output. When all the rays from one obliquity were finished,

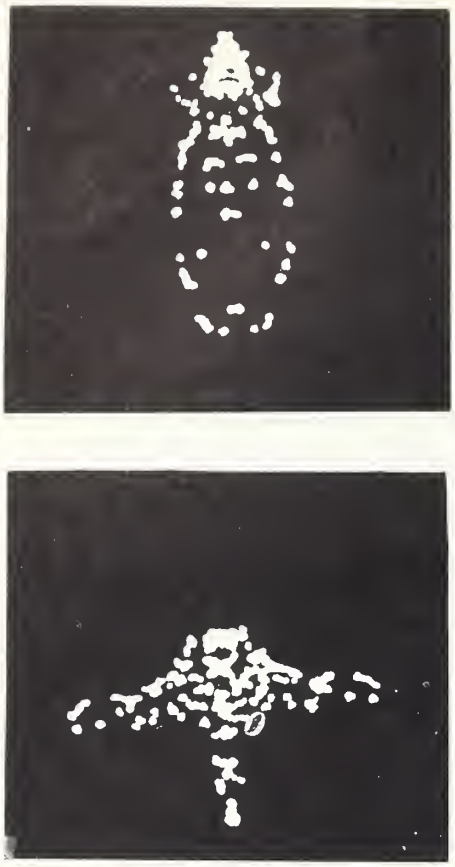

FIGURE 4. *Spot diagrams produced by oscilloscope.*

The dots are larger than those in a spot diagram produced by an inked stylus and fewer spots are used. The contrast range in the reproduction process used here does not illustrate the build-up of the intensity of overlapping spots.

the machine would automatically proceed to the next obliquity or, if all obliquities had been completed, halt. In this program, each ray was traced to five separate focal planes, three of which were usually selected for spot diagram presentation.

Both the CPC and SEAC programs were limited to rotationally symmetric optical systems consisting of spherical surfaces. It was therefore necessary to trace rays only on one side of the meridian plane, as the remainder were obtainable from the symmetry of the system. Although for every lens analyzed thus far the object has been at infinity, finite object points could also be considered by changing slightly the input data.

Experience showed the SEAC code to be more efficient for a large computer. When the primary computation tool of the National Bureau of Standards was changed to the IBM 704 computer in June 1957, and to the IBM 7090 in November 1961, this code was programmed for the new machines without any basic change.

One of the inherent difficulties in routine production of spot diagrams is the reduction of the computed results to a graphical format. Clearly an automatic method is called for. In the procedures using the CPC and in the codes for the SEAC and the 704, provision was made for the output, in the form of punched cards, to be used in conjunction with an automatic plotter to produce the final spot diagram. Each punched card contained the data for a single ray. The data specified the obliquity angle and coordinates of the ray on the entrance pupil plane and on each of five given image planes. The entrance pupil plots and the spot diagrams could thus be plotted from one deck of cards.

Output in the form of punched cards had an additional advantage. By sorting the cards on one coordinate on the focal plane, a profile of the flux distribution in the image could be obtained. This process, reported in detail by Lucy [11], was used in earlier analyses to predict radial and tangential resolving power.

Although the use of card decks and plotting machine was reasonably convenient, delays frequently resulted from plotting machine breakdown. In one suggested improvement in the procedure, a cathode ray tube would be connected directly to the output circuits of a computing machine. The spot diagram could be displayed visually and recorded photographically as it was being computed. In addition, the position of the focal plane could be controlled directly by the operator to find the plane of best focus by simple visual inspection, thus eliminating both manual calculation and the necessity for handling punched cards.

The use of such a device would have an additional advantage over the plotting machine process where points are printed by an inked stylus. With the inked stylus method, a number of superimposed points appears only as a single point, and makes a spot diagram with a dense core and a weak flare distributed over a large area appear less favorable than it really is. However, with the cathode ray tube display process, the intensity of overlapping points increases materially in the image, and a much more accurate diagram results.

A simpler although less accurate procedure for the routine production of spot diagrams has been reported by Miyamoto [12]. The coordinates of the points of a spot diagram are calculated on a digital computer which is then programmed to print out a display of periods with these coordinates.

Some experiments for displaying spot diagrams on the face of a cathode ray tube were completed in 1959 which made use of both the IBM 7090 and SEAC [13]. Some trial results are shown in figure 4. The output of the IBM 7090 was on magnetic tape rather than on punched cards, and the information so recorded consisted of direction cosines of the rays as well as their coordinates of intersections with a fixed image plane. The data was then fed into SEAC where it was converted into analog voltages that controlled the cathode ray tube in plotting the spot diagrams. Using the direction cosine data, the operator was able to shift the position of the plane of the spot diagram and thus find the location of the plane of best focus visually.

Other procedures for the routine production of spot diagrams have been applied elsewhere. One flexible approach, described by Herzberger [14], does not use higher degree polynomials where the coefficients are determined by interpolation. Instead lower degree polynomials are fitted by a least squares method. In this case the number of traced rays need not be fixed. This least squares approach results in a small loss of accuracy that would certainly be less than that introduced by the plotting machine errors. Herzberger goes further in interpreting the coefficients as aberration coefficients and has applied this concept successfully to designing lenses.

3. Interpreting Spot Diagrams

3.1. Direct Visual Inspection To Obtain Subjective Comparisons

The spot diagrams presented in the appendix are, by definition, pictorial representations (through geometrical ray tracing) of the point imagery of the lens system analyzed. Thus, within the scope of the validity of geometrical optics, they would show, by visual inspection, the crude distinction between two lenses of widely differing image quality, with the smaller spot diagram indicating better imagery. The directness of presenting a graphical display of numerical results and the simplicity of interpretation when the above criterion can be applied constitute the obvious appeals of the spot diagram approach to image evaluation. However, it should be borne in mind that some rare lenses of very high quality are diffraction limited, and in these cases the spot diagram serves only to indicate this possibility by its very small size. Such a case is shown in figure 5. An accurate evaluation of such exceptional lenses thus falls beyond the scope of this Monograph.

Even when making only visual comparisons, one usually finds it necessary to draw a finer distinction between two lens designs than that based on total sizes of the spot diagrams. Such a qualitative distinction can often be based on the relative sizes of the cores of the spot diagrams, with the smaller core indicating better imagery. The word "core" is merely a term used to specify subjectively that region of the spot diagram where the point density is highest. For most lens designs with even reasonably good imagery, experience has shown that such a region usually is unique and rather easy to distinguish in each of the spot diagrams. Another convenient term "flare", may be subjectively defined in a similar way. The region of lowest point density occurring outside the core is called flare. It usually consists of a relatively thin scattering of points toward the periphery of the diagram. These terms are found to be useful because they allow one to make comments on the general characteristics of a given spot diagram. They are applied to star images as well. See figures 6 and 7.

Core size can also be associated, at least to some extent, with the resolving power of a lens. Further qualitative considerations, based on an experimental knowledge of the effect of the type of emulsion used, are helpful in the use of core size as a rough guide to resolving power. These considerations will be mentioned, largely because they form a starting point for developing more exact methods. For instance, when using a high contrast emulsion, exposed and developed properly, one could reasonably expect only the core to be recorded. In this case, the smaller core of two diagrams would be associated with a higher resolving power. On the other hand, when using an emulsion of lower contrast, one could expect not only the core, but also some additional points from the region immediately surrounding the core, to contribute to the record. By examining the size of this extended core region, one might thus

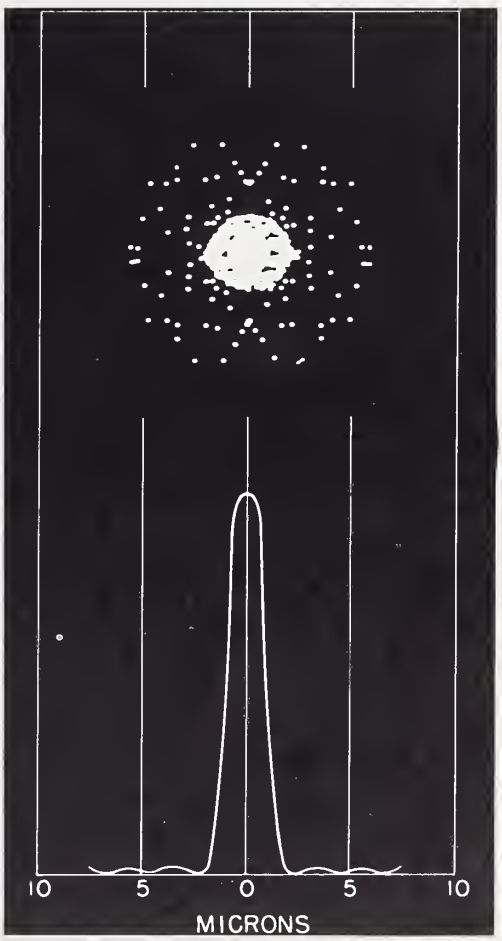

FIGURE 5. *The diffraction limited case.*

The spot diagram was calculated for a 6 in. f/3.5 lens (006BC035 15) at 0° obliquity on the plane of best focus. The graph drawn to the same scale shows the energy distribution in an image formed by a perfect f/3.5 lens. (Data from Jenkins and White [15]). The diffraction effects clearly dominate the geometrical aberrations.

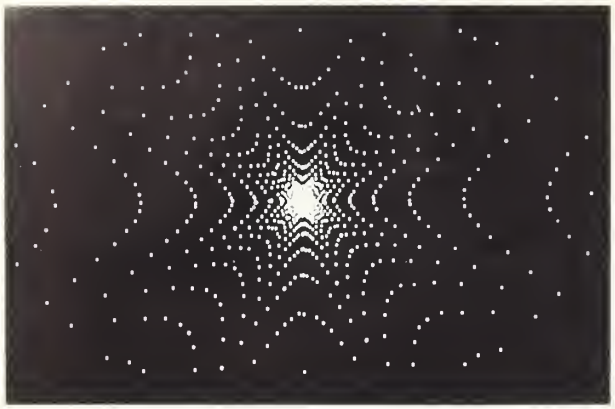

FIGURE 6. *Illustrating core and flare.*

Shown is a greatly enlarged spot diagram. The departure from left-right symmetry is due to plotting errors. A spot diagram with a well-defined core and a large, uniform flare.

expect to obtain a relative estimate of low contrast resolving power. The remaining points of the diagram would be considered to constitute the flare, which contributes nothing to the record except that it may serve to sensitize the emulsion in the area around the image.

Though such visual estimations might be sufficient to facilitate a choice between two lenses in some instances, it is easy to show that, in general, better methods are needed. The chief difficulty of such a visual method appears to be that it might, in many cases, require an experienced and judicious observer to determine accurately just how much of the spot diagram constitutes the extended core region, as used for low contrast resolving power predictions. The core itself is much easier to distinguish, since it is a characteristic feature of many spot diagrams, but, to a lesser degree, the same difficulty sometimes arises in being sure that the proper region of the diagram has been demarcated. It is thus clear that purely visual estimates of resolving power are definitely limited in accuracy, particularly in terms of obtaining absolute, rather than relative, estimates.

The curvature of the field of a lens becomes apparent when spot diagrams of a number of object points are observed at several focal planes, as shown in figure 8. The locus of best focus of all object points can indicate the surface on which an extended object is best imaged. The location of the plane of overall best definition can then be estimated.

3.2. Interpreting Supplementary Tables and Graphs Obtained From the Numerical Data Generated by Spot Diagrams

The production of spot diagrams generates all the data needed for obtaining entrance pupil plots, which represent the set of rays transmitted by the analyzed lens system at a given obliquity. Through comparisons of their entrance pupil plots, the light collecting abilities of different lenses for

FIGURE 7. *Illustrating core and flare.*

Shown is a greatly enlarged spot diagram. The departure from left-right symmetry is due to plotting error. The core in this spot diagram is not well defined. The flare is weak and not uniformly distributed.

corresponding object points can be estimated. For an axial object point, the entrance pupil plots for all lenses with the same focal length and f-number should have the same diameter. As the object point is moved off the axis, the typical lens exhibits a narrowing of the entrance pupil as shown in figure 9. This narrowing is detrimental since it reduces the amount of light reaching the edge of the field. An ideal situation would be one in which the area of the entrance pupil projected onto a plane perpendicular to the principal ray remained constant. Under that condition, the energy associated with the image of a point object would be the same over the entire field of the lens, to the accuracy obtainable by geometrical optics.

For determining the chromatic aberrations, the Conrady "D–d" method [16, 17] may be used. It is a particularly convenient method to apply in conjunction with a ray-tracing code, such as that used in computing spot diagrams, and a knowledge of it should be more widespread. The method makes use of the fact that the optical path length between an object point and any point on an emanating wave front is constant, together with Fermat's principle, which states that the optical path length of a ray between two fixed points possesses a stationary value with respect to arbitrary variation.

The application of the method will be described here for the usual case in which the final medium is air. Suppose it is required that a lens be corrected over the wavelength region from F(4861A) to C(6563Å). Rays are traced only at an intermediate wavelength, usually that of sodium D(5893Å). For each type of glass in the lens, the value of ΔN is obtained, where $\Delta N = N_F - N_C$, that is, the difference between indices of refraction at the F and C wavelengths. Defining D as the length of a given ray in a glass medium and d as the corresponding length of the principal ray, one then calculates the quantity $(D-d)\ \Delta N$ for each glass of the lens system. The sum of these quantities is called the Conrady Sum for that ray. By computing the Conrady Sum for each ray in a meridian fan of rays and plotting it against the coordinate of the ray in the entrance pupil, one obtains the Conrady Sums curves given in the appendix.

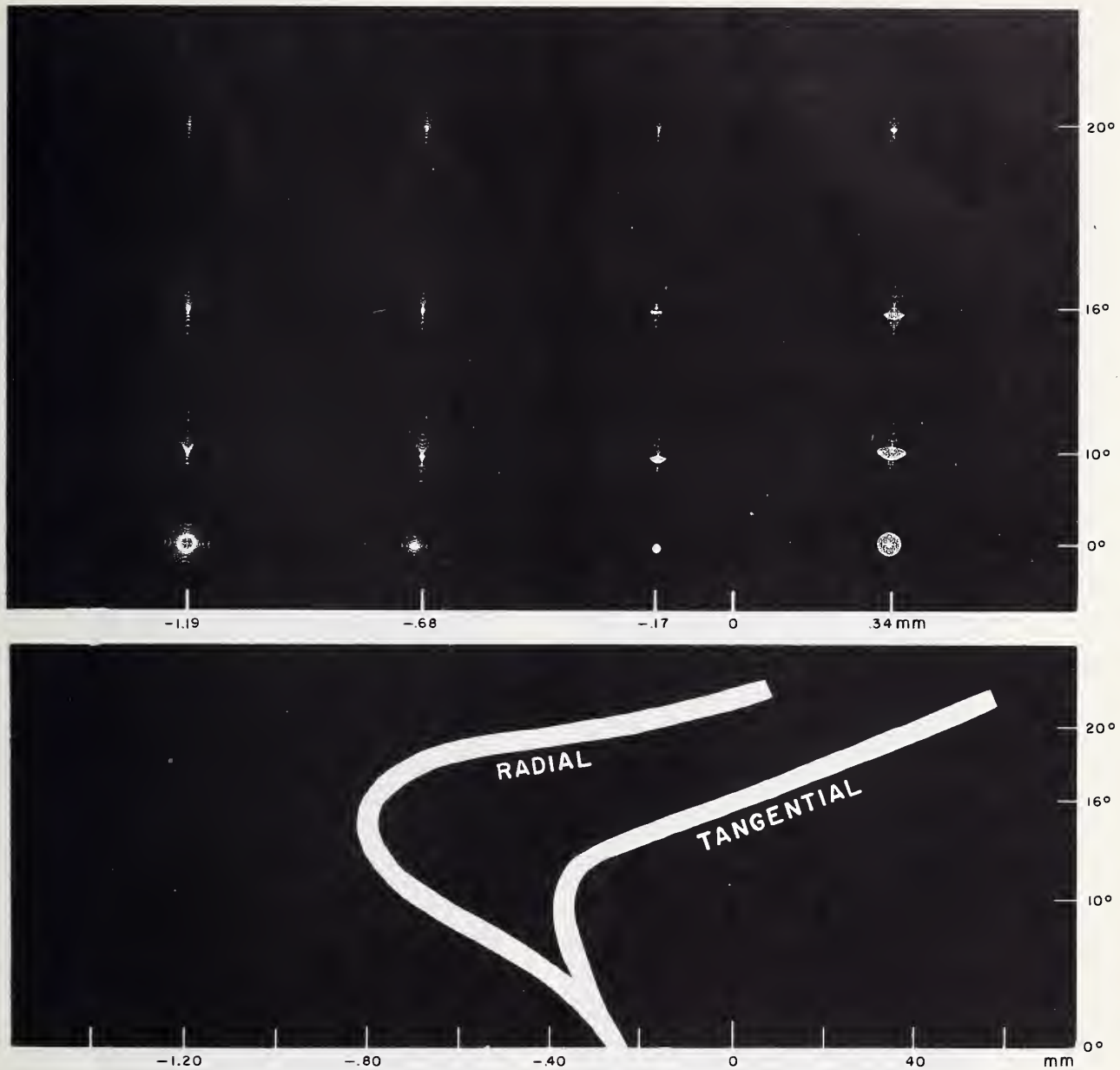

FIGURE 8. *Estimated field curvature and astigmatism from spot diagrams.*

In the upper panel are four sets of spot diagrams each at the focus as indicated (zero indicates the location of the Gaussian image plane). For each obliquity angle, the location of the best tangential focus (where the spot diagram resembles most a horizontal straight line) and the location of the best radial focus (where the spot diagram resembles most a vertical line) are estimated. These estimates are plotted in the lower panel and two curves are drawn through the points. The two curves represent a profile of the tangential and radial focal surfaces. The distance between them is a measure of the astigmatism of the lens. The field curvature can be represented by a curve representing the average of these two curves.

A detailed derivation of formulas relating such curves to the chromatic aberrations obtained by ray-intercept methods may be found in [16]. Here we will simply illustrate certain principles used as a guide to interpreting the plots of Conrady Sums directly. Figures 10 and 11 show idealized plots of the curves produced by specified pure types of chromatic aberration. When mixtures of these pure types are present, the overall slope of a typical Conrady Sums curve provides a good representation of the lateral color aberration, and the deviations of the curve from a straight line of that indicated slope are a measure of the longitudinal color aberration.

In a quantitative analysis by means of spot diagrams, the principal problem is to predict the resolving power of the fabricated lens. It is not the purpose of this Monograph to go into the question of the meaning of resolving power and its relevance in lens specifications. Measurement of resolving power is essentially subjective, as it depends ultimately upon the ability of the observer

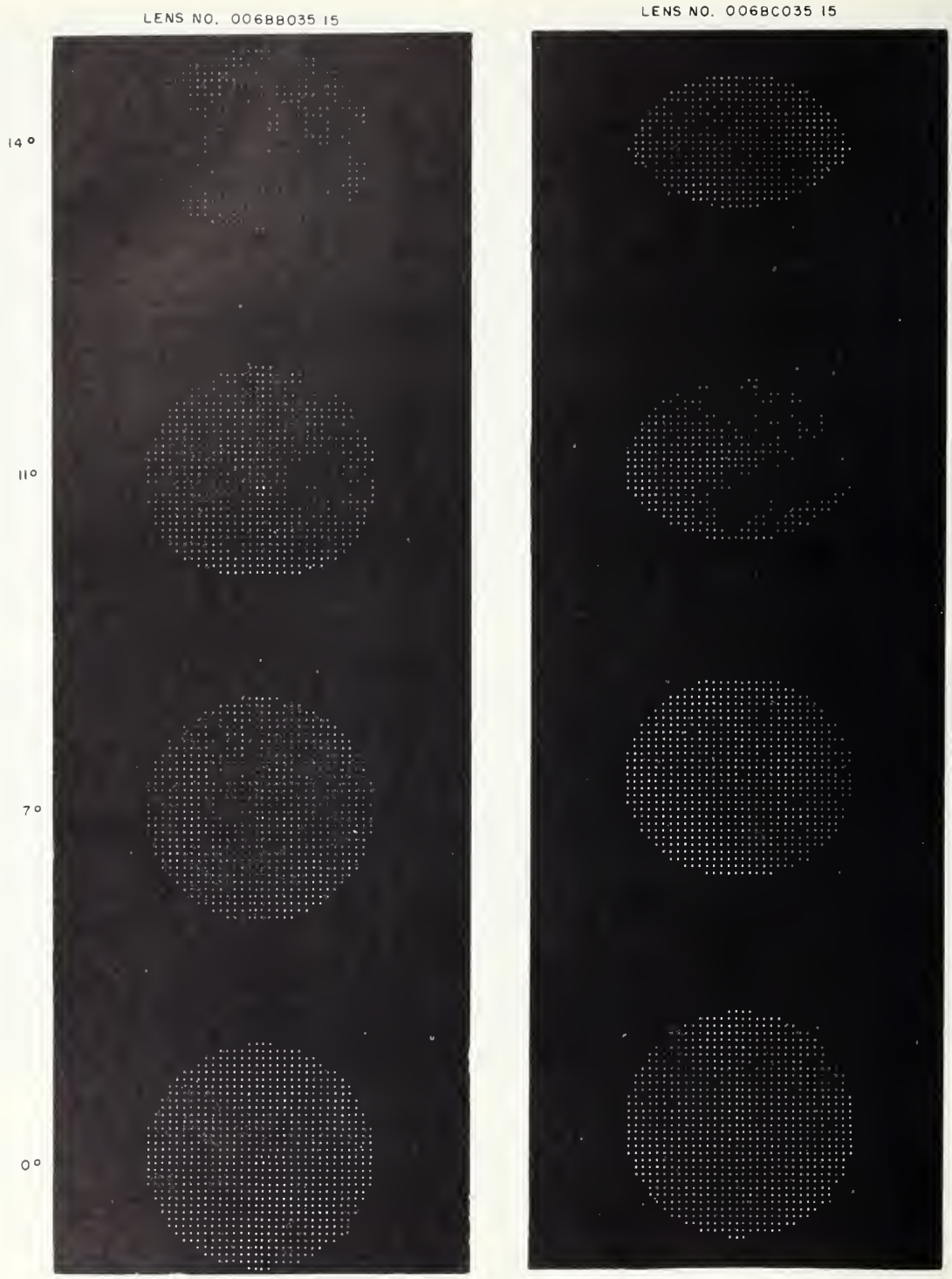

FIGURE 9. *Entrance pupil plots for two 6 in. f/3.5 lenses designed for a 30° field angle.*

Left is 006BB035 15; right is 006BC035 15. These plots indicate that the left lens is more efficient resulting in a more even distribution of light over the focal plane.

to find that spacing of the lines on a test target which renders its image barely perceptible. Nevertheless, resolving power is used to describe the performance of lenses and therefore it is proper to consider means of predicting resolving power. What is needed is a set of numbers that agree generally with the results of some procedure for measuring resolving power. The desired goal is that a qualitative ordering of lenses in terms of predicted resolving power should agree with the ordering of the same lenses in terms of measured resolving power. Once this goal is reached the

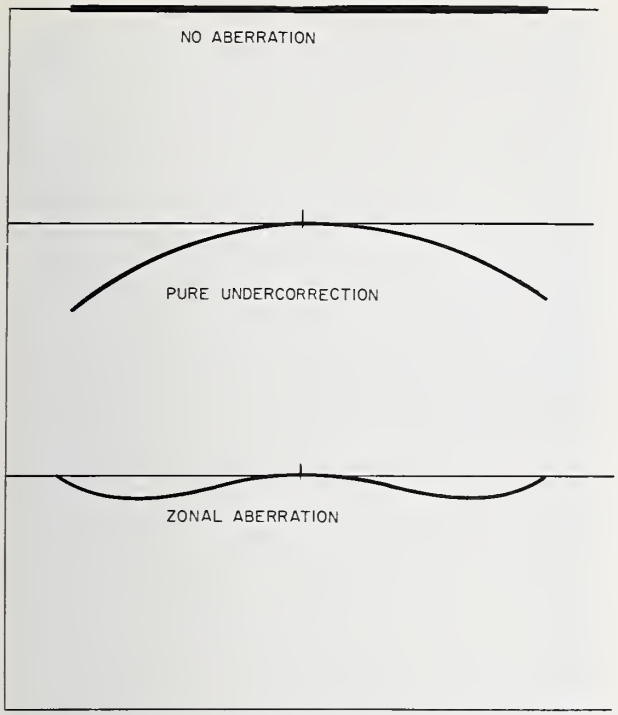

FIGURE 10. *Interpreting Conrady sums.*

Axial rays.

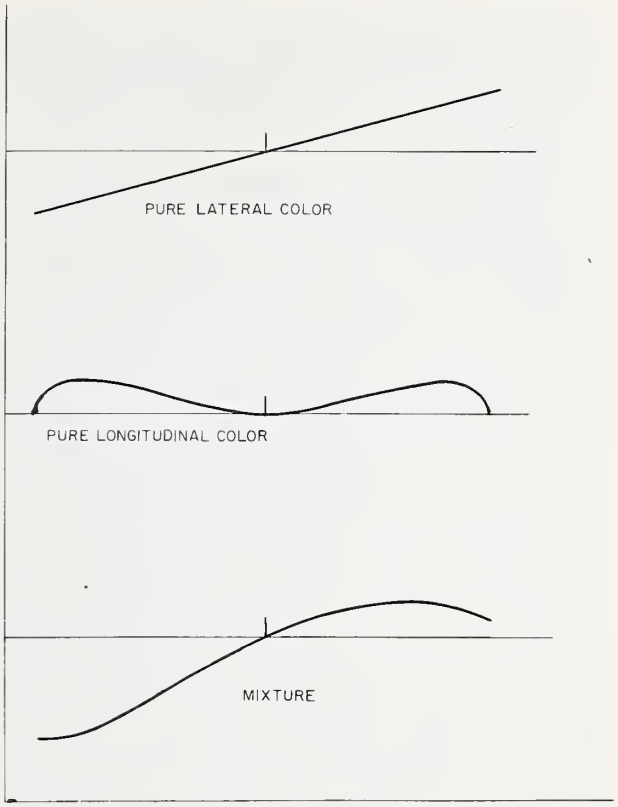

FIGURE 11. *Interpreting Conrady sums.*

Off-axis rays.

problem is one of improving the quality of the predictions to agree better with the measured values.

The most straightforward approach is to prepare profiles of the density of points in a spot diagram in radial and tangential directions [10, 11]. From considerations of the widths of these profiles, and the type of emulsions to be used, an estimate of radial and tangential resolving power can be made. This procedure is based on the assumption that a straight line on an object can be considered as a sequence of colinear overlapping spot diagrams on the image. The point density contour of the image of the line can then be approximated by counting points in strips of equal width parallel to the ideal image of the line. Let P_i represent the number of points in the ith strip and D_i the displacement of the center of this strip from the ideal position. Then a smooth curve drawn through a plot of P_i against D_i gives a profile of the flux density distribution in the image of the line. Estimates of resolving power based on the measure of the half-width of the main peak in such a profile can be easily obtained. However, the above assumption is true only for lines of zero thickness. Because the object lines on a resolving power chart have finite widths, their energy profiles are not the same as those of zero width lines. The spot diagrams should also be integrated in the proper direction to simulate a line of a finite thickness. A typical energy distribution profile is shown in figure 12.

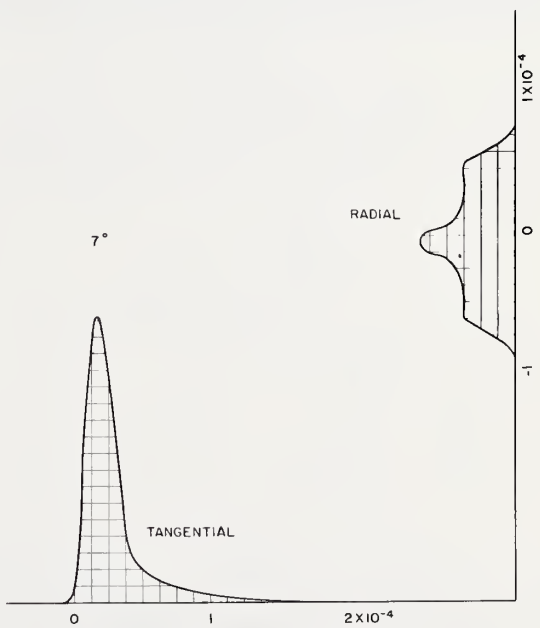

FIGURE 12. *Energy distribution profile.*

Parallel lines are ruled on a spot diagram and the number of points in each strip is determined. These counts are then plotted against the location of the center of the strip and a smooth curve is drawn through the points. Counts are taken with the parallel lines oriented in two directions.

The Bureau's method for obtaining routine resolving power predictions from spot diagrams uses a formula developed by Hopkins, Oxley, and Eyer [18]. The high contrast resolving power, R, is given by

$$R=\frac{K}{(d_f^2+d_s^2)^{1/2}}$$

(which shall be referred to hereafter as the *resolution formula*) where K is an empirically determined constant; d_f is the mean grain diameter, in microns, of the film emulsion; and d_s is the diameter, in microns, of a circle centered on the vertical line of symmetry of the spot diagram and containing 30 percent of the diagram points. Furthermore, the center of this circle is to be located along the vertical line of symmetry at that point which minimizes d_s (i.e., in the "densest" region of the diagram). Although the resolution formula was originally derived for application only to rotationally symmetric spot diagrams, we have arbitrarily applied it to all with a view toward obtaining a correlation of the result with the geometric mean of the radial and tangential resolving powers. Further research will be necessary if a more accurate extension of the resolution formula turns out to be desirable.

A machine program was written to locate the center and compute the radius of the smallest circle containing 30 percent of the points in a spot diagram, where the center is to be somewhere on the vertical line of symmetry of the diagram. The point representing the principal ray can be used as a first estimate for the center. For a specified center, a high-speed calculator can compute the squares of the distances, from this center, of all points on the right side of the diagram, sort these values into an ascending list, and select from the list the squared radius of the circle with that center which just contains 30 percent of the points. This process is done in a few seconds and may be repeated for each of several vertical shifts of the center, so that for each trial center a corresponding radius is calculated. Between two centers where a minimum radius is in evidence, more vertical shifts may be made with a smaller interval between trial centers, thus locating a center for which the corresponding radius is a minimum. Though this location program is carried out automatically within the calculator, a detailed graph of the function to be minimized was prepared for the spot diagram shown in figure 13. As illustrated in figure 14, the minimum abscissa is sought as function of the ordinate. It should be noted that an out-of-focus spot diagram may have more than one minimum. However, the minimum radius is very easily found, even though the center of the minimum 30 percent circle, as shown in figure 14, may not be well defined.

Having located the center of concentration of the points by the process just described, the machine program uses that center to compute the 10 radii of a set of concentric circles containing 10, 20, and so on to 100 percent of the points of the spot diagram. The results can then be used in the resolution formula to obtain estimates of resolving power. The use of the resolution formula for estimates of high contrast resolution can be based on the diameter of either a 20 or a 30 percent circle for the value of d_s. However, Hopkins [19] recommended the 30 percent circle as preferable, and in this case K is 600 and d_f is 10 μ. For estimates of low contrast resolution, the diameter of the 50 percent circle is used as the value of d_s, and here K is 871 and d_f is 35 μ.

This approach to the problem avoids the subjectivity involved in trying to make a direct measurement of a visually demarcated core region and then using the result in some nonuniform estimation procedure. An objective method which can be applied in a routine way is naturally a desirable goal. Such a goal is more nearly attained by some method of the type described here, which gives a strict percentage definition for the region of high point density and specifies use of its diameter in a definite estimation formula. It should be emphasized that the method currently in use here, as described above, is certainly open to improvement with respect to accuracy of the estimates, and the need for further research to that end is clear.

Measurements of resolving power for some of the lenses of this Monograph have been provided by the Air Force and are included in the appendix. For nine of the lenses measured, estimates of the high contrast resolving power had been made by using the resolution formula. In some cases the estimates had been based on the use of a 20 percent circle, but information on the size of the 30 percent circle was available to allow calculation of estimates of the preferred 30 percent-circle type. The results are listed in table 1, where it is noted that the results for lenses A, B, and G are subject to special conditions which dictate their exclusion from a comparison of the predictions and measurements. The pertinent results for the remaining six lenses have been carried over to table 2 for comparison purposes.

One can of course compute the linear correlation coefficient between the compared columns of table 2, which gives the value of r as $+0.625$, but it should be noted that the sample consists of only six items. Though a high degree of accuracy can hardly be claimed from such a result, the deviations listed in the last column of table 2 do not appear extreme for estimations of such intrinsic difficulty. An attempt was made to account for the source of these deviations, by reference to our records of the computations done for these lens. In the case of lens C, it appeared very likely that most of the deviation was due to a difference in the choice of the plane of best overall focus. It also appeared possible, somewhat less conclusively, that the same consideration applied to lens E.

When making predictions from the spot diagrams, as indeed again when the resolving power is later independently measured, one must choose a compromise plane of imagery which he judges to be best over the entire field. In both cases

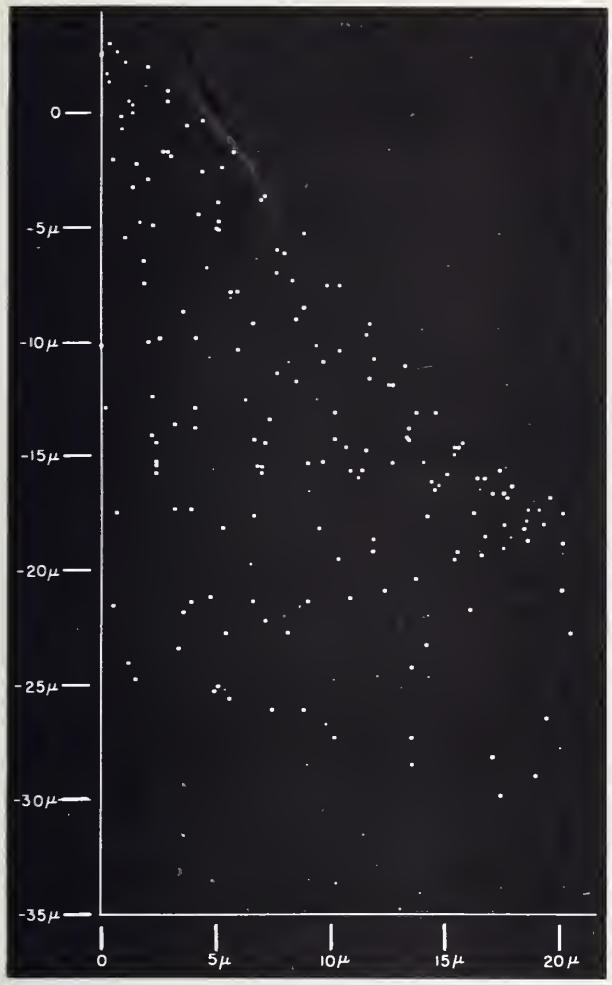

FIGURE 13. *The determination of the 30-percent circle.*

A greatly enlarged core of that portion of a spot diagram to the right of the meridian plane. The ordinate scale shows distances from the principal ray. The abscissa is measured from the meridian plane.

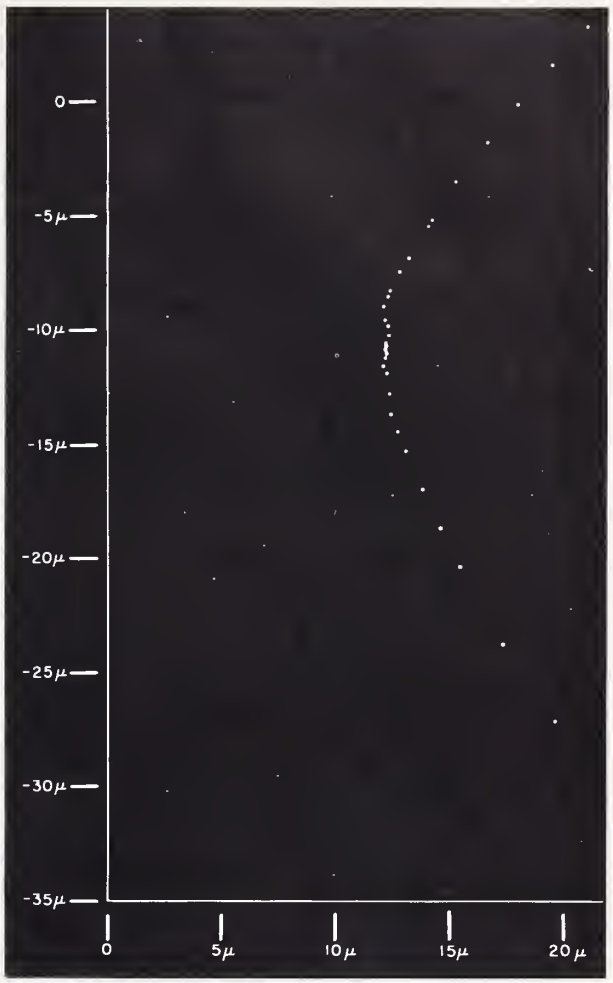

FIGURE 14. *The determination of the 30-percent circle.*

Centers versus radii. The ordinate shows the location on the meridian plane of the center of a circle containing 30 percent of the points in the spot diagram (shown in figure 13) measured from the principal ray. The abscissa represents the radius of that circle. The minimum radius is used in the resolution formula. Note also that the location of the minimum, although not well defined, could be used to provide an estimate of distortion.

TABLE 1. *Predicted and measured resolving power in lines/mm on axis*

Lens name	Resolving power (high contrast)				
	Predicted		Measured		
	From 20% circle	From 30% circle	R= radial	T= tangential	$\sqrt{RT}$
A* (006BC035 15)	47*	60*	32	32	32.0
B* (BAC-2)	—	56	49.7*	35.3	41.9*
C (006BB035 15)	45	49	63	56	59.4
D (C03AA015 28)	45	53	56	56	56.0
E (006AA015 28)	45	52	41.0	41.0	41.0
F (024BB060 23)	—	44	36	36	36.0
G* (024AA060 23)	41	49	—(28)*	—	—
H (006AA025 28)	34	34	35.3	31.4	33.3
K (024CC060 23)	32	34	42.0	42.0	42.0

*Notes on 3 of the above lenses—
Lens A: This lens is diffraction limited on axis, so predictions are unreliable.
Lens B: The measurements show too wide a spread between R and T to be reliable.
Lens G: The mean of thirty measurements labeled "Lowest resolution, radial or tangential."

TABLE 2. *Predicted and measured values for six lenses from table 1*

Predicted values based on 30% circle
Measured values taken as $\sqrt{RT}$

Lens name	Prediction	Measurement	(Prediction—measurement)
C	49	59.4	(−10.4)
D	53	56.0	(− 3.0)
E	52	41.0	(+11.0)
F	44	36.0	(+ 8.0)
H	34	33.3	(+ 0.7)
K	34	42.0	(− 8.0)
	Σ=266	Σ=267.7	Σ=(−1.7)

such a choice is, at least to a degree, subjective, and a more precise definition of this plane would, for some particular lenses, be desirable. However, future improvements toward flexibility in making the required computations, which would facilitate the choice of this plane for the spot diagrams, might be reasonably expected to increase the accuracy of the predictions to some extent.

Any judgments as to the accuracy of the predictions are naturally limited by the fact that the measurement of resolving power is itself subject to experimental error. We were not given nor could we reasonably expect to obtain for these measurements, any exact bounds on the experimental error. Only the measured values were made available to us, and, for that matter, there would always be the possibility of human error. Another possibility is that errors of lens construction, such as decentrations, would affect the apparent accuracy of predictions computed from blueprint data. Nevertheless, our experience with such measurements indicates that they should have at least enough accuracy to make clear the need for improvement in the present accuracy of the predictions.

Table 3 gives a compilation of further data on the same nine lenses used in table 1. Here, we give the available information, at certain off-axis obliquities, which makes possible comparisons, as before, between the predicted and measured values of high contrast resolving power. Whenever possible, estimates based on both 20 and 30 percent circles are listed. However, as in the case of resolution on axis, comparisons with the measurements will again be made using the preferred 30-percent-circle results. Unfortunately, this requires the omission of lens H from the tabulations carried over to table 4, since the diameter of the 30 percent circle was not included in the data listed at the time of the report on lens H. To keep a minimum of six other lenses in section 1 of table 3, we have thus included results for lens G, but with the measured value in parentheses, along with a footnote which points out its probable lower accuracy as a measure of $\sqrt{RT}$.

It should be noticed that, in section 2 of table 3, data at exactly matching obliquities for the predictions and measurements were not available in that the entries for these tables must be compiled from data that had been obtained in earlier independent reports. When this mismatching of the available obliquities is small, it can be allowed for, to some extent, by listing measurements in the manner shown in table 3 for lenses A and C. However, in general, a detailed study of the accuracy of the predictions cannot be made when the obliquities are not matched.

For section 1 of table 3 there is exact matching of obliquities at 20°, and the numerical results are carried over to table 4, where the deviations of predictions from measurements are also listed. The entries for lenses G and F are listed below a horizontal line in table 4 as a reminder that there are reasons for considering their measured values less reliable than the others.

A noticeable contrast between the comparisons in table 4 and table 2 is observed in that, for table 4, the predictions are lower than the measurements for each lens. Though the sample size of compared lenses is small, this observation indicates that predictions of this type, obtained by the unmodified extension of the resolution formula to an off-axis obliquity as high as 20°, are likely to err on the side of conservatism. Judged only by the data of table 4, the 20° predictions appear to be at least providing lower bounds for the measured resolving powers of the lenses.

These off-axis values had been computed in the hope that they would provide predicted values adequate for specifying a relative ranking of lenses, at least for lenses of rather widely different resolving power performance. Table 4, though, provides so few contrasts in measured lens performance that it affords only a marginal basis for judging this aspect of the predictions. We can only note that, if there were valid reasons for omitting lenses F and K, the remaining lenses could be properly ranked from the predictions in the order D, B, E, and G (E and G considered equal). Even then, though, the range of measured values between lenses D and G would be only 10.3 lines. Some of the wide discrepancy exhibited by lens F could conceivably be attributed to the measured value, $R=38$, about which we have expressed doubts in the footnote on lens F in table 3. The supplementary data supplied in that

TABLE 3. *Predicted and measured resolving power in lines/mm off-axis*

Lens name	Max. half-field	Resolving power (high contrast)						
		Predicted			Measured			
		At obliquity of	From 20% circle	From 30% circle	At obliquity of	R= radial	T= tangential	$\sqrt{RT}$
Sec. 1								
B	27.5°	20°	10	8	20°	17.5	20.8	19.1
D	28°	20°	15	11	20°	25	28	26.5
E	28°	20°	8	7	20°	13.6	20.0	16.5
F*	23°	20°	9	7	20°	38*	25*	31*
G**	23°	20°	8	7	20°	(16.2)**		
H	28°	20°	15		20°	18.7	19.8	19.2
K	23°	20°	15	12	20°	18.5	18.5	18.5
Sec. 2								
A	15°	11°	30	22	10°	31	31	31
		14°	28	21	12.5°	31	31	31
					15°	31	31	31
C	15°	11°	36	42	10°	43	49	45.9
		14°	28	33	12.5°	34	45	39.1
					15°	31	37	33.9

*For lens F, the spread between R and T is 13 lines, which appears questionable when compared with the spreads at 15° and 25°. The R values at 15°, 20°, and 25° were measured as, respectively, 22, 38, and 17 lines, with corresponding T values of 24, 25, and 19 lines.

**For lens G, we list 16.2 lines as the only value available, using parentheses as a reminder that this is the mean of thirty measurements labeled "Lowest resolution, radial or tangential."

TABLE 4. *Predicted and measured values at 20° obliquity for six lenses from table 3*

P=Predicted values based on 30% circle
M=Measured values taken at $\sqrt{RT}$

Lens name	P	M	$[\Delta P]=[P-M]$
B	8	19.1	−11.1
D	11	26.5	−15.5
E	7	16.5	−9.5
K	12	18.5	−6.5
G*	7	(16.2)	(−9.2)
F*	7	31	−24

*Footnotes of table 3 still apply to measured values.

footnote suggest that one might have expected this value of R to be about 23, rather than 38, lines. If that were the case, the last measured value in table 4 would be changed from 31 to about 24 lines. However, such a conjecture also makes it clear that all of the discrepancy of lens F could hardly be explained in this way.

For the comparisons made so far, it appears that, at least in terms of absolute accuracy, the predictions for the higher obliquities show a greater need for improvement than the predictions for the on-axis case. Further research effort would be needed to provide a reliable basis for effecting such an improvement, if the resulting method of prediction were intended to be usable over a reasonably wide range of obliquities and measured resolving powers. We must remember that there would be a restriction on the applicability of any method based on considerations of geometrical optics alone, since there are some high quality lenses in which the imagery is dominated by diffraction effects. Nevertheless, the existence of such a category of lenses does not, in itself, preclude the consideration of ways to improve the present method of predicting resolving power for other lenses.

First of all, an improved method of choosing the plane of best overall focus would be helpful, but this alone would probably be insufficient, since the off-axis imagery is almost always considerably less sensitive than the on-axis imagery to small shifts of the focal plane. Beyond this first means of obtaining a small improvement, it might be possible to formulate some generalization of the present method which would give a greater improvement in accuracy, by virtue of a more efficient use of the information content of the spot diagram.

An obvious defect in the application of the resolution formula is the presupposition that the 30 percent circle coincides with the core of a spot diagram. Certainly in the case of an off-axis spot diagram the shape of the core would hardly be circular. A casual examination of on-axis spot diagrams would indicate that these cores very often are larger or smaller than the 30 percent circle. Kubota and Miyamoto [20] offer two very simple alternate procedures. In one they simply measure the length and width of the core of the spot diagram thus obtaining two quantities which they relate to the radial and tangential resolving power. In the second method a sequence of concentric circles is constructed; the number of points within each circle is counted and a curve of circle radius versus the number of points enclosed is plotted. Where the circle passes through the edge of the core of a spot diagram the slope of the curve should change abruptly due to the sudden change of the spot density. The curve is therefore inspected and the location of this inflection point determines the radius of the circle which best fits the core.

Kubota and Miyamoto use as estimates of the resolving power the reciprocal of either the radius of best fitting circle or of the measured semi-axes. In the latter case both the radial and tangential resolving power is estimated. This method was tested on two lenses by comparing predicted and measured resolving power. The results are encouraging.

Another approach taken by Miyamoto [12] and Kubota and Miyamoto [20] has been the application of the Fourier transformation to spot diagrams to obtain what might be described as a geometrical analog to the transfer function. Their results indicate that the frequency response estimates are valid over a fairly large frequency range.

Estimates of distortion used in the routine calculations are made in the usual way by taking the difference between the ideal image height and the height of the principal ray on the Gaussian focal plane. The ideal image height is the product of the tangent of the angle between the axis and object point and the focal length of the lens, the latter being determined from paraxial ray tracing.

The principal ray is defined as the central ray of the bundle of rays from the object point that is transmitted by the lens and in practice is taken to be the ray that passes through the axial point on the entrance pupil.

A study of figures 15 and 16 shows, however, that the principal ray is not necessarily at the center of a spot diagram or even at the center of the core. This is particularly true when coma is present in which case the principal ray is located at the vertex of the comatic figure. The procedure in which the principal ray is used to calculate distortion therefore seems questionable; consequently, some estimation of the center of the core of a spot diagram would be preferable. An attempt has been made to use the center of the 30 percent circle determined in the resolving power predictions as shown in figure 14 but the uncertainty in locating this point, as mentioned above, makes this procedure questionable.

Figures 15 and 16 suggest that it is possible for the distortion characteristics of a lens to change with the *f*-number. Some preliminary studies have been made to determine whether this phenomenon can be observed but the results have been inconclusive.

These studies indicate that spot diagrams are useful in predicting the performance of lenses from their design data. However the crudity of the predictions so obtained leaves much to be desired. Means to improve their accuracy and reliability may be found in two areas. First, the information content of spot diagrams should be broadened to include physical data such as measures of phase and signal strength as well as ray coordinates, from which diffraction calculations can be made. Second, the Hopkins formula seems to be capable of a generalization based on ellipses rather than circles, which may provide a more reliable means of predicting off-axis resolving power.

769-553 O—65——2

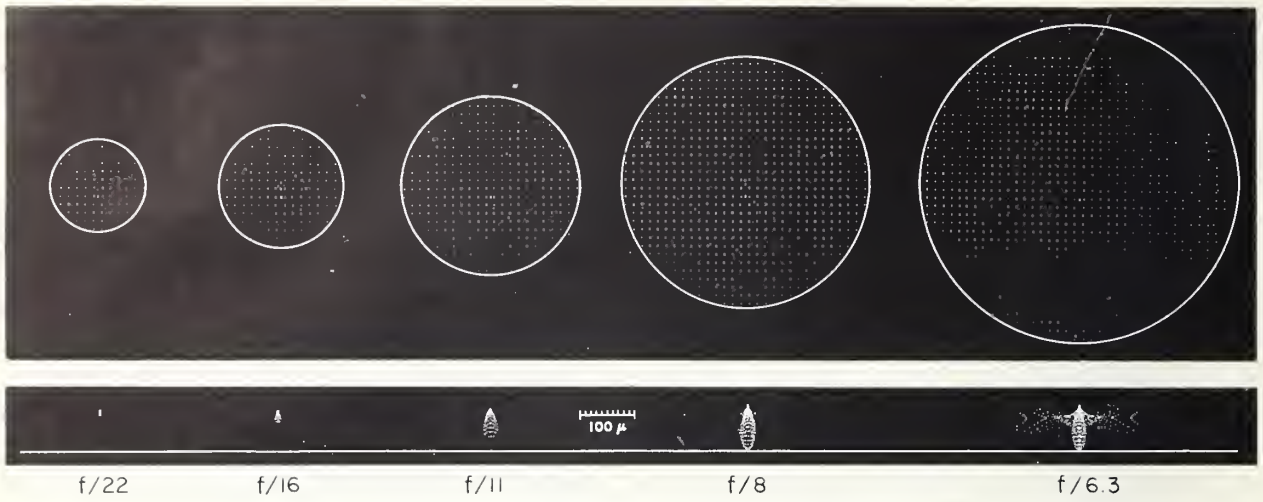

FIGURE 15. *Spot diagrams for various f-numbers.*

A series of spot diagrams for a 6-in. lens showing the effects of reducing the stop opening. Above are the entrance pupil plots. The core appears to move downward as the diaphragm is opened indicating a change in the distortion characteristics.

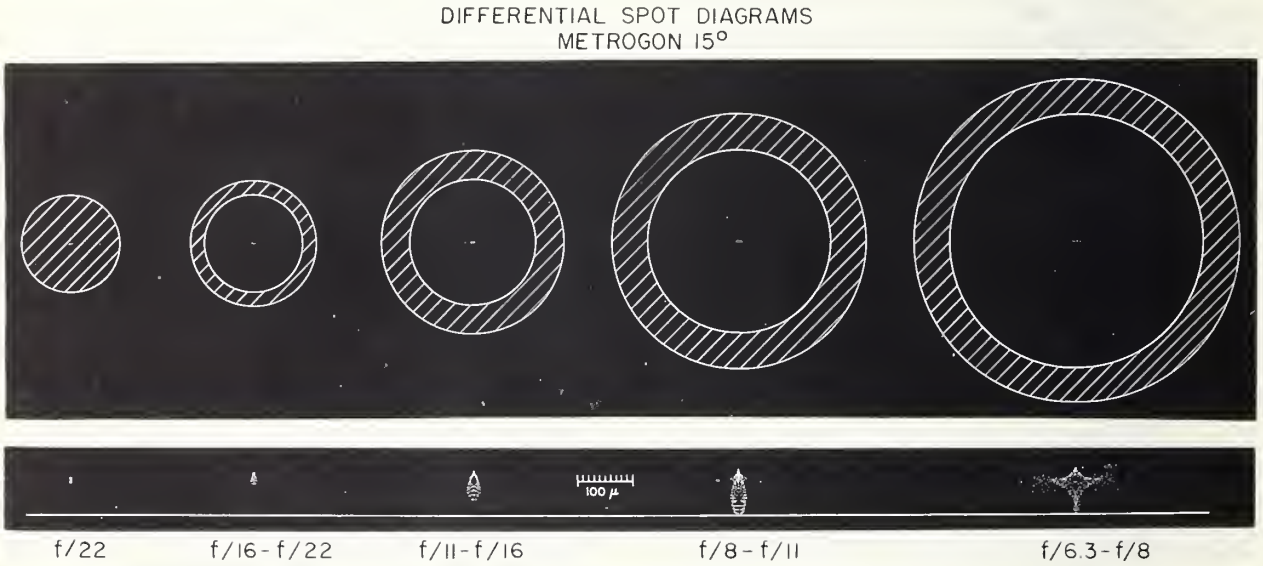

FIGURE 16. *Differential spot diagrams obtained from the data used in figure 12.*

Rays passing through concentric zones in the entrance pupil are plotted. The contribution of the outer zones to the core is negligible indicating that image quality may be enhanced by stopping down the lens with no loss of intensity.

The authors wish to acknowledge the important contribution of Donald P. Feder, under whose direction this project was conceived and under whose supervision the difficult pioneer work was done.

Those to whom we owe thanks are legion: the staff, past and present, of the Computation Section, who have been most helpful even to the extent of relinquishing some of their valuable space for our equipment; the staff, past and present, of the Photographic Laboratory, to whom fell the difficult task of reproducing spot diagrams clearly and to the proper scale; Edgar Watts, whose preparation of the illustrations has been of the highest quality; to John Whitmore of the Editorial Section for his invaluable advice and assistance in preparing this manuscript; the staff of the Naval Ordnance Laboratory who prepared our earlier spot diagrams; and the many colleagues and friends whose comments and criticisms have contributed to the success of this work.

4. References

[1] Hartmann, J. Objectivuntersuchungen, Zeit. f. Instrumenk. **24,** 1–21, 33–47 (1904).

[2] Hawkins, D., and Linfoot, E. H., An improved type of Schmidt telescope, Monthly Notices Roy. Astron. Soc. 105-334 (1945).

[3] Herzberger, M., Light distribution in the optical image, J. Opt. Soc. Am. **37,** 485–93 (1947).

[4] Sommerfield, A., Optics, Academic Press, New York (1945).

[5] Grosch, H. R. J., Ray tracing with punched card equipment (abstract), J. Opt. Soc. Am. **35,** 803 (1945).

[6] Feder, D. P., Optical calculations with automatic computing machinery, J. Opt. Soc. Am. **41,** 630–35 (1951).

[7] Allen, W. A., and Stark, R. H., Ray tracing using the IBM Card Programmed Electronic Calculator, J. Opt. Soc. Am. **41,** 636-40 (1951).

[8] Herzberger, M., Some remarks on ray tracing, J. Opt. Soc. Am. **41,** 805–7 (1951).

[9] Solution of skew ray problem, NBS Tech. News Bull. **34,** 125 (1950).

[10] Stavroudis, O. N., and Feder, D. P., Automatic computation of spot diagrams, J. Opt. Soc. Am. **44,** 163–70 (1954).

[11] Lucy, F. A., Image quality criteria derived from skew traces, J. Opt. Soc. Am. **46,** 699 (1956).

[12] Miyamoto, K., Image evaluation by spot diagram using a computer, Applied Optics **2,** 1247–1250 (1963).

[13] Lenstar aids lens design, NBS Tech. News Bull. **43,** 191 (1959).

[14] Herzberger, M., Analysis of spot diagrams, J. Opt. Soc. Am. **47,** 584–94 (1957).

[15] Jenkins, Francis A., and White, Harvey E., Fundamentals of optics, Second Edition, McGraw Hill, New York. p. 294 (1950).

[16] Feder, D. P., Conrady's chromatic condition, J. Research NBS **52,** 43–49 (1954).

[17] Conrady, A. E., Monthly notices, Roy. Astron. Soc. **64,** 182, 458 (1904).

[18] Hopkins, R. E., Oxley, S., and Eyer, J., The problem of evaluating a white light image, J. Opt. Soc. Am. **44,** 692–98 (1954).

[19] Hopkins, R. E. (Unpublished communications).

[20] Kubota, H., and Miyamoto, K. On the study of the image of photographic lens by means of spot diagram, Report of the Institute of Industrial Science, University of Tokyo, **13,** 38–53 (1963).

5. Appendix. A Compendium of Analyses

This section consists of a collection of spot diagram analyses of lenses completed at the National Bureau of Standards. All but two of the designs are the property of the U.S. Air Force. One is the property of the Eastman Kodak Company. The remaining one was taken from the patent literature. With the exception of the latter, the lenses are identified only in terms of a code number, no reference being made to designer or manufacturer.

Unless otherwise noted, the values of refractive index for the glasses listed in this appendix are those specified on the lens blueprint by the designer. Thus, in some cases, these specified index values used in the computations are for special melts not listed in standard glass catalogs.

The spot diagrams of this appendix are all shown at a scale which is 50 times the size of the actual images formed by the lenses. If a scale line is included on the illustration, it merely serves as an approximate indication of this scaling. However, the scaling of the entrance pupil plots will vary from lens to lens, since these are given only to show the relative sizes of the transmitted beams of a single lens.

For each of these lenses, the object point was at infinity, and each off-axis beam was traced from an object point located on the meridian plane and below the optic axis.

We wish to thank the Eastman Kodak Company and the U.S. Air Force for permission to reproduce the design data contained herein.

Contents

Focal length	f-number	Lens	Special designation
in.			
2.75	f/8	275CB080 61	
3	f/1.5	003AA015 28	D
6	f/1.5	006AA015 28	E
6	f/2	Lens No. 2 (006POL20 25)	
6	f/2	Lens No. 1	
6	f/2.5	003AA025 28	H
6	f/2.5	BAC-2	B
6	f/3.5	006BB035 15	C
6	f/3.5	006BC035 15	A
6	f/5.6	006XA056 45	
6	f/6.3	PL-9	
6	f/6.3	ME-10	
12	f/4	CO-1	
12	f/4.5	012AA045 40	
24	f/6	024AA060 23	G
24	f/6	024BB060 23	F
24	f/6	024CC060 23	K
36	f/3.7	ALPHA	
36	f/4	BETA	
48	f/4.5	CO-3	
48	f/4.5	BA-4	

Special designation	Lens	f-number	Focal length
			in.
A	006BC035 15	f/3.5	6
B	BAC-2	f/2.5	6
C	006BB035 15	f/3.5	6
D	003AA015 28	f/1.5	3
E	006AA015 28	f/1.5	6
F	024BB060 23	f/6	24
G	024AA060 23	f/6	24
H	003AA025 28	f/2.5	6
K	024CC060 23	f/6	24

275CB080 61—The Roossinov 2.75 in. (69.88 mm) *f*/8 122° field Wide-angle orthoscopic anastigmat

The data for this analysis (shown in figures 17a–17e) were taken from the patent literature (U.S. Patent No. 2,516,724) and, therefore, these results may not represent the optimum performance that can be expected from a lens of this type. The important feature of this lens is shown in the increase in the size of the vignetted aperture on the entrance pupil as the obliquity increases. This property represents an important achievement in the development of wide-angle lenses where there is usually a rapid decrease of the size of the entrance pupil accompanied by a decrease in the exposure at the edge of the field. This feature, along with what might be described as a reasonable performance in image quality, is achieved with unusual economy, as the lens consists of only six elements.

275CB080 61—M. M. Roossinov
2.75 in. (69.88 mm) *f*/8 122° field
Wide-angle orthoscopic anastigmat
Source of data: U.S. Patent No. 2,516,724 Example II

	Radii	Separations	Outside diameters	Clear apertures	Glass *	Index	Abbe No.
	mm	*mm*	*mm*	*mm*			
1	35.370						
		2.15	67	66	JI–67	1.6395	43.3
2	22.960						
		35.58					
3	47.565						
		9.20	30	28	JI–24	1.6126	58.6
4	−24.540						
		3.07	30	20	JI–28	1.5480	45.9
5	131.918						
		0.493					
6	−129.540						
		3.029	30	11	JI–28	1.5480	45.9
7	24.100						
		9.04	30	28	JI–24	1.6126	58.6
8	−46.700						
		34.94					
9	−22.270						
		2.11	66	65	JI–3	1.6242	35.9
10	−34.550						

*Described as from Lenzos Co. Catalog of 1936.

Relative entrance pupil area (275CB080 61)

Field angle	No. transmitted rays	Percent of 0°
deg		
0	824	100.0
25	886	107.5
42	1054	127.9
54	1318	160.0
61	1582	192.0

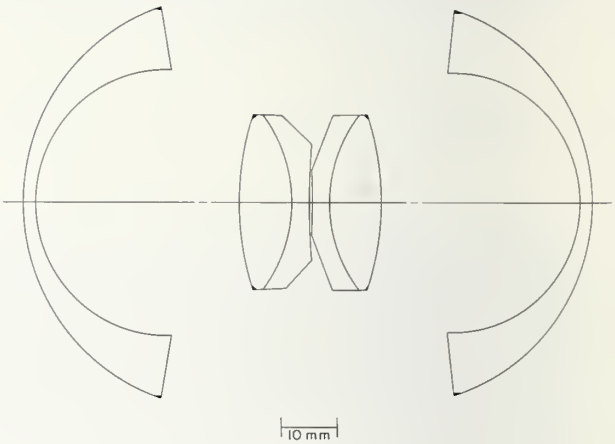

FIGURE 17a.

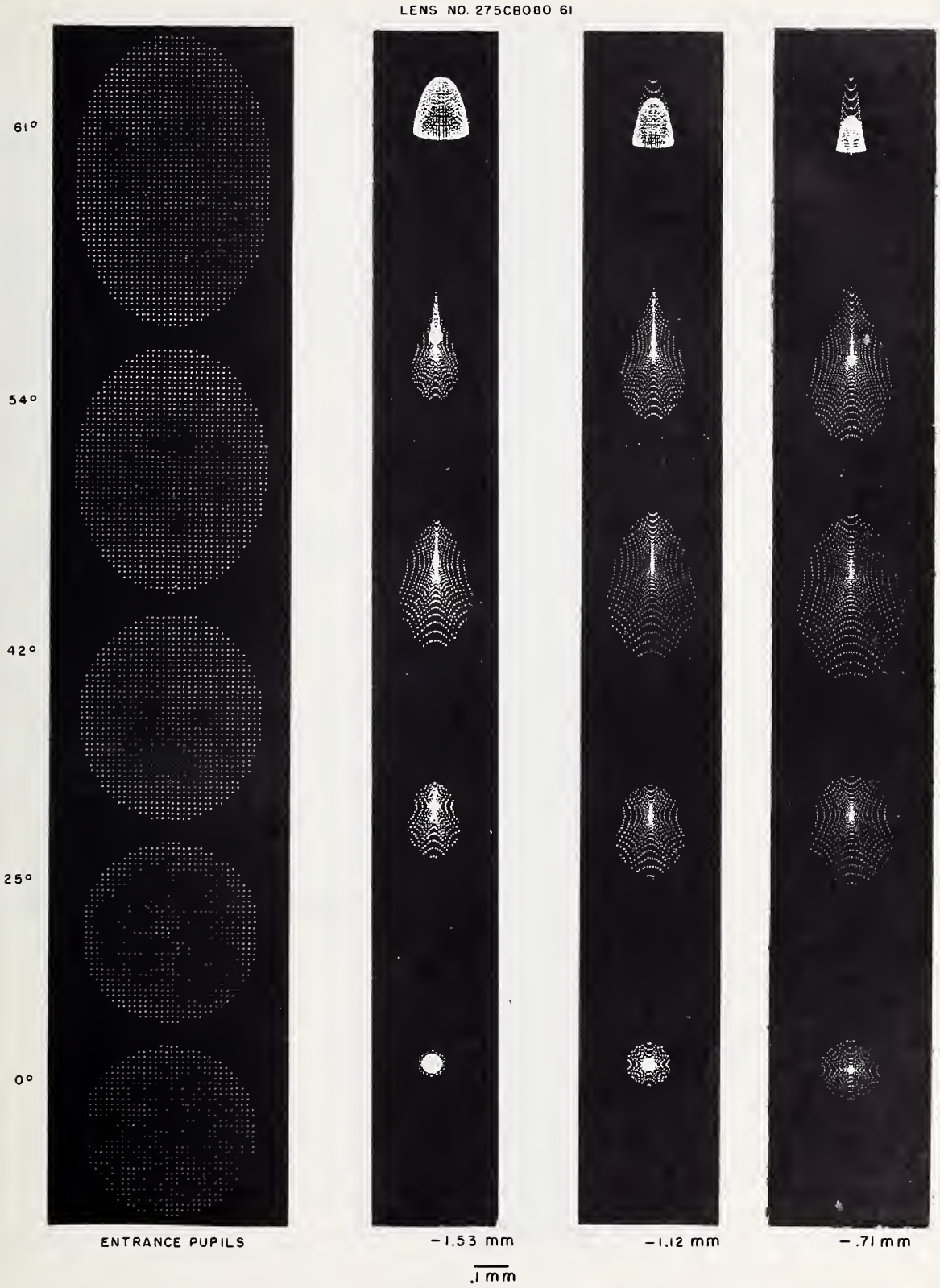

FIGURE 17b, c, d, e.

003AA015 28—3 in. $f/1.5$, 2¼×2¼ in. format—Aerial camera lens

The spot diagrams (see figures 18a–18f) indicate that this lens is characterized by a small amount of astigmatism, and a fair amount of coma and spherical aberration. The field is fairly flat. The lens was evidently designed for optimal correction of the 0° rays. The degree of light-collecting ability, insofar as it may be judged by the relative areas of the entrance pupil plots, is about average for a lens having such a low f-number.

The curves for the Conrady sums and the lateral color table show that there is considerable chromatic aberration.

The distortion table indicates that over the entire field distortion is well under 0.1 percent.

003AA015 28—3 in. $f/1.5$ aerial camera lens for a 2¼×2¼ in. format

	Radii	Separations	Outside diameters	Clear apertures	Glass	Index	Abbe No.
	mm	*mm*	*mm*	*mm*			
1	+50.015		69.0	67.0			
		16.0			EK-210	1.73400	51.2
2	−567.5						
		3.8			751277	1.75100	27.7
3	+131.47			56.0			
		—0.10—					
4	+29.908		45.6	43.6			
		5.37			EK-210	1.73400	51.2
5	+44.33			42.0			
		—1.085—					
6	+43.43		45.6	40.0			
		4.52			649338	1.64900	33.8
7	+18.194			29.5			
		—19.84—					
8	−19.550		43.0	27.5			
		3.41			720293	1.72000	29.3
9	−36.76			36.0			
		— .025—					
10	−62.62		43.0	40.0			
		7.57			EK-210	1.73400	51.2
11	−27.295			42.0			
		— .10 —					
12	+215.6		63.0	55.0			
		3.0			751277	1.75100	27.7
13	+65.0						
		15.4			EK-210	1.73400	51.2
14	−83.16			60.0			

Stop position: 10.8 mm from surface 7.
Opening: 28.3 mm at $f/1.5$.

Relative entrance pupil area (003AA015 28)

Field angle	No. transmitted rays	Percent of 0°
deg		
0	1102	100.0
12	942	85.5
20	730	66.2
25	508	46.1

Distortion and lateral color (003AA015 28)

Field angle (nominal)	Tangent	Distortion	Distortion	H_F–H_C
deg		*in.*	%	*in.*
12	0.21256	-20.38×10^{-5}	−0.032	-33.3×10^{-5}
20	.36397	−95.26	−.087	−48.9
25	.46631	−103.58	−.074	−24.6

Resolving power (003AA015 28)

Field angle	Predicted resolving power in lines/mm		Measured resolving power in lines/mm *		
	High contrast	Low contrast	R	T	$\sqrt{RT}$
deg					
0	45	24	56	56	56.0
5			47	49	48.0
10			28	38	32.6
12	16	5			
15			23	28	25.4
20	15	4	25	28	26.5
25	13	5	24	20	21.9

*Courtesy of the U.S. Air Force Reconnaissance Laboratory, Wright Field.

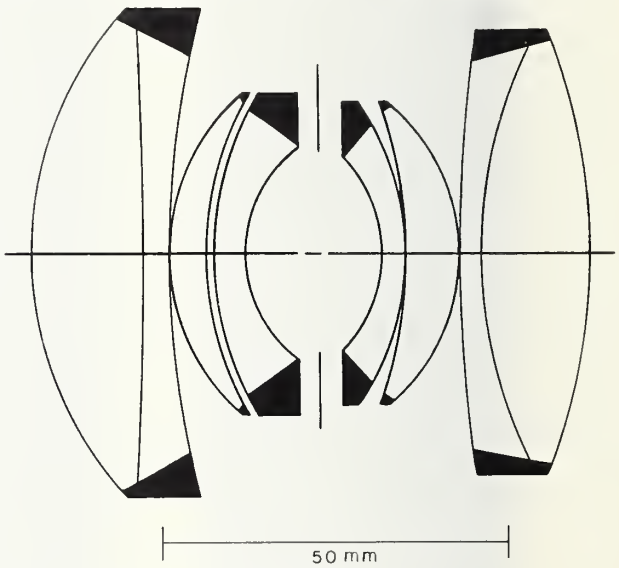

FIGURE 18a.

FIGURE 18b.

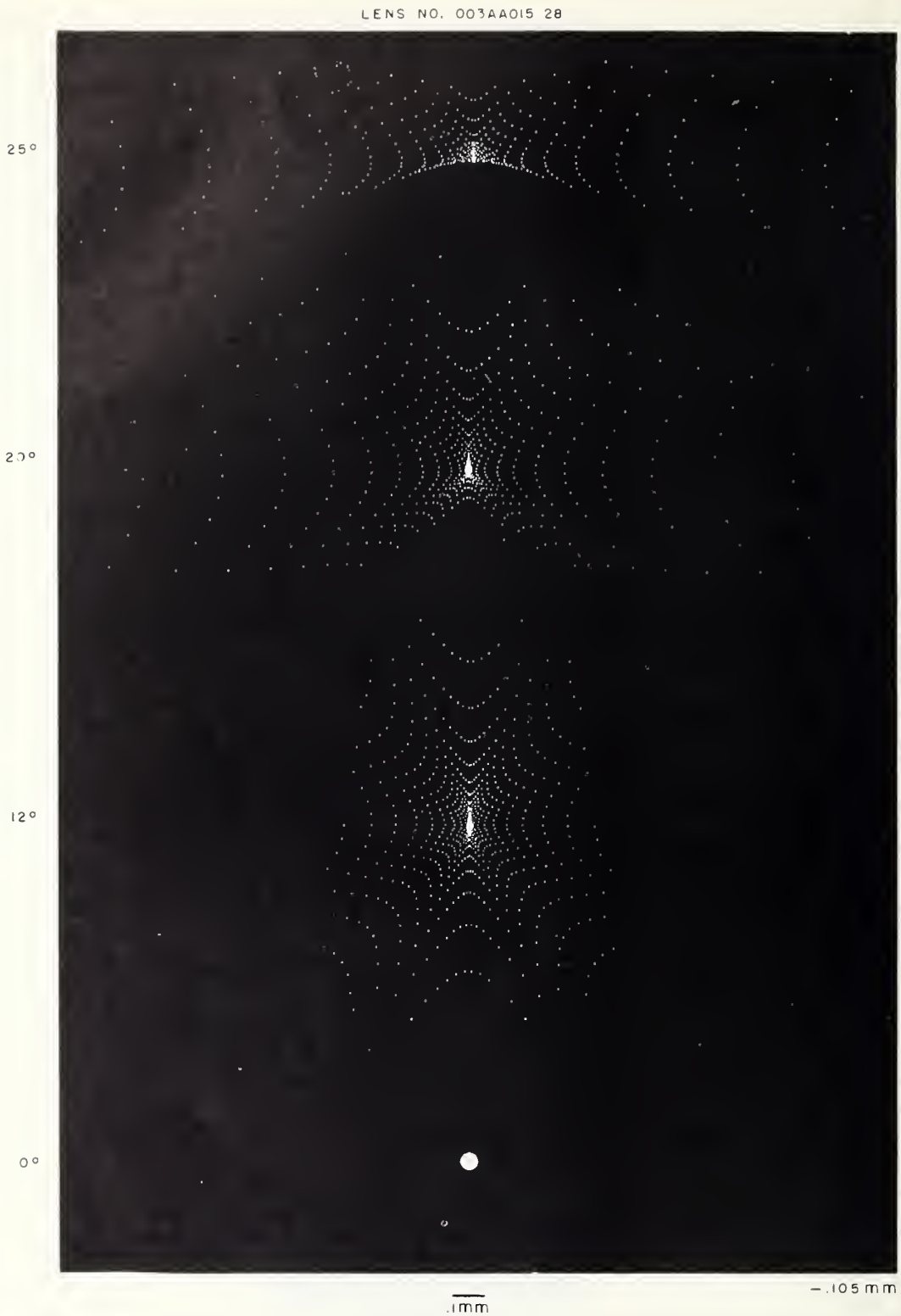

FIGURE 18c.

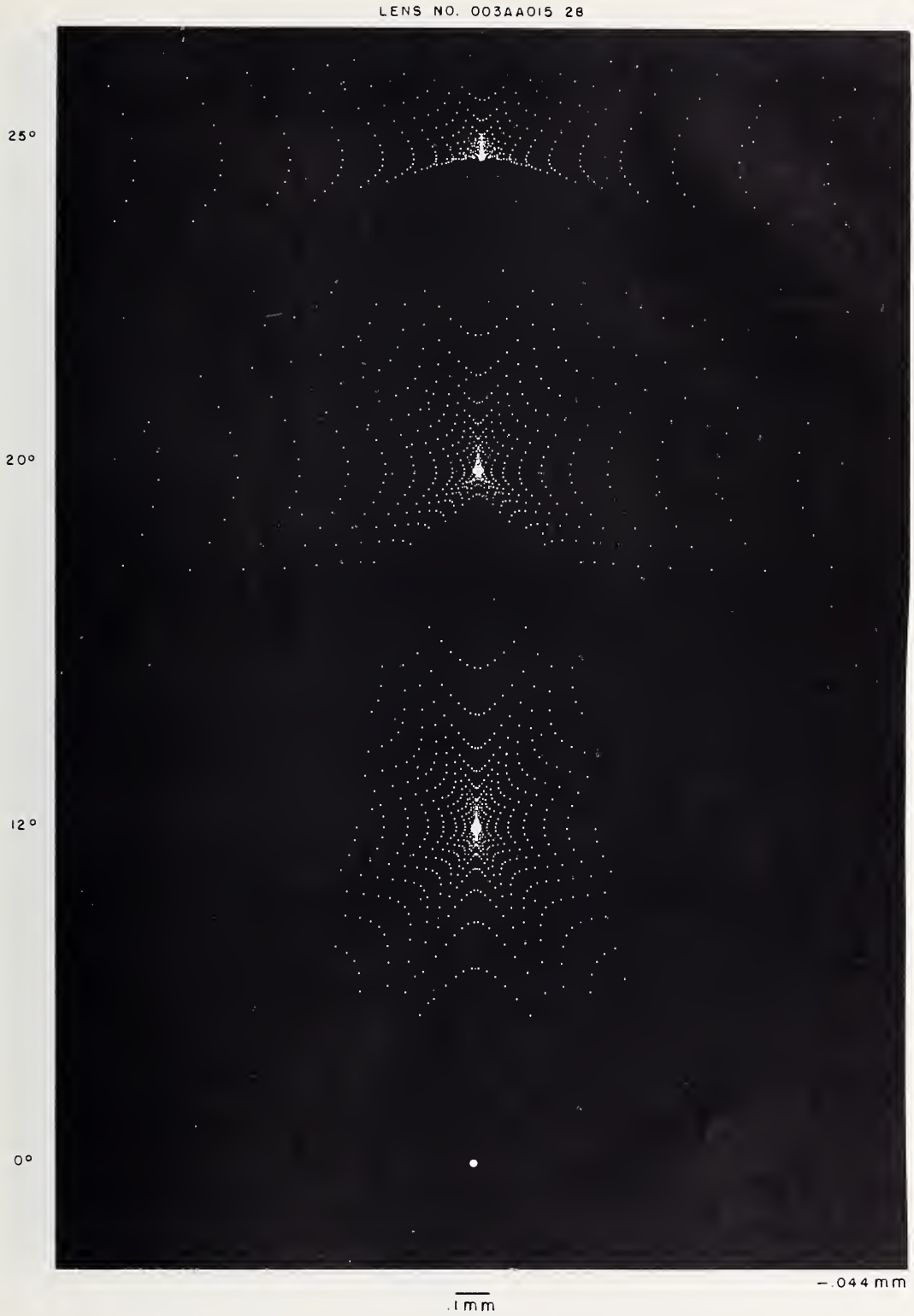

FIGURE 18d.

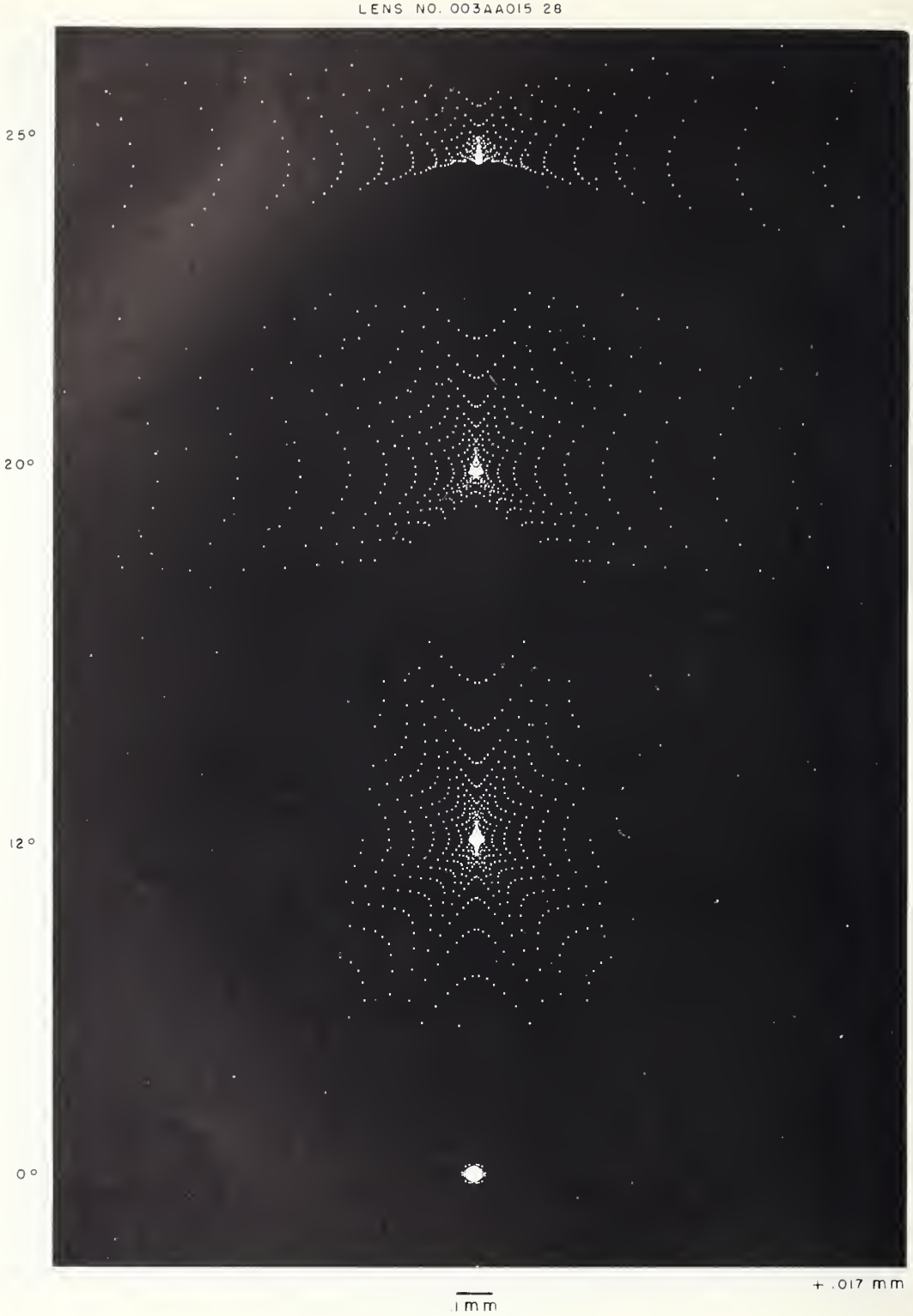

FIGURE 18e.

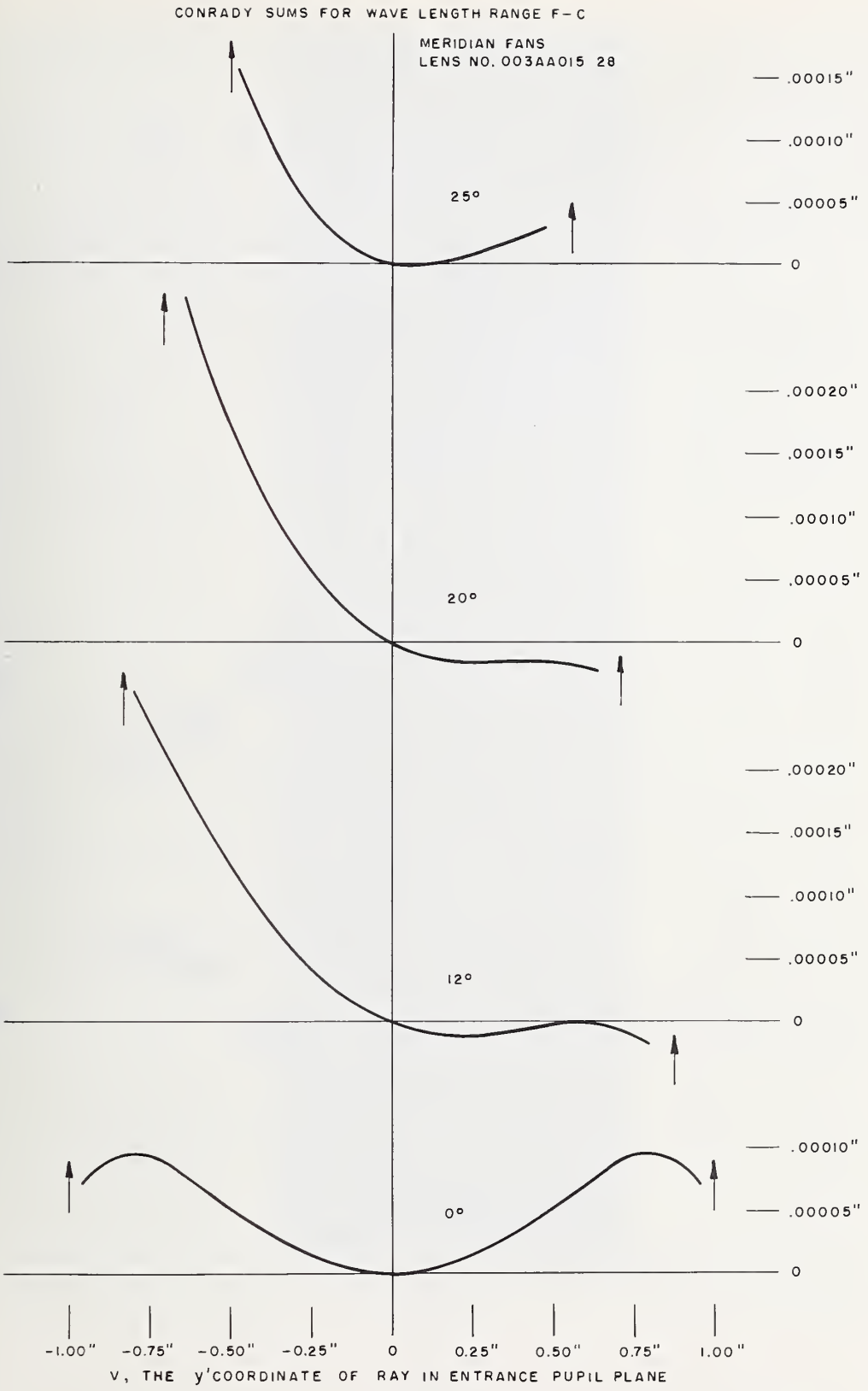
CONRADY SUMS FOR WAVE LENGTH RANGE F-C
MERIDIAN FANS
LENS NO. 003AA015 28
.00015"
.00010"
.00005"
0
25°
.00020"
.00015"
.00010"
.00005"
0
20°
.00020"
.00015"
.00010"
.00005"
0
12°
.00010"
.00005"
0
0°
-1.00"
-0.75"
-0.50"
-0.25"
0
0.25"
0.50"
0.75"
1.00"
V, THE y'COORDINATE OF RAY IN ENTRANCE PUPIL PLANE

FIGURE 18f.

006AA015 28—6 in. $f/1.5$, $4\frac{1}{2}\times4\frac{1}{2}$ in. format

The axial bundle for this lens is very well corrected. (See figures 19a–19f.) However, the spot diagrams for the off-axis obliquities exhibit a considerable amount of spherical aberration, together with smaller amounts of astigmatism and coma. As a result, the table on resolving power shows a definite decrease in resolution for the higher field angles. The light-collecting ability is about average out to 20° and drops off somewhat at 25°, as indicated by the plots of the entrance pupil areas.

The curves for the Conrady sums indicate that considerable amounts of both longitudinal and lateral chromatic aberration are present.

006 AA015 28—6 in. $f/1.5$ aerial camera lens for $4\frac{1}{2}\times4\frac{1}{2}$ in. format

	Radii	Separations	Outside diameters	Clear apertures	Glass	Index*	Abbe No.
	mm	*mm*	*mm*	*mm*			
1	+100.03		139	134			
		32.1			EK-210	1.7343	51.2
2	+2000.00						
		7.5			751277	1.75226	27.7
3	+208.19		139	112			
		—0.10—					
4	+61.947		95	87.2			
		12.53			EK-210	1.7342	51.2
5	+104.12			84.0			
		—1.215—					
6	+91.81		95	80.0			
		11.13			649338	1.64854	33.8
7	+35.905			59.0			
		—38.86—					
8	−41.424		90	55.0			
		7.12			720293	1.7203	29.3
9	−87.16			72.0			
		—.035—					
10	−209.71		90	80.0			
		19.50			EK-210	1.7342	51.2
11	−61.502			84.0			
		—.10—					
12	+354.7		119	102			
		5.7			751277	1.75226	27.7
13	+118.0						
		29.3			EK-210	1.7343	51.2
14	−175.55		119	112			

*Melt data.

Stop position: 23.368 mm from surface 7.
Opening 54.7 mm at $f/1.5$.

Relative entrance pupil area (006 AA015 28)

Field angle	No. transmitted rays	Percent of 0°
deg		
0	1090	100.0
12	934	85.7
20	672	61.7
25	336	30.8

Distortion and lateral color (006 AA015 28)

Field angle (nominal)	Tangent	Distortion	Distortion	H_F-H_C
deg		*in.*	*%*	*in.*
12	0.21256	−0.007609	−0.597	-15.1×10^{-3}
20	.36397	−.043350	−1.985	−34.2
25	.46631	−.100580	−3.595	−47.2

Resolving power (006 AA015 28)

Field angle	Predicted resolving power in lines/mm		Measured resolving power* in lines/mm		
	High contrast	Low contrast	R	T	$\sqrt{RT}$
deg					
0	45	24	41.0	41.0	41.0
5			36.8	32.6	34.6
10			24.1	22.5	23.3
12	9	3			
15			14.8	19.2	16.9
20	8	3	13.6	20.0	16.5
25	10	6	10.4	10.0	10.2

*Courtesy of the U.S. Air Force Reconnaissance Laboratory, Wright Field.

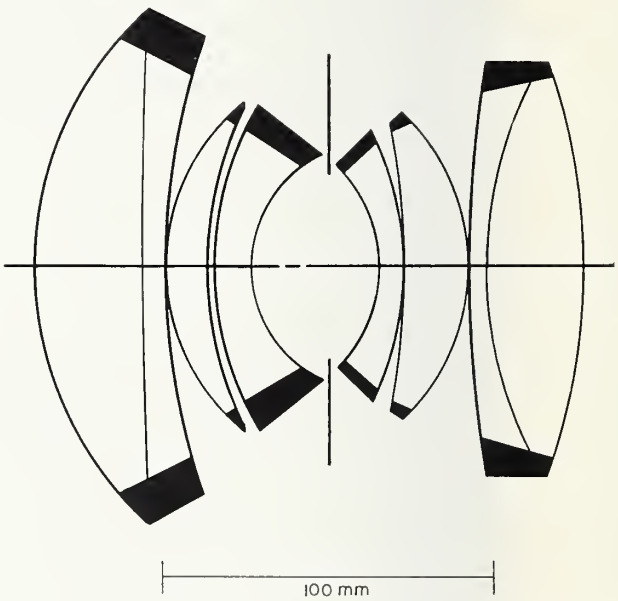

FIGURE 19a.

FIGURE 19b.

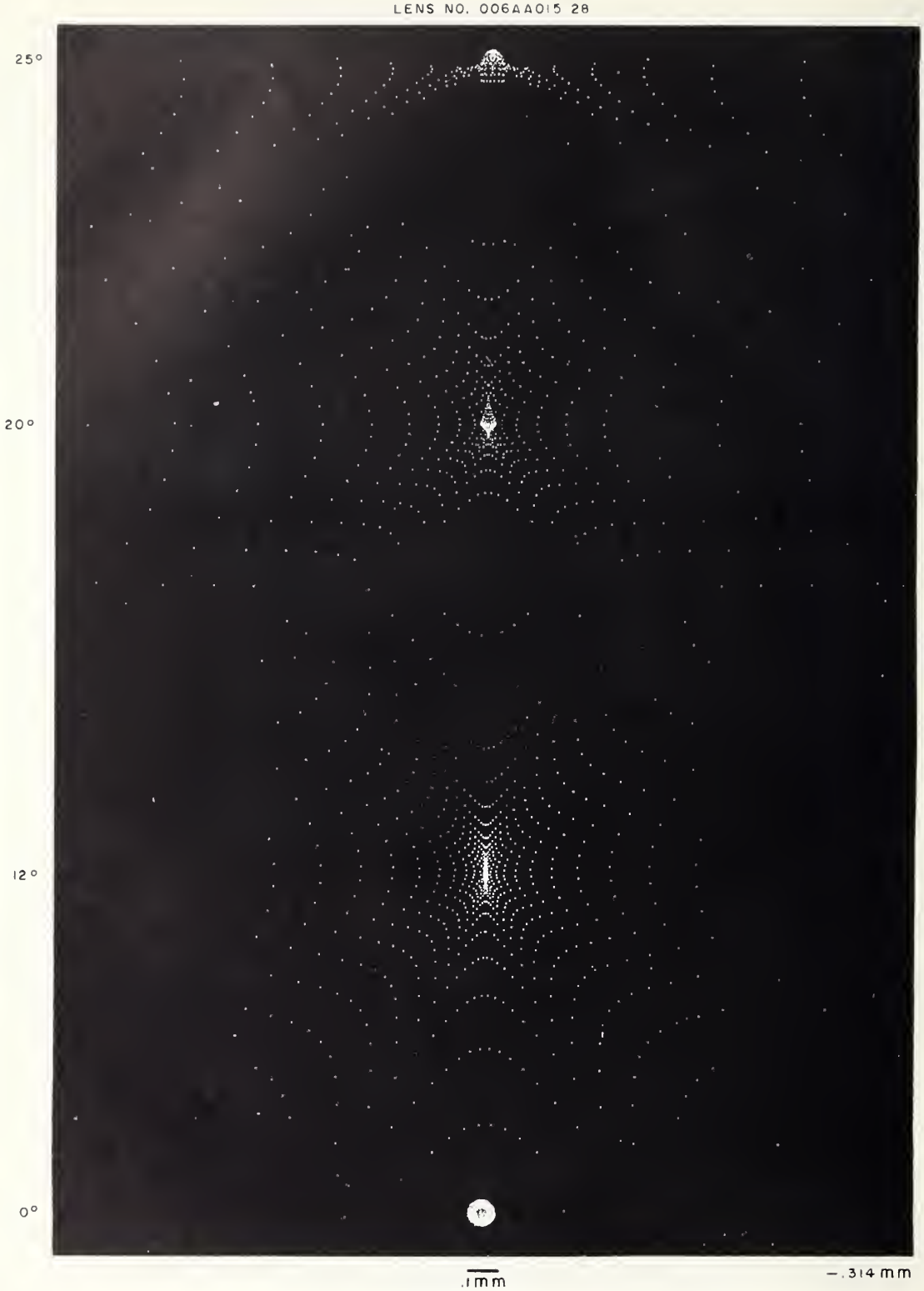

FIGURE 19c.

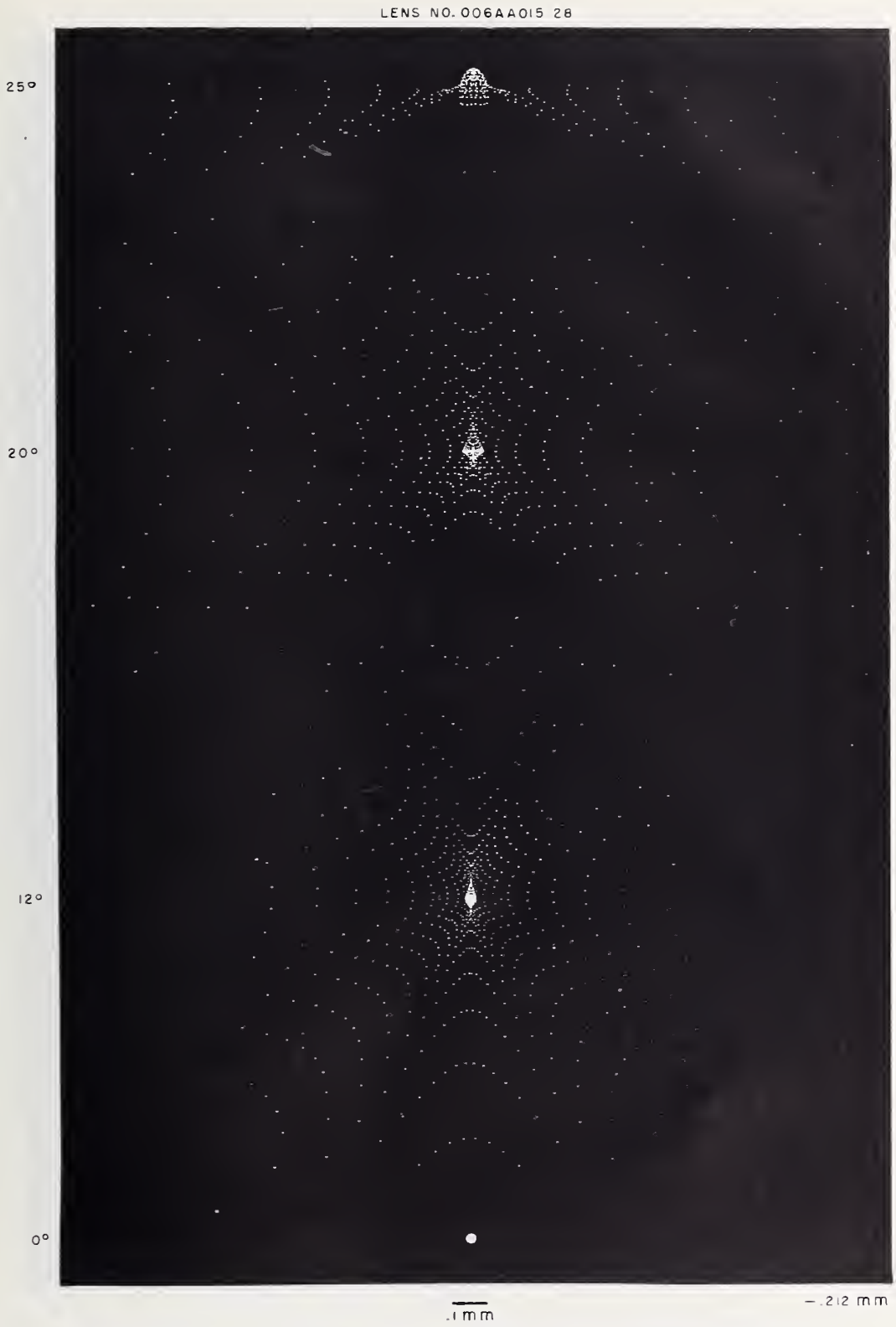

FIGURE 19d.

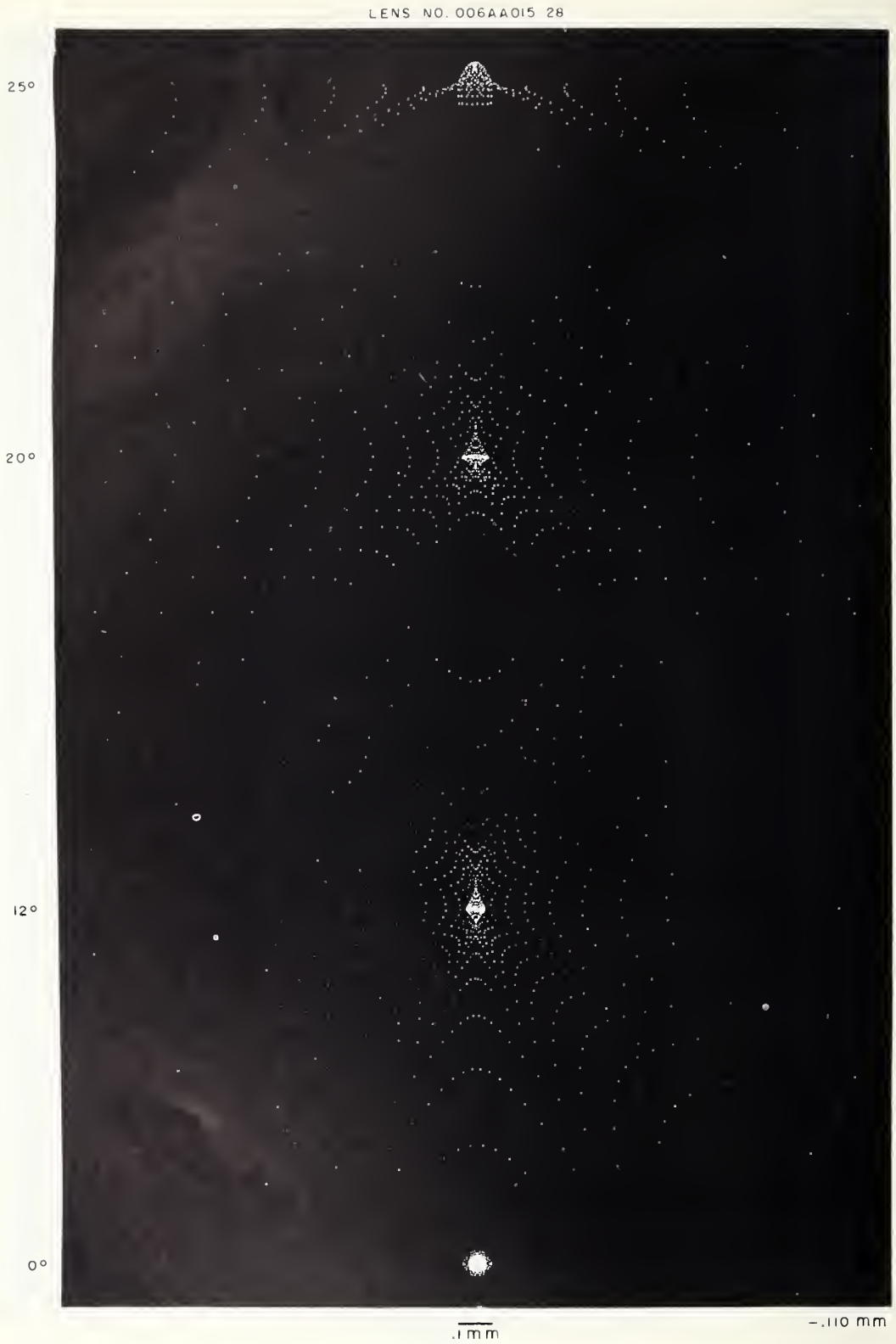

FIGURE 19c.

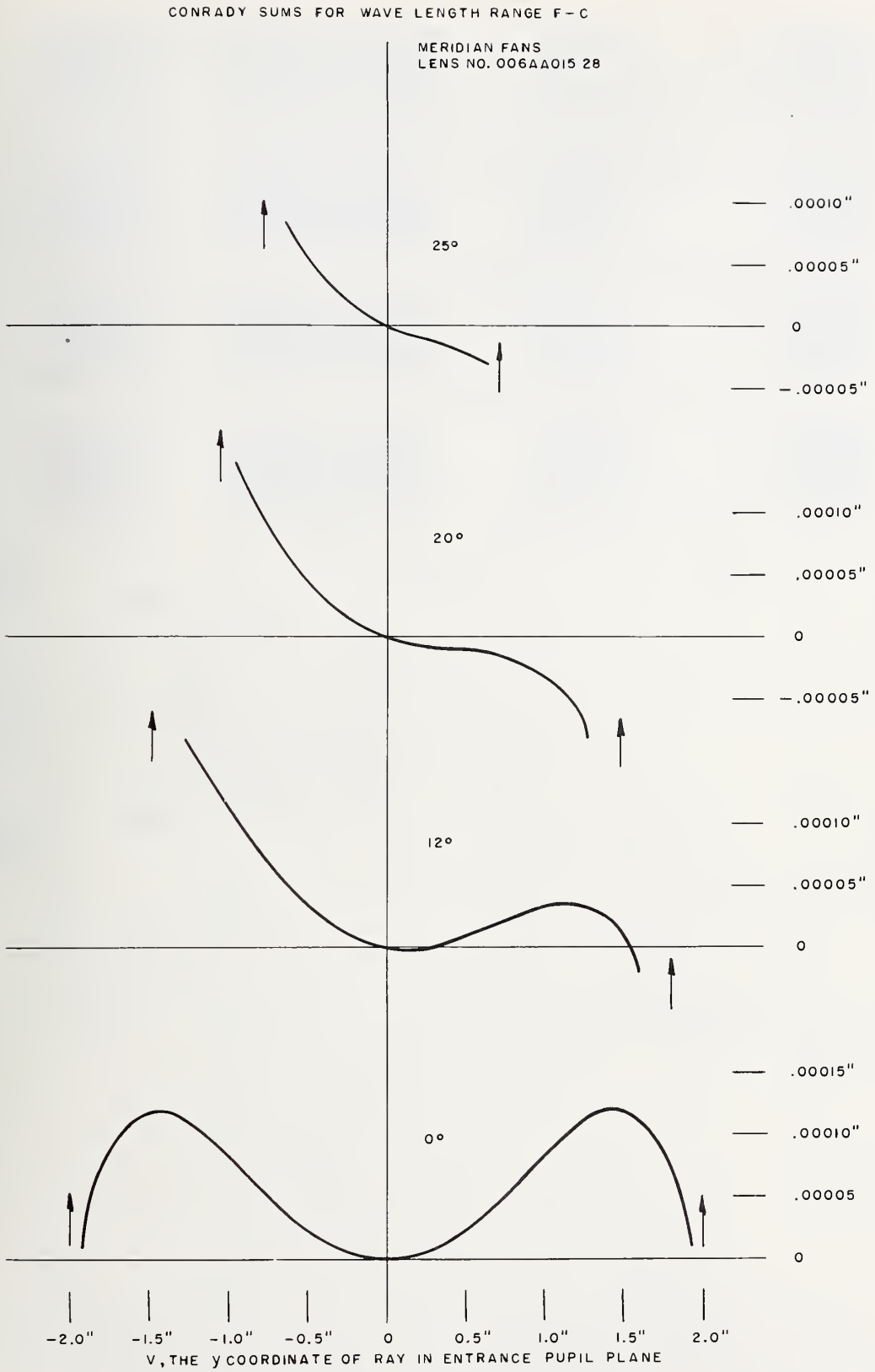

FIGURE 19f.

769-553 O—65——3

Lens No. 2 (006POL20 25) 6 in. $f/2$, 50° field

This lens was one for which only the spot diagrams and resolving power estimates were requested. (See figures 20a–20c.) However, the analysis produced information on the number of transmitted rays. This information is given here as a table. The results indicate that illumination should be maintained rather well over the field in this case.

The plane of best focus is at about −0.185 mm. Here the spot diagrams exhibit definitely better than average image quality, and particularly so for an $f/2$ lens. The cores of the images remain relatively small even in the diagrams for 18° and 25°. These higher obliquities show a moderate amount of flare, but enough rays are retained in the cores to keep them relatively solid, indicating that resolving power should be maintained to a corresponding degree over the entire field.

Lens No. 2 (006POL20 25) 6 in. f/2 aerial camera lens for a 50° field

	Radii	Separations	Outside diameters	Clear apertures	Index	Abbe No.
	mm	*mm*	*mm*	*mm*		
1	+131.379	8.832	81.2	78.2	1.7551	47.2
2	+819.36	7.620				
3	−155.510	4.572	79.2	76.2	1.7551	47.2
4	−1385.5	13.411				
5	+317.50	8.382	79.2	76.2	1.72	29.3
6	+152.400	19.705			1.611	58.8
7	−115.454	8.382			1.621	36.2
8	+146.583	9.144				
9	−435.43	9.144	79.2	71.4	1.611	58.8
10	−133.813	0.457				
11	+106.350	6.096	101.6	87.4	1.605	37.9
12	+83.55	28.956			1.611	58.8
13	−338.216	73.289		98.4		
14	−69.210	3.048	124.0	104.0	1.611	58.8
15	−508.00	25.073		121.0		

Stop position: 12.289 mm from fourth surfaee.
Opening: 73.8 mm at f/2.

Relative entrance pupil area lens No. 2 (006POL20 25)

Field angle	No. transmitted rays	Pereent of 0°
deg		
0	1094	100.0
10	950	86.8
18	784	71.7
25	624	57.0

Resolving power lens No. 2 (006POL20 25)

Field angle	Predicted resolving power in lines/mm	
	High contrast	Low contrast
deg		
0	47	24
10	37	21
18	24	17
25	22	17

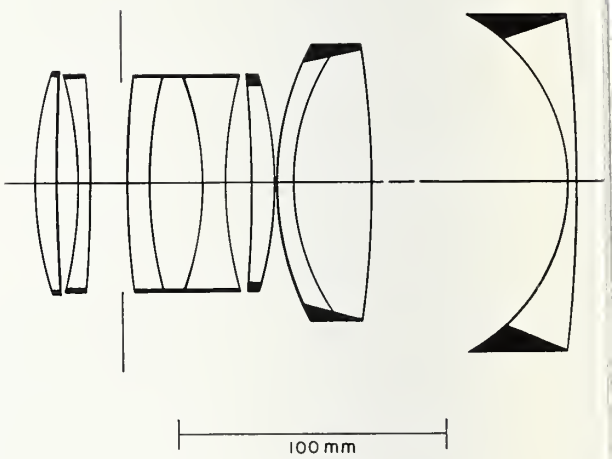

FIGURE 20a.

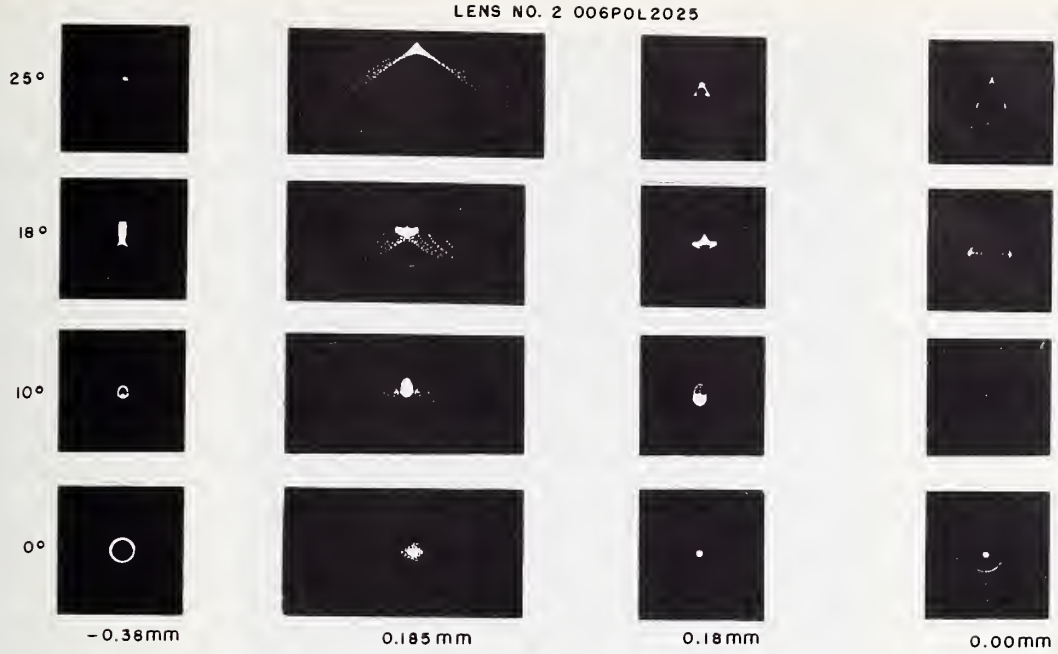

FIGURE 20b.

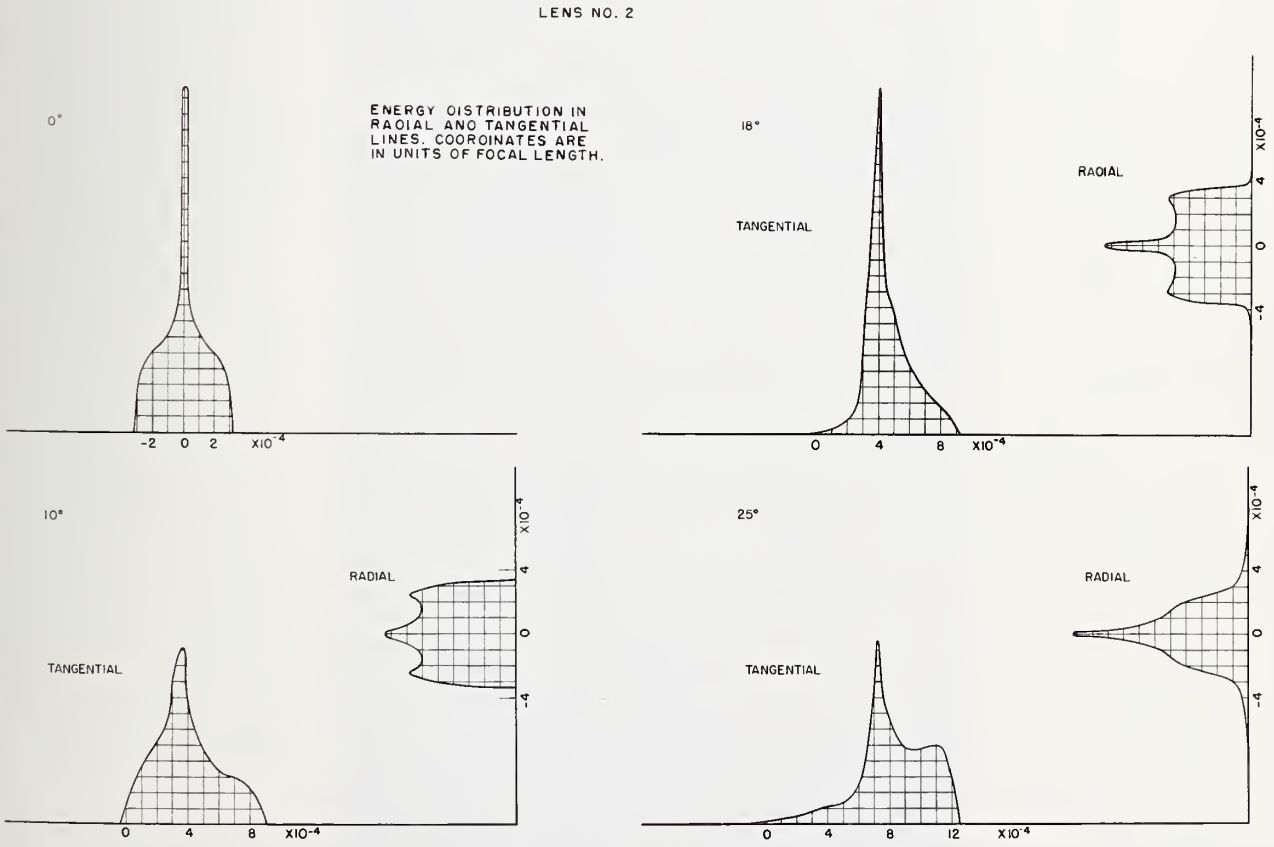

FIGURE 20c. *Lens No. 2—Energy distribution in radial and tangential lines.*

Coordinates are in units of focal length. Curves shown are for the Gaussian focal plane.

Lens No. 1—6 in. *f*/2, 50° field

This lens was not studied in as complete detail as usual since only spot diagrams were requested for the analysis. (See figures 21a–21e.) However, information on the light-gathering ability of the lens was incidentally obtained which indicated about average performance in terms of illumination. The entrance pupil at 25° took on a typical cat's-eye shape with an area of a little less than half the area of the 0° entrance pupil.

The spot diagrams show a rather small core at 0° with a flare which covers only a relatively small area. At off-axis obliquities the flare becomes very enlarged and its extreme edges were omitted for reasons of space. At 10° and 18° the cores are also enlarged, but only by a moderate amount compared with the enlargement of the flares. The core is again quite small at 25°, but it is apparent that only a small percentage of the rays are involved in forming this core. The presence of astigmatism may be noted from the horizontal or vertical "lines" formed in the off-axis imagery as the focal position changes.

Lens No. 1—6 in. *f*/2 aerial camera lens for a 50° field

	Radii	Separations	Outside diameter	Clear aperture	Glass	Index	Abbe No.
	mm	*mm*	*mm*	*mm*			
1	+117.8	11.0	80.0	76.3	D.B.C.6001-83	1.6203	60.3
2	+585.0	0.8					
3	+52.3	16.8	72.0	70.3	D.B.C.6001-83	1.6203	60.3
4	+245.0	5.0			L.F.8502-30	1.5800	41.0
5	+37.0	26.4		54.0			
6	−52.3	5.0		52.0	L.F.8502-15	1.5725	42.5
7	+117.8	16.6		63.0	D.B.C.6001-83	1.6203	60.3
8	−72.75	4.7	66.0	63.0			
9	+1767.0	10.7	84.0	82.0	D.C.B.6001-83	1.6203	60.3
10	−119.5	53.7					
11	−585.0	12.0	142.0	139.0	B.S.C.3002-35	1.517	54.5
12	+189.0	18.0			D.B.C.6001-83	1.6203	60.3
13	−1767.0		142.0	139.0			

Stop position: 17.1 mm from fifth surface.
Opening: 53.0 mm at f/2.

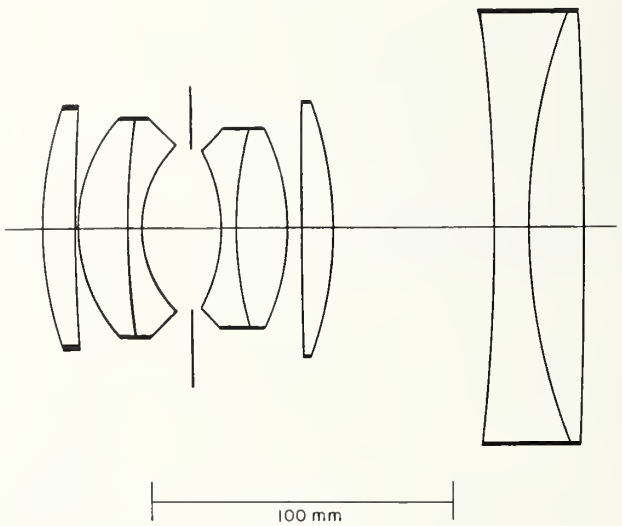

FIGURE 21a.

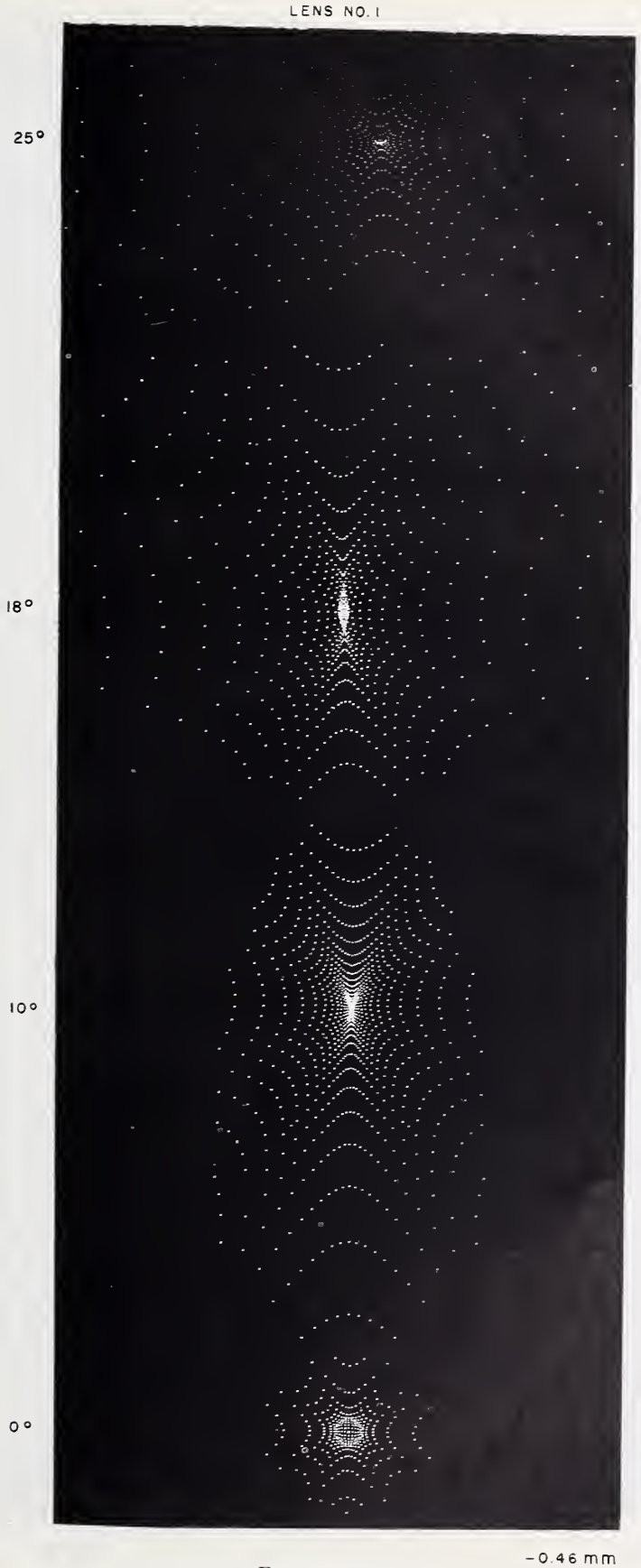

FIGURE 21b.

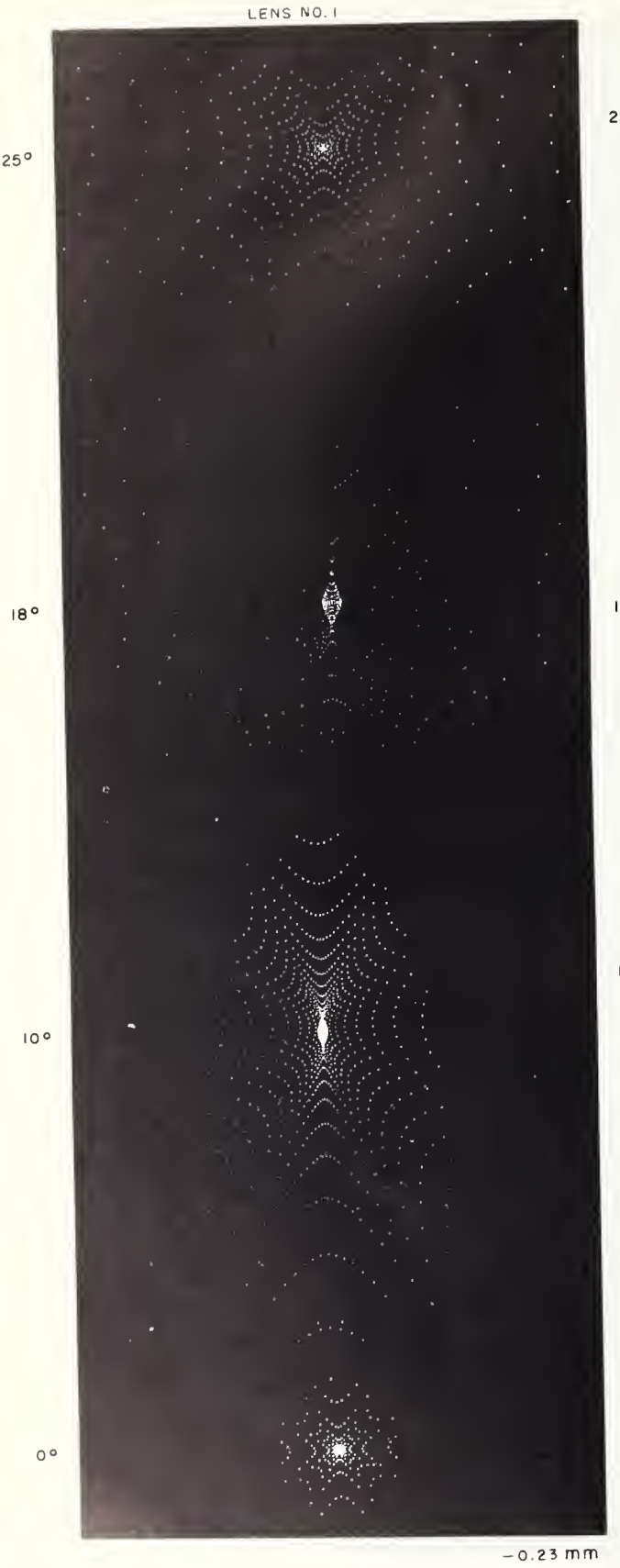

FIGURE 21c.

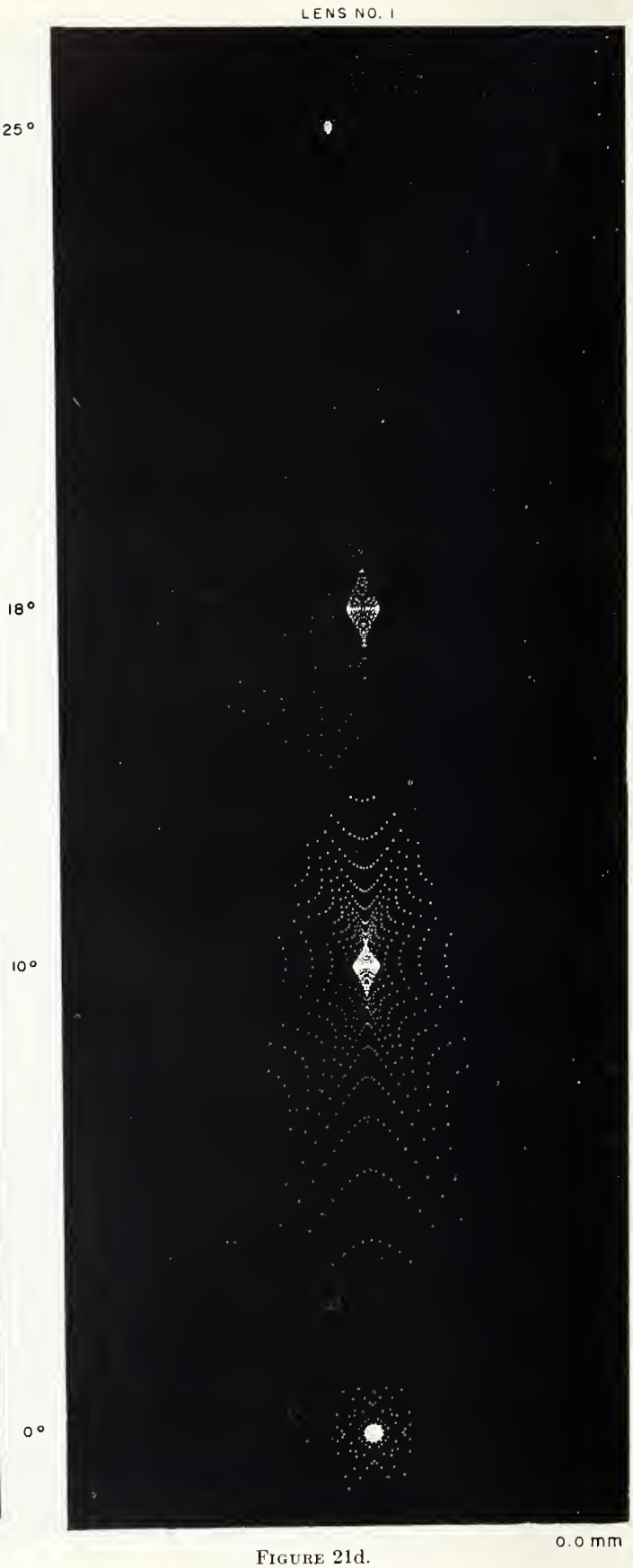

FIGURE 21d.

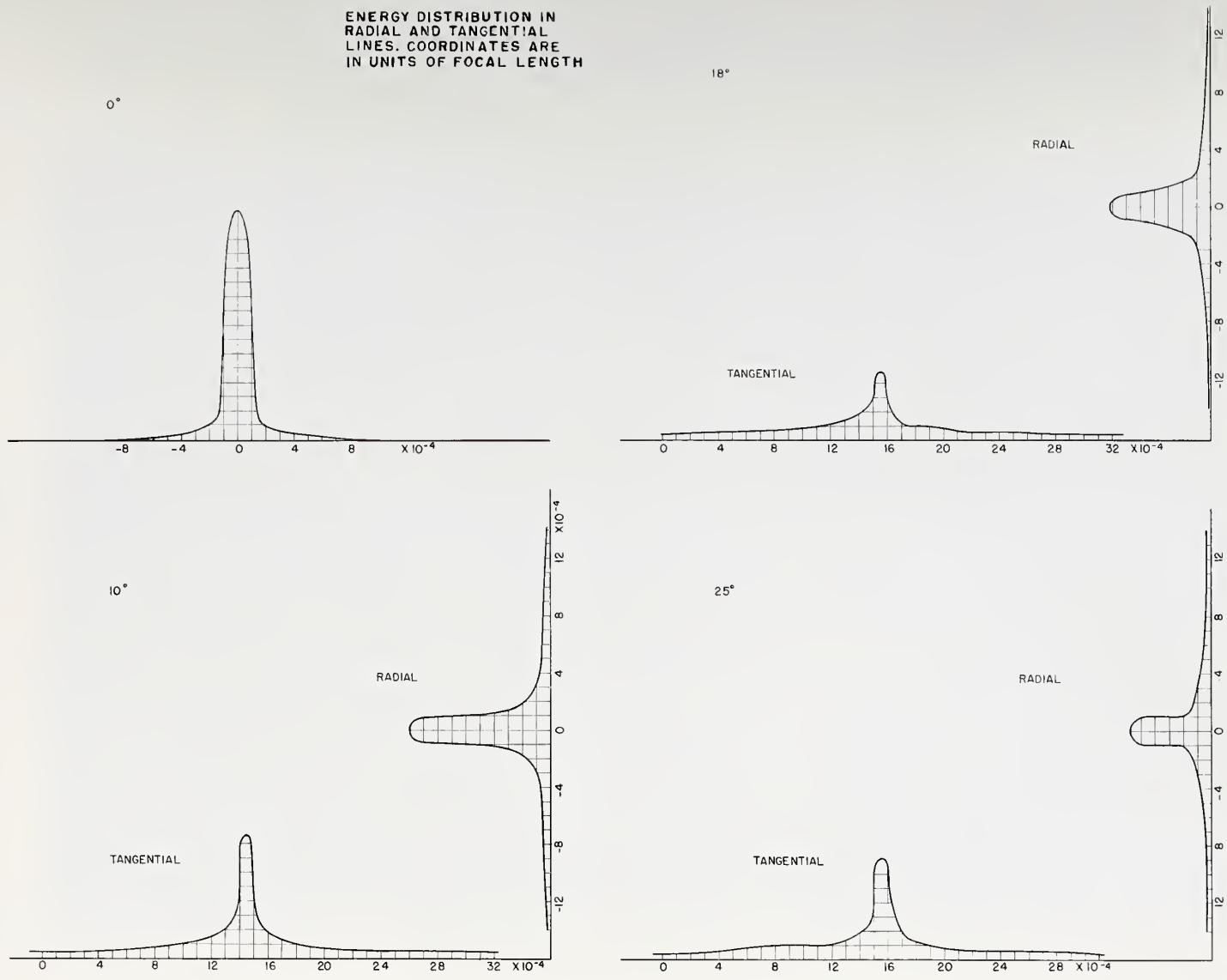

FIGURE 21e. *Lens No. 1—Energy distribution in radial and tangential lines.*

Coordinates are in units of focal length. Curves shown are for the Gaussian focal plane.

006AA025 28—6 in. *f*/2.5, 4½×4½ in. format

The cores of the spot diagrams for this lens (see figures 22a–22g) exhibit more than average symmetry, which indicates a good correction for astigmatism. Some curvature of field may be observed from the fact that the best focus for the 12 and 20° rays is inward from the best overall focus of −0.39 mm. Although there is a noticeable light flare in the 25° spot diagram, the small size of the core apparently compensates for this and maintains good high-contrast resolution here.

This lens appears about average in terms of light-collecting ability and quite good with respect to distortion. The lateral color correction looks better than average, with the longitudinal color not quite up to the same level.

006AA025 28—6 in. aerial camera lens for a 4½×4½ in. format

	Radii	Separations	Outside diameter	Clear aperture	Glass	Index	Abbe No.
	mm	*mm*	*mm*				
1	+79.40	7.01	67.0	65.00	EK-330	1.7551	47.2
2	+141.10	1.52					
3	+63.90	9.75	62.00	60.00	EK-210	1.7340	51.0
4	+443.80	5.33			DF-2	1.6170	36.6
5	+43.90	24.85		50.00			
6	−43.16	3.05		48.00	EDF-2	1.6890	30.9
7	+571.00	9.53			EK-430	1.77670	44.7
8	−54.45	5.28	54.0	52.00			
9	−302.20	5.61	59.00	57.00	EK-448	1.88040	41.1
10	−86.66	2.42					
11	−67.10	3.58	62.00	60.00	EK-450	1.80370	41.8
12	−89.96						

Stop position: 12.75 mm from fifth surface.
Opening: 47.44 mm at f/2.5.

Relative entrance pupil area 006AA025 28

Field angle	No. transmitted rays	Percent of 0°
deg		
0	1012	100.0
12	822	81.2
20	614	60.7
25	438	43.3

Distortion and lateral color 006AA025 28

Field angle (nominal)	Tangent	Distortion	Distortion	$H_F—H_C$
deg		*mm*	%	*mm*
12	0.21256	−0.00865	−0.027	−0.0048
20	.36397	−.04974	−.090	−.0053
25	.46631	−.10909	−.153	−.0021

Resolving power 006AA025 28

Field angle	Predicted resolving power in lines/mm		Measured resolving power* in lines/mm		
	High contrast	Low contrast	*R*	*T*	$\sqrt{RT}$
deg					
0	34	20	35.3	31.4	33.3
5			33.3	39.3	36.2
10			43.7	40.7	42.2
12	22	16			
15			27.0	20.7	23.6
20	15	14	18.7	19.8	19.2
25	13	6	26.9	32.5	29.6
27½			9.0	7.4	8.2

*Courtesy of the U.S. Air Force Reconnaissance Laboratories, Wright Field.

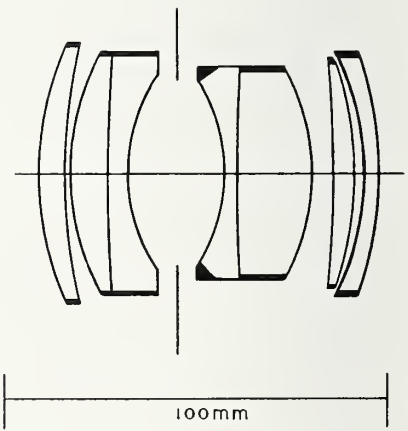

FIGURE 22a.

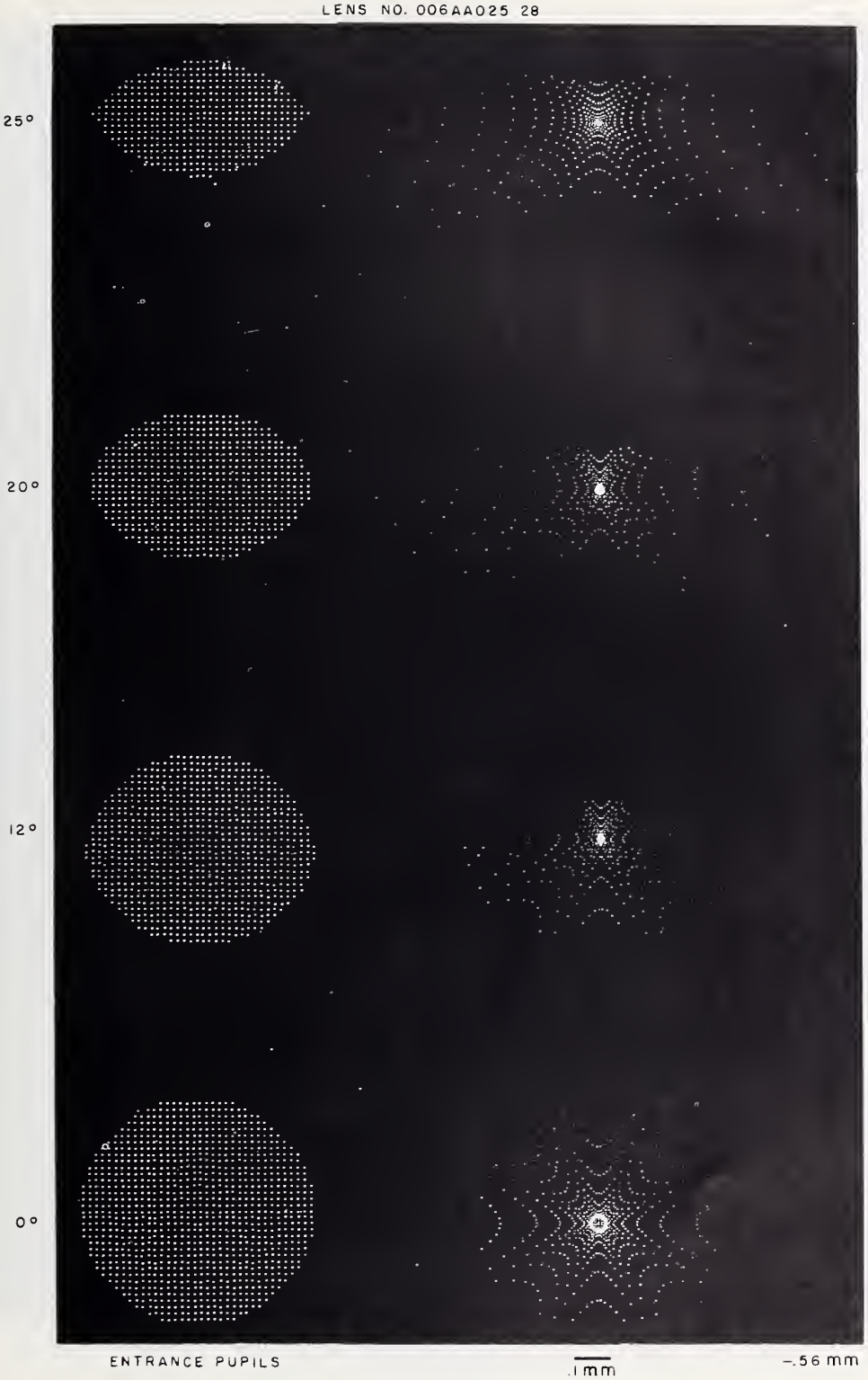

FIGURE 22b, c.

FIGURE 22d, e.

FIGURE 22f.

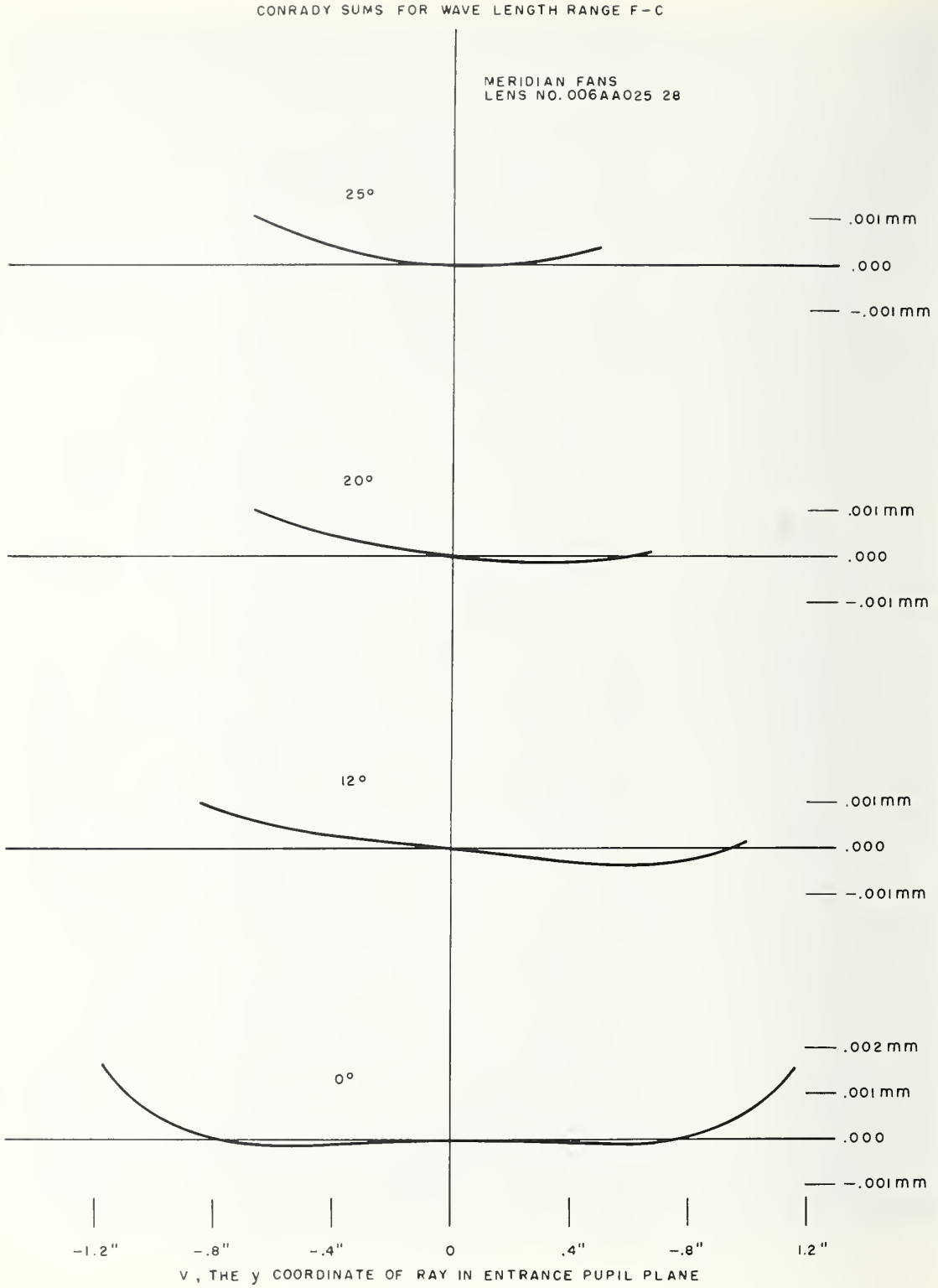
CONRADY SUMS FOR WAVE LENGTH RANGE F-C
MERIDIAN FANS
LENS NO. 006AA025 28
25°
20°
12°
0°
.001 mm
.000
-.001 mm
.002 mm
-1.2"
-.8"
-.4"
0
.4"
.8"
1.2"
V, THE y COORDINATE OF RAY IN ENTRANCE PUPIL PLANE

FIGURE 22g.

BAC–2—6 in. *f*/2.5, 55° field

Spot diagrams for this lens (see figures 23a–23c) were originally prepared for image planes at −0.225, 0, and +0.225 mm from the Gaussian focus. These results were used to locate the plane of best focus, shown at −0.150 mm, and estimates of resolving power were made for this focal position. One could expect that the image quality would be quite good on axis, falling off appreciably at the higher obliquities. The spot diagrams show definite, if somewhat large, cores at 12 and 20°, but the extensive spreading of the points at 25° indicates that loss of resolution will be more noticeable at this obliquity. It should be noted, of course, that this lens operates at a relatively low *f*-number, which normally increases the difficulty of obtaining good imagery over the entire field.

Illumination appears about average through 20° and drops off somewhat at 25°. The values of distortion remain quite low indeed out to slightly beyond 20° and then increase rapidly closer to the edge of the field. However, the distortion correction is still adequate for ordinary purposes.

BAC–2–6 in. *f*/2.5 aerial camera lens for a 55° field

	Radii	Separations	Outside diameters	Clear apertures	Glass	Index	Abbe No.
	in.	*in.*	*in.*	*in.*			
	+4.900	0.250	3.175	3.075	EK-110	1.69680	56.15
2	+18.140			3.015			
		—.012—					
3	+3.855	.390	2.970	2.870	EK-110	1.69680	56.15
4	+30.000			2.800	DF-375	1.621	
5	+3.740	.180		2.540			
		—.012—					
6	+2.345	.552	2.500	2.400	DF-375	1.621	
7	+1.664			1.890			
		—.930—					
8	−2.100	.787	2.562	1.870	EDF-977	1.649	
9	−3.337			2.300			
		—.012—					
10	−6.667	.150	2.562	2.300	EDF-977	1.649	
11	+6.000			2.440	EK-110	1.69680	56.15
12	−3.668	.450		2.450			
		—.012—					
13	−29.27	.240	2.700	2.570	EK-110	1.69680	56.15
14	−5.882			2.600			

Stop position: 0.517 in. from seventh surface.
Opening: 1.712 in. at *f*/2.5.

Relative entrance pupil area (BAC–2)

Field angle	No. transmitted rays	Percent of 0°
deg		
0	1012	100.0
12	1000	98.8
20	688	68.0
25	392	38.7

Resolving power (BAC–2)

Field angle	Predicted resolving power in lines/mm		Measured resolving power*		
	High contrast	Low contrast	R	T	$\sqrt{RT}$
deg					
0	56	25	49.7	35.3	41.9
5			33.2	29.4	31.2
10			20.6	25.5	22.9
12	10	9			
15			15.2	23.2	18.8
20	8	5	17.5	20.8	19.1
25	7	4	12.0	15.3	13.5

*Courtesy of the U.S. Air Force Reconnaissance Laboratory, Wright Field.

Distortion (BAC–2)

Field angle (nominal)	Tangent	Distortion	Distortion
deg		*in.*	%
12	0.21256	-28.8×10^{-5}	−0.022
20	.36397	+86.3	+.039
25	.46631	+723.6	+.257

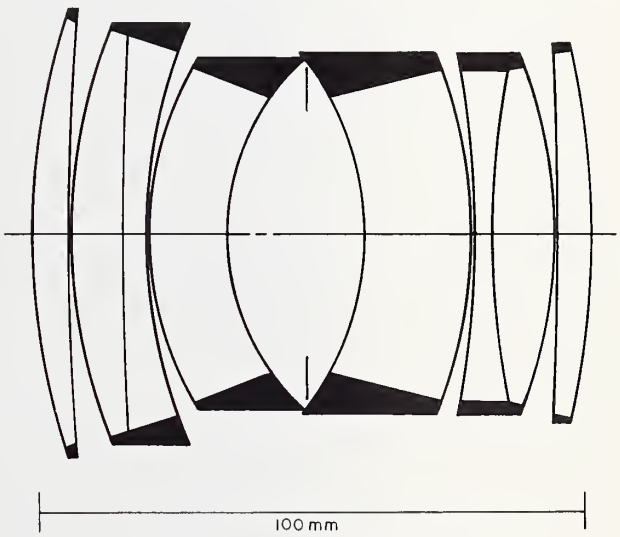

FIGURE 23a.

FIGURE 23b1.

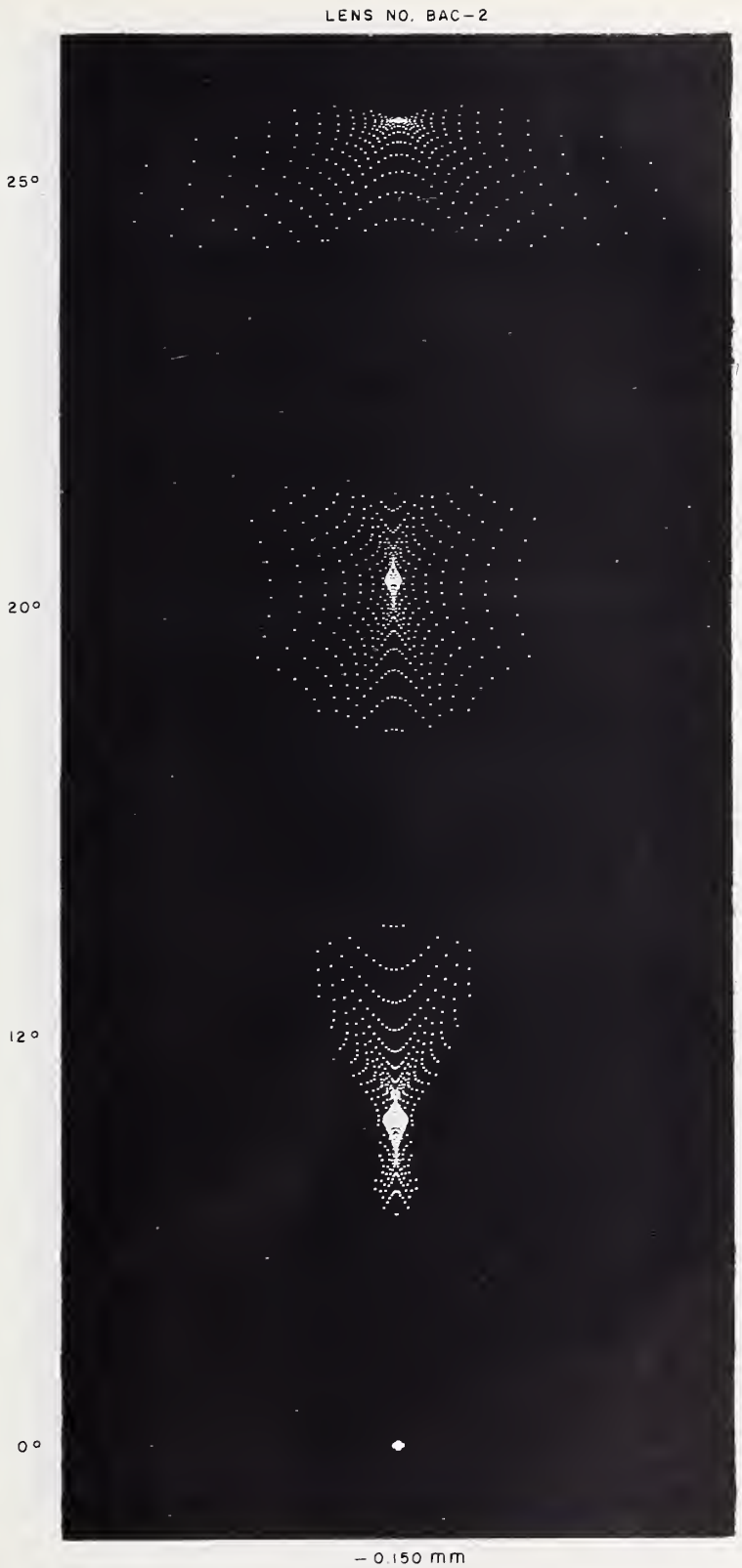

FIGURE 23b2.

FIGURE 23c1.

FIGURE 23c2.

006BB035 15—6 in. *f*/3.54, 2¼×2¼ in. format

The most evident feature of the spot diagrams for this lens (see figures 24a–24f) is the overall compactness of the image points depicted. This qualitative impression of a well-corrected design is borne out by the table on resolving power, which shows that some of the measured values of resolving power turned out to be higher than the predicted numerical estimates.

For this lens, illumination and curvature of field should present no problems, and the correction of distortion appears reasonable for ordinary applications. The flatness of the curves for the Conrady sums indicates good correction of longitudinal chromatic aberration, although there is a definite residual of lateral color.

006BB035 15—6 in f/3.54 aerial camera lens for a 2¼×2¼ in. format

	Radii	Separations	Clear apertures	Glass	Index	Abbe No.
	mm	*mm*	*mm*			
1	+72.87	9.60	62.00	EK–320	1.74450	45.8
2	+135.3	0.62	58.68			
3	+43.71	10.58	54.22	EK–110	1.69680	56.2
4	+83.14	5.29	49.30	EDF–2	1.68900	30.9
5	+31.21	52.07	40.34			
6	−36.42	3.09	39.07	EDF–15	1.67252	32.2
7	−2327.0	9.52	46.91	EK–415	1.74450	43.9
8	−45.90	0.19	49.18			
9	−1570.0	7.52	53.42	EK–310	1.74500	46.4
10	−114.6		55.00			

Stop position: 26.14 mm from fifth surface.
Opening: 28.76 mm at *f*/3.54.

Relative entrance pupil area 006BB035 15

Field angle	No. transmitted rays	Percent of 0°
deg		
0	816	100.0
7	806	98.8
11	770	94.4
14	662	81.1

Distortion and lateral color 006BB035 15

Field angle (nominal)	Tangent	Distortion	Distortion	H_F-H_C
deg		*in.*	%	*in.*
7	0.12278	-85.3×10^{-5}	−0.117	-12.9×10^{-5}
11	.19438	-353.6×10^{-5}	−.306	-24.1×10^{-5}
14	.24933	-779.2×10^{-5}	−.526	-36.3×10^{-5}

Resolving power—High contrast target—Supper XX 006BB035 15

Field angle	Predicted resolving power in lines/mm	Measured resolving power*		
		R	*T*	$\sqrt{RT}$
deg				
0	45–49	63	56	59.4
2.5		53	56	54.5
5		63	57	59.9
7	40–44			
7.5		56	49	52.4
10		43	49	45.9
11	36–42			
12.5		34	45	39.1
14	28–33			
15		31	37	33.9

*Courtesy of the U.S. Air Force Reconnaissance Laboratory, Wright Field.

Resolving power—Low contrast target—Pan X—006BB-035 15

Field angle	Predicted resolving power in lines/mm	Measured resolving power*		
		R	*T*	$\sqrt{RT}$
deg				
0	23	56	44	49.6
2.5		42	47	44.4
5		47	47	47.0
7	23			
7.5		40	39	39.5
10		24	36	29.4
11	23			
12.5		24	34	28.6
14	22			
15		24	31	27.3

*Courtesy of the U.S. Air Force Reconnaissance Laboratory, Wright Field.

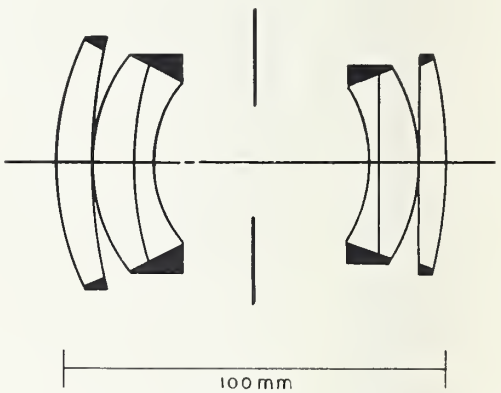

FIGURE 24a.

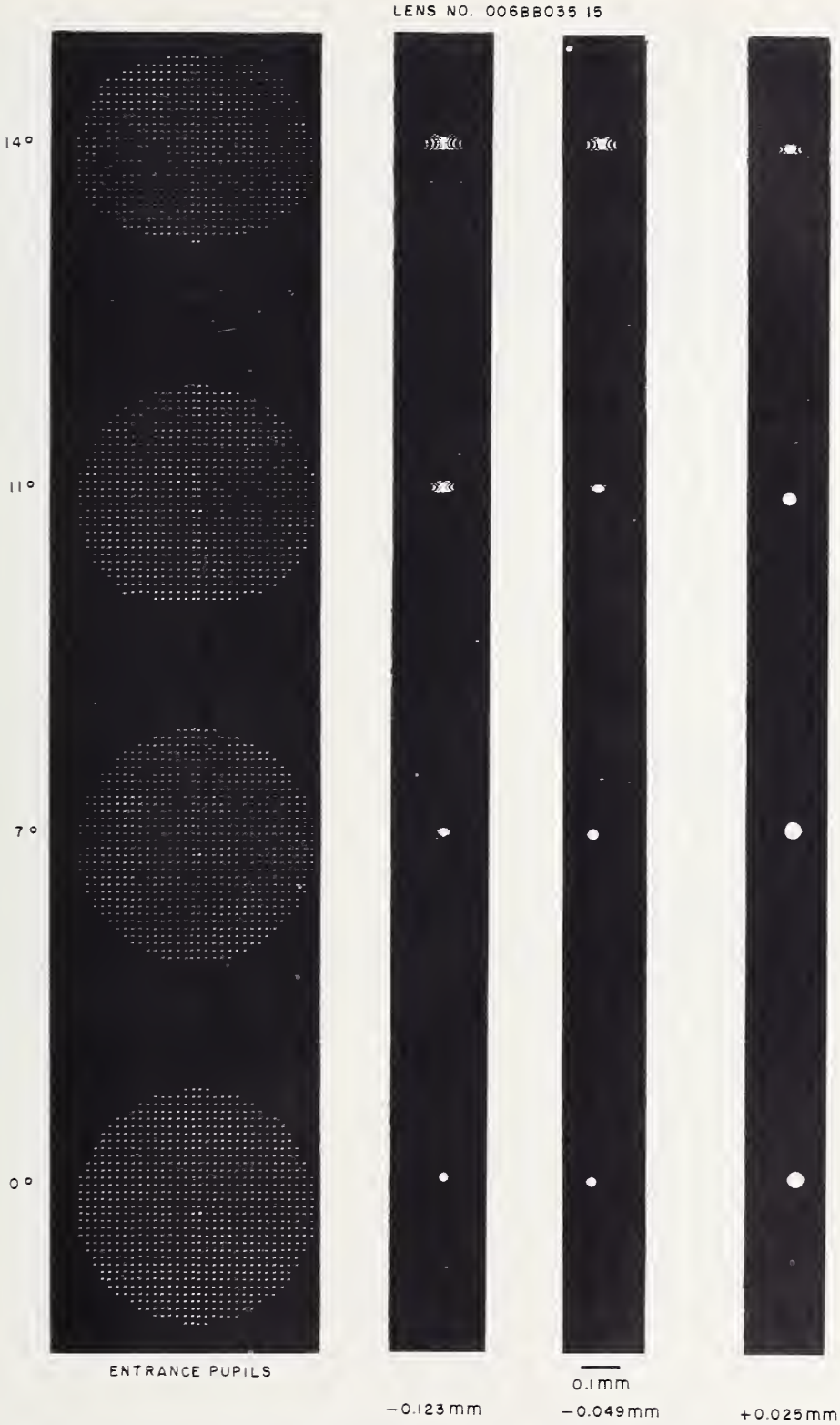

FIGURE 24b, c, d, e.

769–553 O—65——5

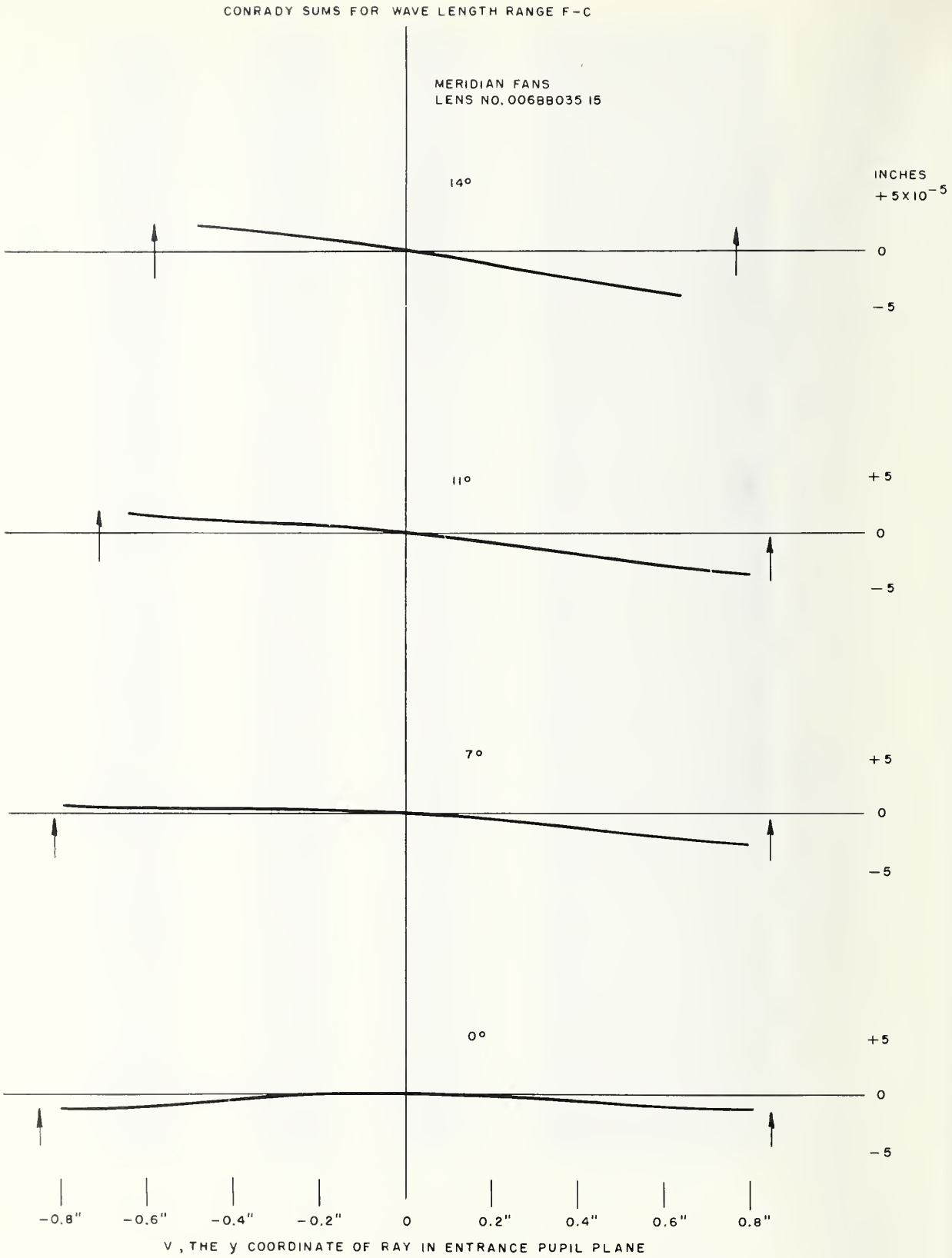
CONRADY SUMS FOR WAVE LENGTH RANGE F-C
MERIDIAN FANS
LENS NO. 006BB035 15
INCHES
+5X10⁻⁵
14°
11°
7°
0°
+5
0
-5
-0.8"
-0.6"
-0.4"
-0.2"
0
0.2"
0.4"
0.6"
0.8"
V, THE y COORDINATE OF RAY IN ENTRANCE PUPIL PLANE

FIGURE 24f.

006BC035 15—6 in. *f*/3.5, 2¼×2¼ in. format

The off-axis spot diagrams here show dense cores, each with a surrounding flare, but with all the rays converging into quite small areas. (See figures 25a–25f.) In the report on this lens it was noted that the 0° bundle, which shows excellent correction according to geometrical optics, produces a spot diagram which, at best focus (−0.042 mm), is slightly smaller than the corresponding Airy disk of physical optics. (See figure 5.) The resolving power actually obtainable under such a condition will be limited by the effects of diffraction.

This lens appears to have about average light-collecting ability and to be somewhat better than average in the correction of distortion. Both longitudinal and lateral chromatic aberration may be observed in the curves for the Conrady sums.

006BC035 15—6 in. *f*/3.5 aerial camera lens for a 2¼×2¼ in. format

	Radii	Separations	Outside diameters	Clear apertures	Glass	Index	Abbe No.
	mm	*mm*	*mm*	*mm*			
1	+58.89	9.9	57.0	54.0	670472	1.66990	47.2
2	+159.9			54.0			
		3.5					
3	+51.10		50.0	46.0			
		18.9			611588	1.611	58.8
4	−106.0						
		2.55			621362	1.621	36.2
5	+28.10		50.0	32.0			
		23.2					
6	−33.20		38.0	32.0			
		7.8			617366	1.617	36.6
7	−50.61			28.7			
		6.1					
8	+4186.4		44.0	40.8			
		12.15			573568	1.5725	56.8
9	−56.26			40.8			

Stop position: 13.2 mm from fifth surface.
Opening: 26.58 mm at *f*/3.5.

Relative entrance pupil area—006BC035 15

Field angle	No. transmitted rays	Percent of 0°
deg		
0	824	100.0
7	726	88.1
11	576	69.9
14	436	52.9

Distortion and lateral color—006BC035 15

Field angle (nominal)	Tangent	Distortion	Distortion	H_F-H_C
deg		*in.*	%	*in.*
7	0.12278	$+59.7\times10^{-5}$	+0.081	$+55.2\times10^{-5}$
11	0.19438	+206.7	+0.178	+67.9
14	0.24933	+364.6	+0.245	+56.8

Resolving Power—006BC035 15

Field angle	Predicted resolving power in lines/mm		Measured resolving power in lines/mm*		
	High contrast	Low contrast	*R*	*T*	$\sqrt{RT}$
deg					
0	47–60	25	32	32	32.0
2.5			32	35	33.5
5			31	31	31.0
7	35–39	17			
7.5			28	28	28.0
10			31	31	31.0
11	22–30	12			
12.5			31	31	31.0
14	21–28	11			
15			31	31	31.0

*Courtesy of the U.S. Air Force Reconnaissance Laboratory, Wright Field.

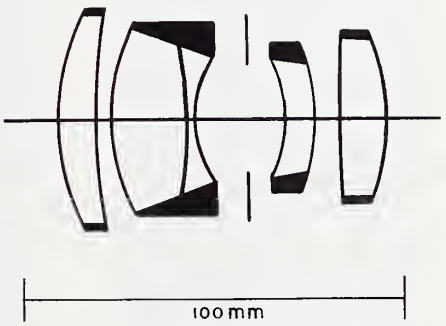

FIGURE 25a.

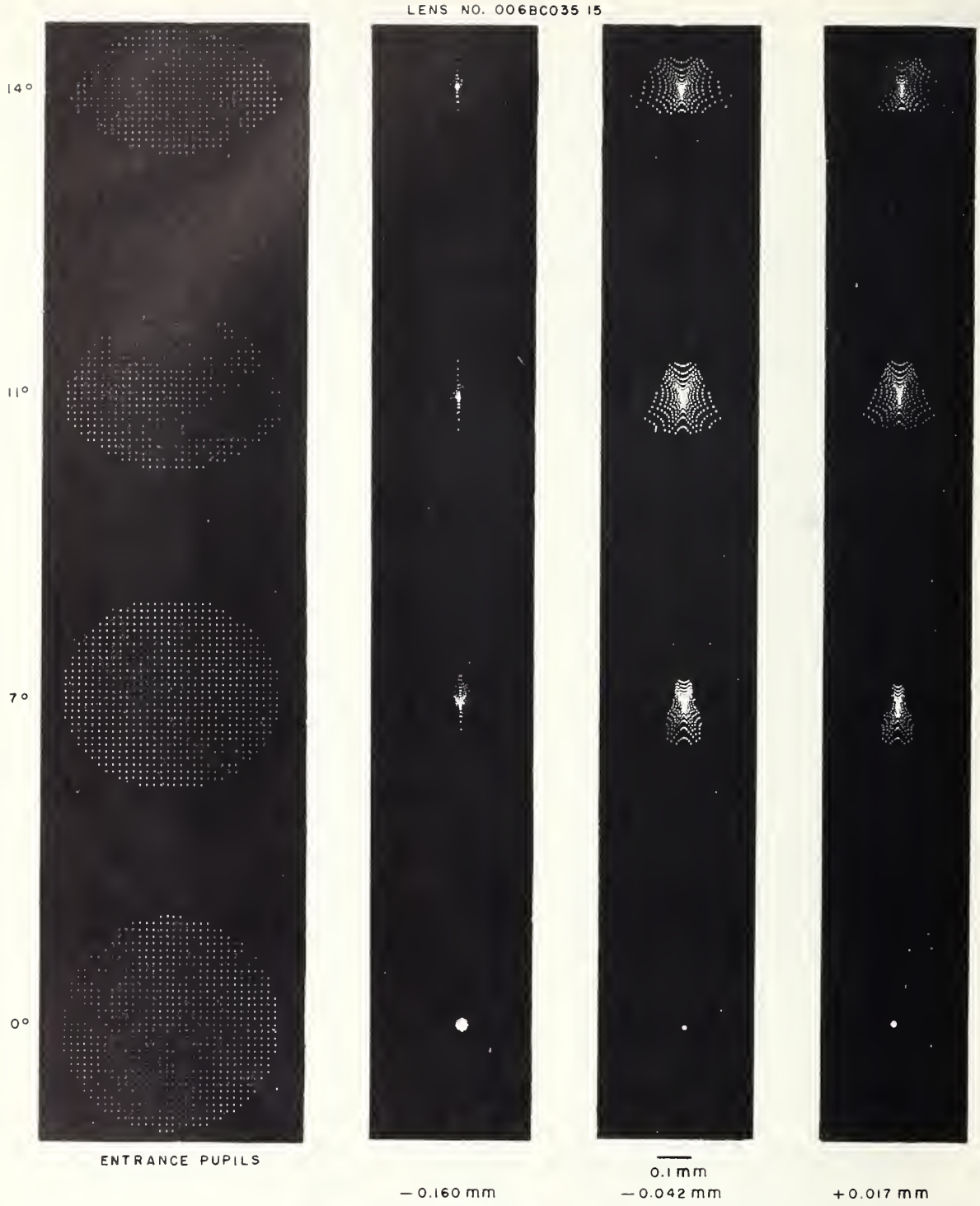

FIGURE 25b, c, d, e.

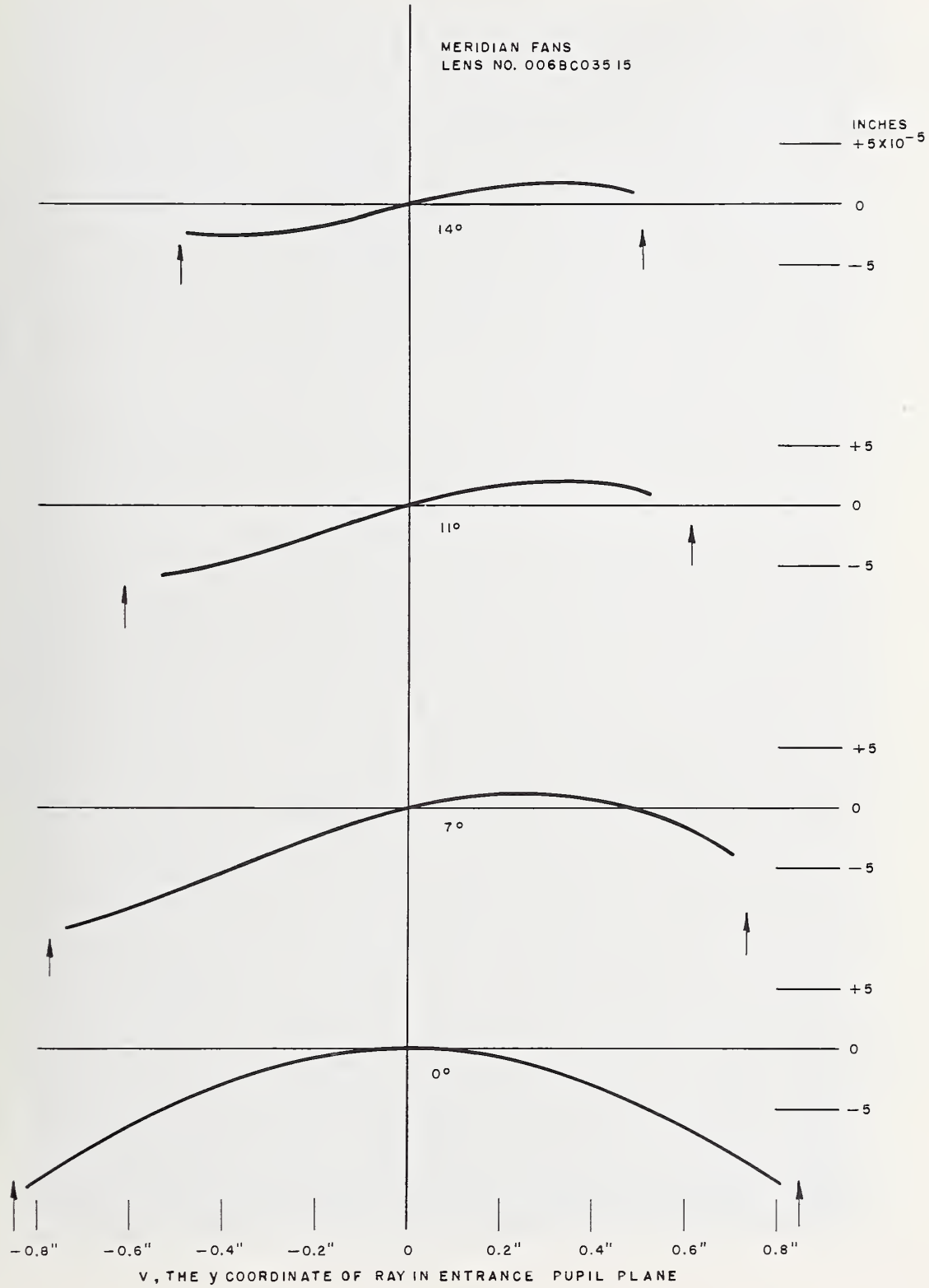
MERIDIAN FANS
LENS NO. 006BC035 15
INCHES
+5X10⁻⁵
0
−5
14°
+5
0
−5
11°
+5
0
−5
7°
+5
0
−5
0°
−0.8"
−0.6"
−0.4"
−0.2"
0
0.2"
0.4"
0.6"
0.8"
V, THE y COORDINATE OF RAY IN ENTRANCE PUPIL PLANE

FIGURE 25f.

006XA056 45—*f*/5.6, 90° field

The plane of best focus for this lens (see figures 26a–26f) was judged to be at the −0.342 mm position although the overall imagery at −0.477 mm is almost equally good. These spot diagrams exhibit dense cores of a small size from 0 through 35°, becoming moderately enlarged for the 40 and 45° obliquities. The light-collecting ability and control of distortion for this lens are superior.

The numbers computed for the table on lateral color are approximately equal to the slopes of the Conrady sum graphs at the origin. Inspection of these graphs shows that due to a displacement of the bundle of rays, the correction of lateral color is actually somewhat better at 40 and 45° than the last two values in the lateral color table would indicate. The Conrady sum graphs also show the presence of longitudinal color, except near the middle of the field at about 27°. The curves range gradually from downward bending at 0° to approximately equal upward bending at 45°.

006XA056 45—6 in. *f*/5.6 aerial camera lens for a 90° field

	Radii	Separation	Outside diameter	Clear aperture	Index	Abbe No.
	in.	*in.*	*in.*	*in.*		
1	+3.1551	0.4922	4.100	4.004	1.617	36.6
2	+4.2068	.2650		3.638		
3	+11.146	.0947	3.765	3.635	1.700	41.0
4	+1.8354	.7004		2.804		
5	+2.1942	.3407	2.595	2.468	1.8004	41.1
6	+6.5220	.2991		2.396		
7	+8.5632	.1514	2.079	1.954	1.670	47.4
8	+0.8605	.5245		1.452	1.607	59.5
9	aspheric	.3029	1.514	1.331		
10	aspheric	.5245	1.471	1.266	1.607	59.5
11	−0.8605	.1514		1.409	1.670	47.4
12	−8.5632	.2991	1.984	1.859		
13	−5.2825	.3407	2.465	2.245	1.8004	41.1
14	−2.0337	1.1752		2.338		
15	−1.8354	.0947	4.131	2.987	1.700	41.0
16	−11.146	.2650		4.004		
17	−10.443	.5096	5.089	4.633	1.575	41.4
18	−5.6355	2.9119		4.962		

Stop position: 0.15145 in. from ninth surface.
Opening: 1.072 in. at *f*/5.6.

Relative entrance pupil area—006XA056 45

Field angle	No. transmitted rays	Percent of 0°
deg		
0	1052	100.0
10	1052	100.0
18	1048	99.6
27	1068	101.5
35	1080	102.7
40	1078	102.5
45	1008	95.8

Distortion and lateral color—006XA056 45

Field angle (nominal)	Tangent	Distortion	Distortion	H_F-H_C
deg		*in.*	%	*in.*
10	0.17633	$+4.2\times10^{-5}$	+0.0039	-42.6×10^{-5}
18	.32492	+22.4	.0114	−69.6
27	.50953	+58.5	.0191	−88.1
35	.70021	+64.2	.0152	−109.4
40	.83910	+23.9	.0047	−164.8
45	1.00000	+27.9	.0046	−353.8

Predicted resolving power—006XA056 45

Field angle	Predicted resolving power in lines/mm	
	High contrast	Low contrast
deg		
0	48	23
10	48	24
18	50	23
27	30	20
35	15	14
40	10	9
45	10	8

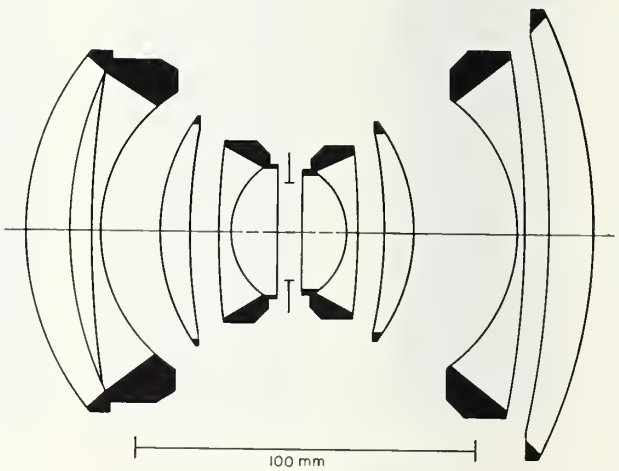

FIGURE 26a.

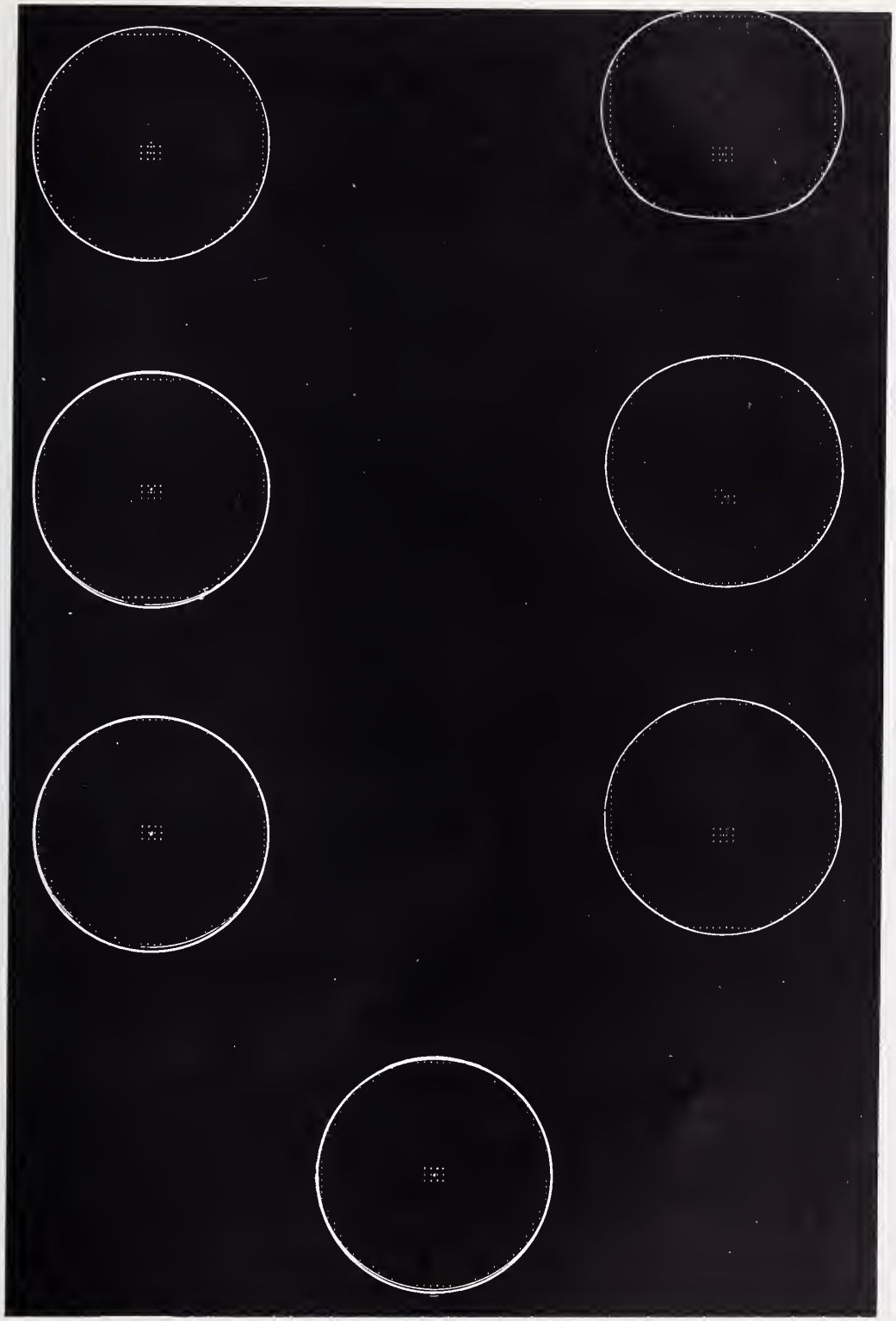

ENTRANCE PUPILS

FIGURE 26b.

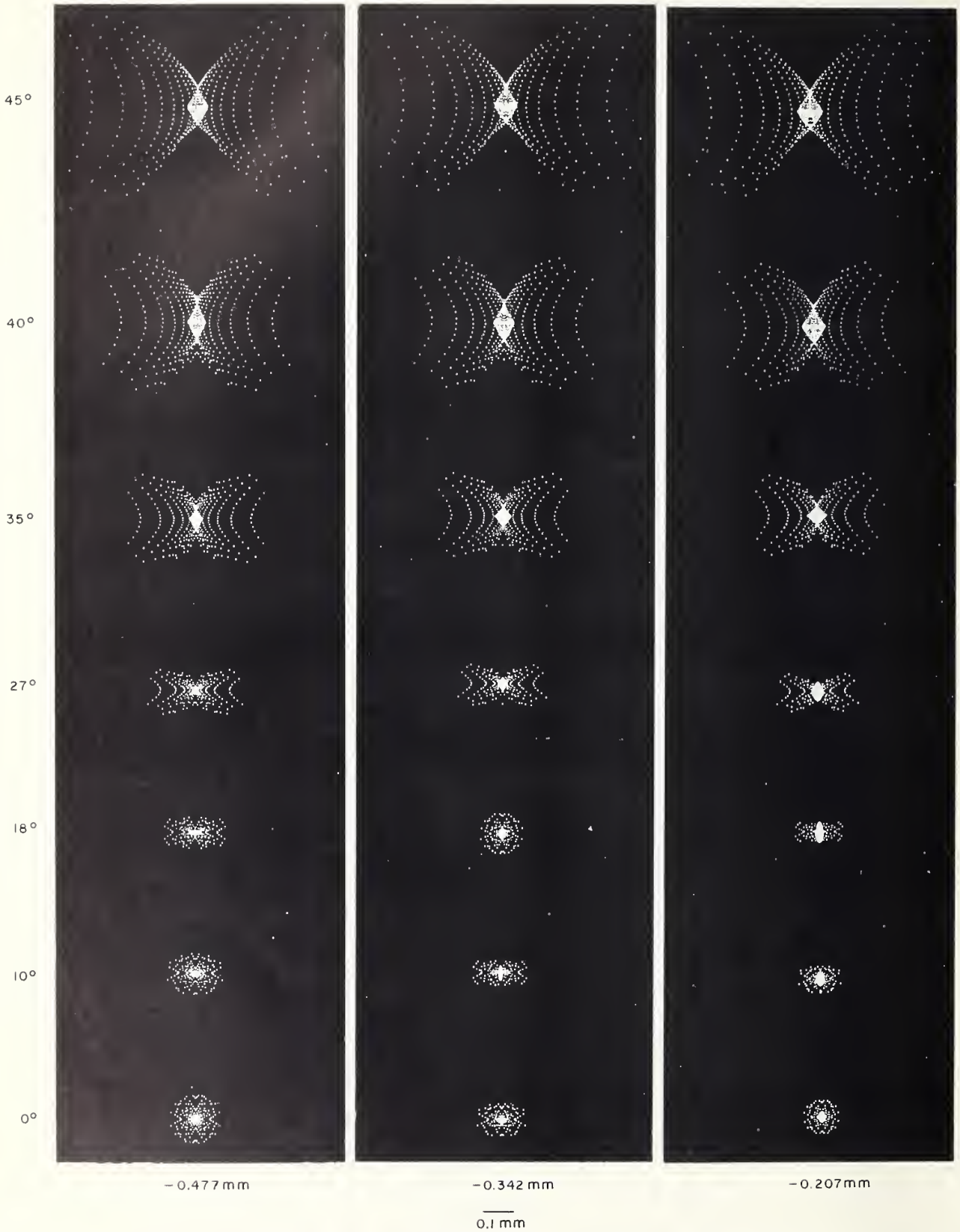

FIGURE 26c, d, e.

CONRADY SUMS FOR WAVE LENGTH RANGE F-C

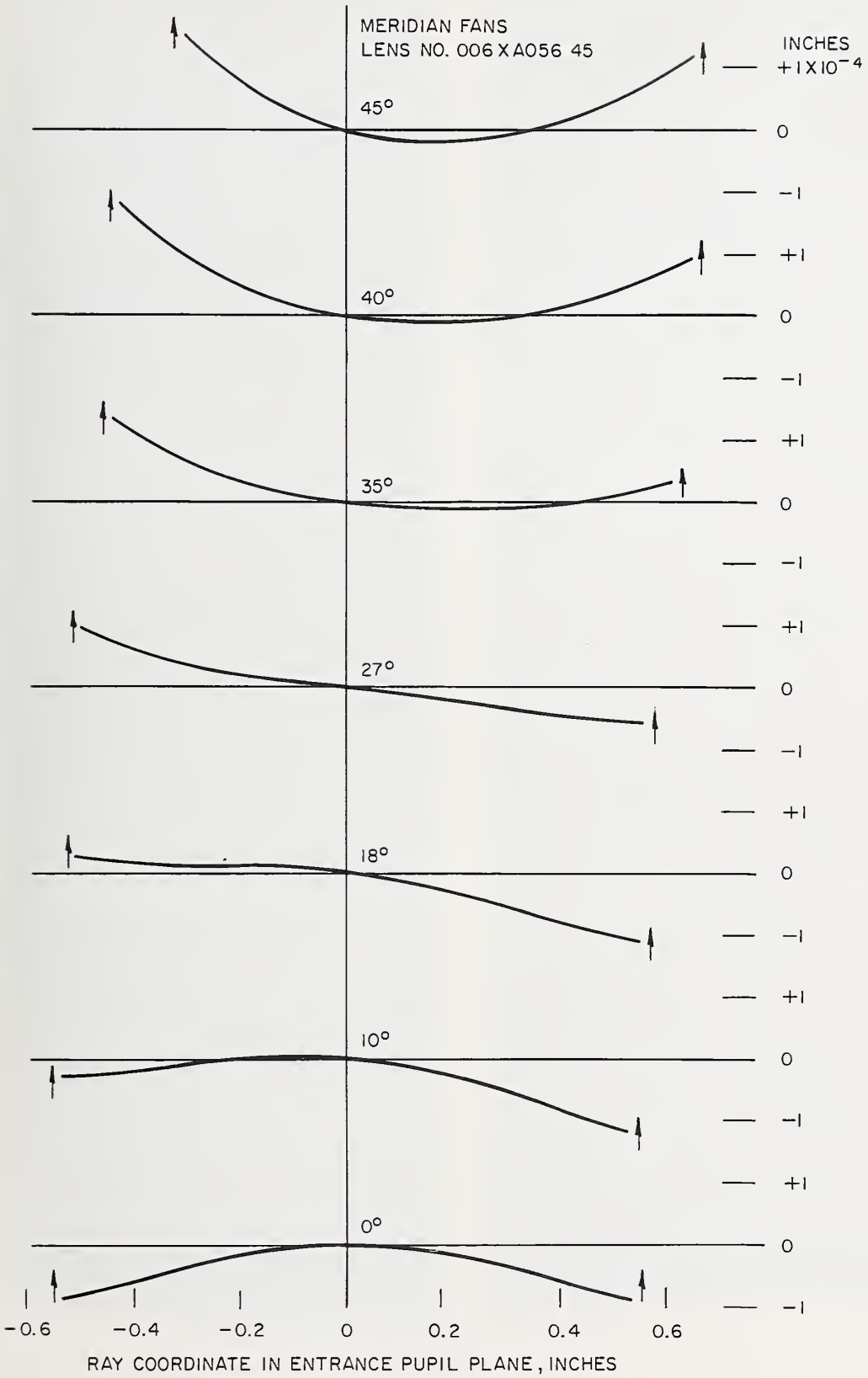

FIGURE 26f.

PL–9—6 in. *f*/6.3, 90° field

The spot diagrams indicate very little curvature of field for this lens. (See figures 27a–27d.) The imagery for the plane at −0.30 mm appears quite favorable for a lens of so few elements which covers a 90° field. It is noteworthy that the pattern of points that produces the central core of the diagram at 20° is, in a general way, retained at the higher obliquities, with a definite core still present in the spot diagram at 45°. Such cores are needed to keep the high-contrast resolution near the edge of the field up to a level comparable with that at low obliquities.

Illumination appears to be reasonably well maintained over the field, in terms of the number of rays transmitted at the various obliquities. This lens shows very good correction for distortion, which remains within 0.02 percent over the entire field.

PL–9—6 in. *f*/6.3 aerial camera lens for a 9×9 in. format

	Radius	Separation	Outside diameter	Clear aperature	Glass	Index	Abbe No.
	mm	*mm*	*mm*	*mm*			
1	30.18	13.32	58.7	58.1	620603	1.6203	60.3
2	44.69						
		.023					
3	22.59	1.42	41.0	40.06	720293	1.7200	29.3
4	18.65						
		33.32					
5	−18.65	1.42	41.0	40.06	720293	1.7200	29.3
6	−22.59						
		.019					
7	−44.69	12.53	58.0	57.40	623569	1.6227	56.9
8	−30.18						
		3.1					
9	∞	41.70		107.7	517645	1.517	64.5
10	∞			152.7			

Stop position: 16.66 mm from fourth surface.
Opening: 17.5 mm at *f*/6.3.

Distortion—PL–9

Field angle (nominal)	Tangent	Distortion	Distortion
deg		*in.*	%
10	0.17633	-4.3×10^{-3}	−0.0041
20	.36397	−11.4	−.0052
35	.70021	56.1	+.0133
40	.83910	97.7	+.0194
42.5	.91633	81.8	+.0149
45	1.00000	−4.1	−.0007

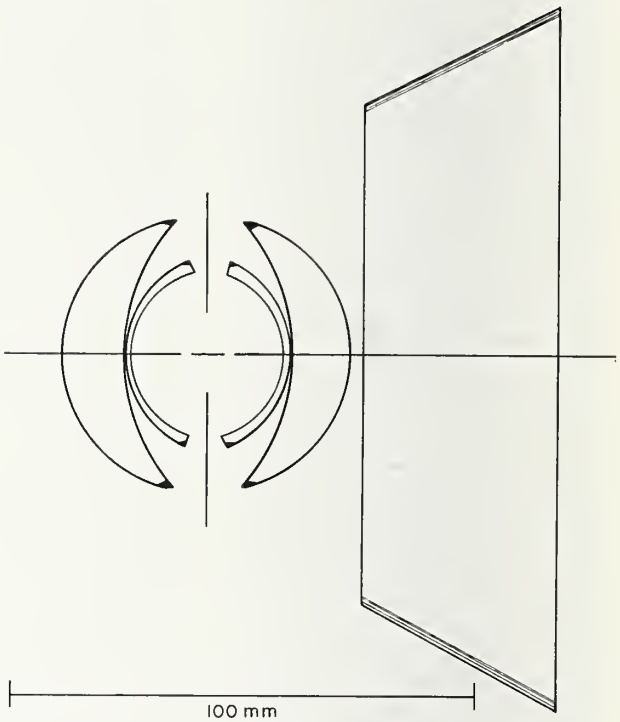

FIGURE 27a.

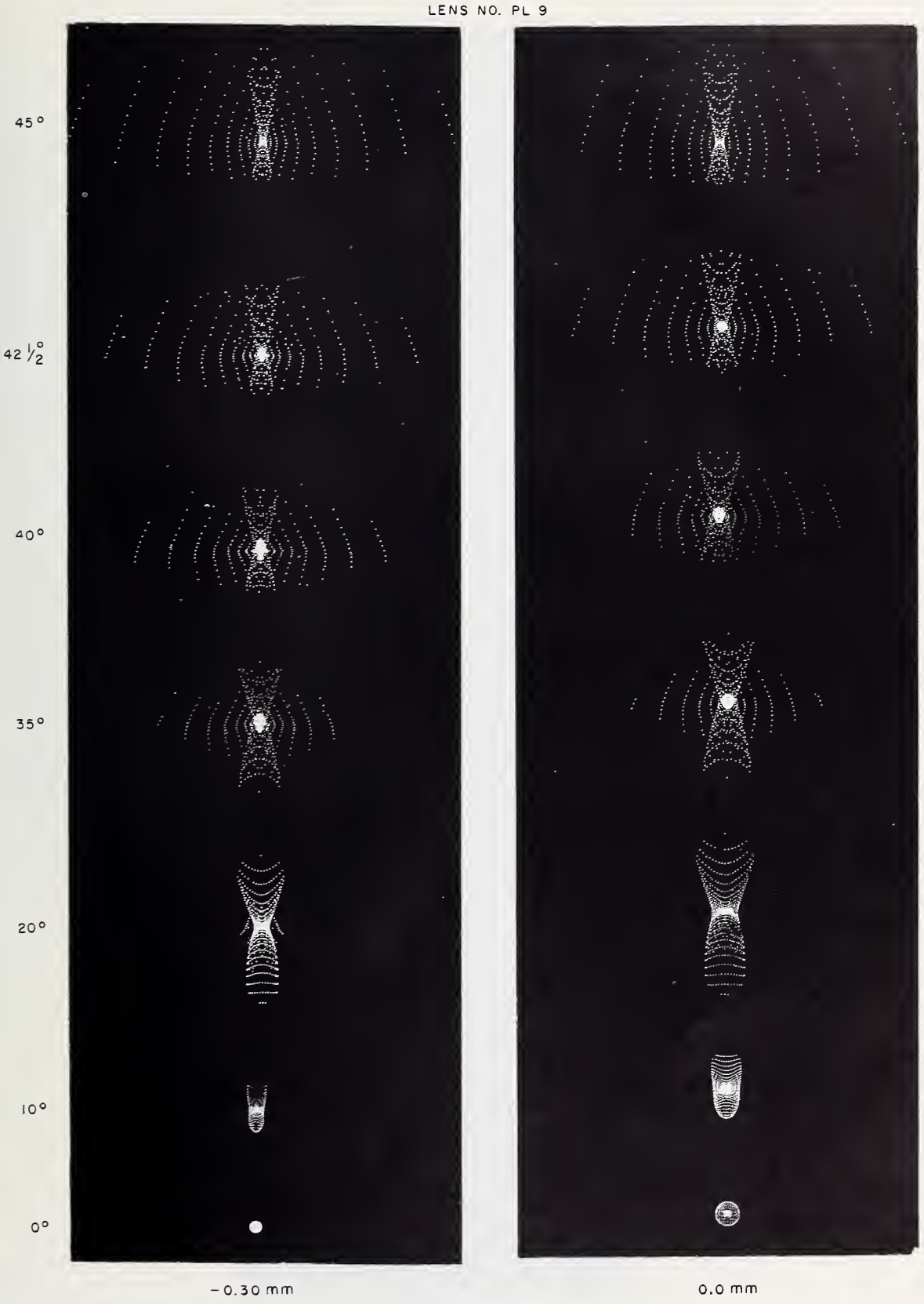

FIGURE 27b, c.

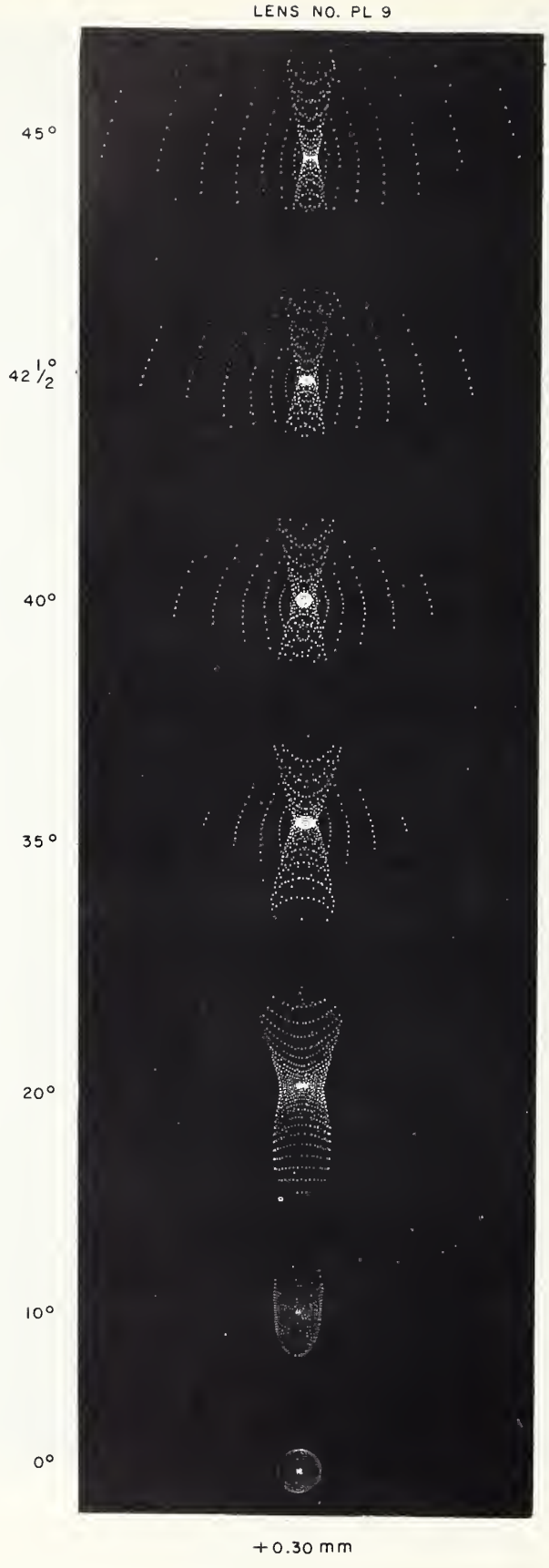

FIGURE 27d.

ME–10—6 in. *f*/6.3, 90° field

The spot diagrams of this four-element lens (see figures 28a–28d) are interesting because they illustrate some of the difficulties of obtaining good imagery over such a wide field. The central cores of these diagrams are quite small at 0 and 10° and still fairly small at 35°—the most important part of the field. Beyond 35°, however, it is clear that the density of the points begins to drop off, and the general pattern of the points at 40, 42.5, and 45° is quite different from the pattern at low obliquities. In some designs the basic pattern of the points does not undergo so much change and, perhaps because of this, there is a somewhat denser core of points in the spot diagrams at 40 to 45°.

Illumination is fairly well maintained over the field, in terms of the relative number of rays transmitted at each obliquity. Distortion reaches a maximum of about 0.1 percent at 35°.

ME–10—6 in. *f*/6.3 aerial camera lens for a 90° field

	Radii	Separations	Outside diameter	Clear aperture	Glass	Index	Abbe No.
	mm	*mm*	*mm*	*mm*			
1	25.01	9.71	47.0		DBC–3	1.611	57.2
2	35.00	1.95		46.0			
3	19.90	1.05	33.5		EDF–3	1.720	29.3
4	16.53	25.28		30.5			
5	−16.53	.99		30.5	EDF–3	1.720	29.3
6	−20.00	3.2	33.5				
7	−40.07	11.0		48.0	DBC–3	1.611	57.2
8	−27.30		50.0				

Stop position: 11.25 mm from fourth surface.
Opening: 18.0 mm at *f*/6.3.

Distortion—ME–10

Field angle (nominal)	Tangent	Distortion	Distortion
deg		*in.*	%
10	0.17633	20.8×10^{-5}	+0.0195
20	.36397	150.7	+.0684
35	.70021	425.8	+.1005
40	.83910	243.0	+.0479
42.5	.91633	−25.6	−.0046
45	1.00000	−493.2	−.0815

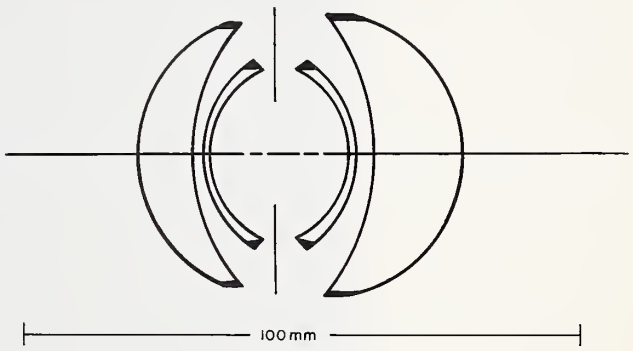

FIGURE 28a.

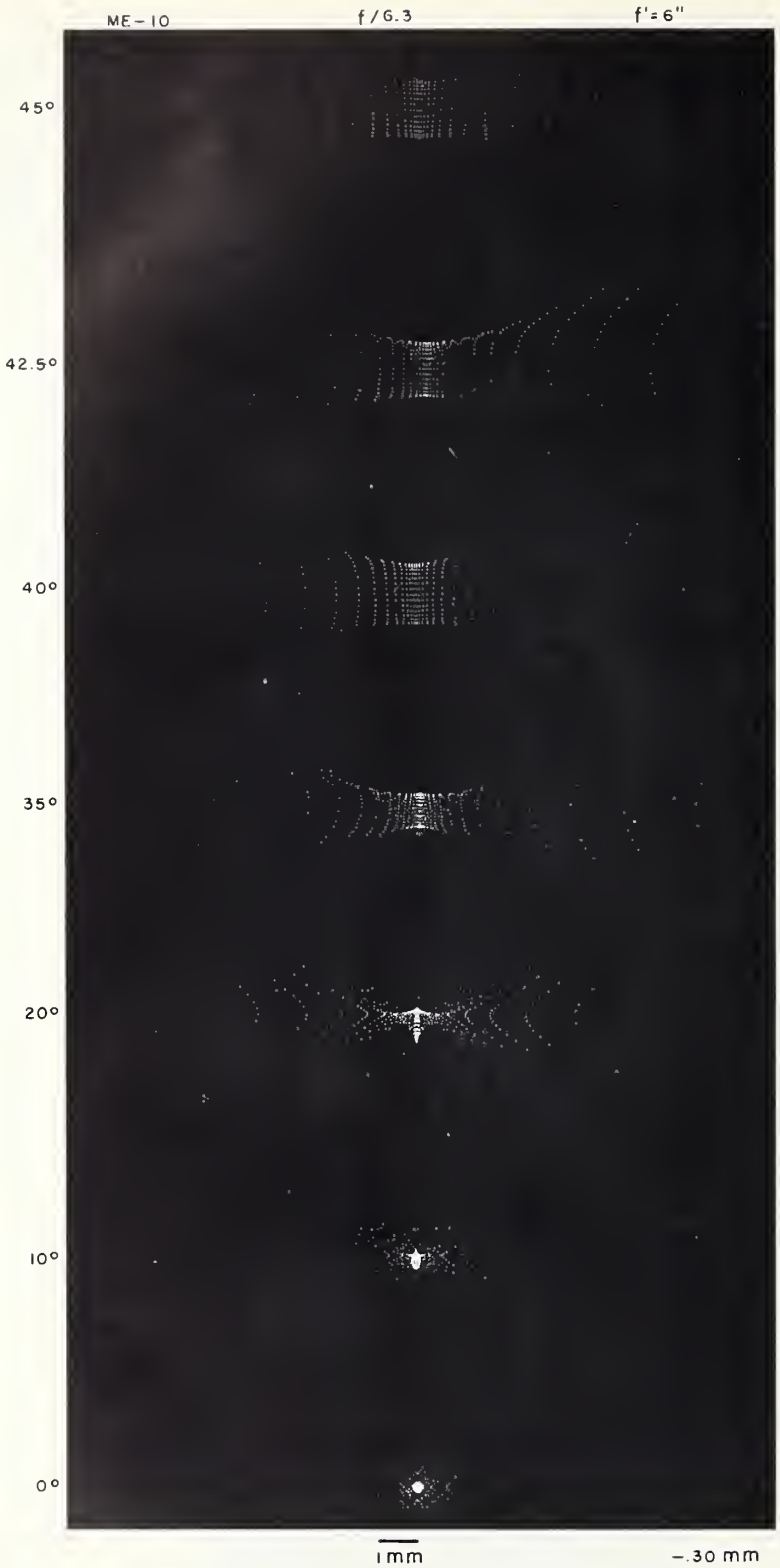

FIGURE 28b.

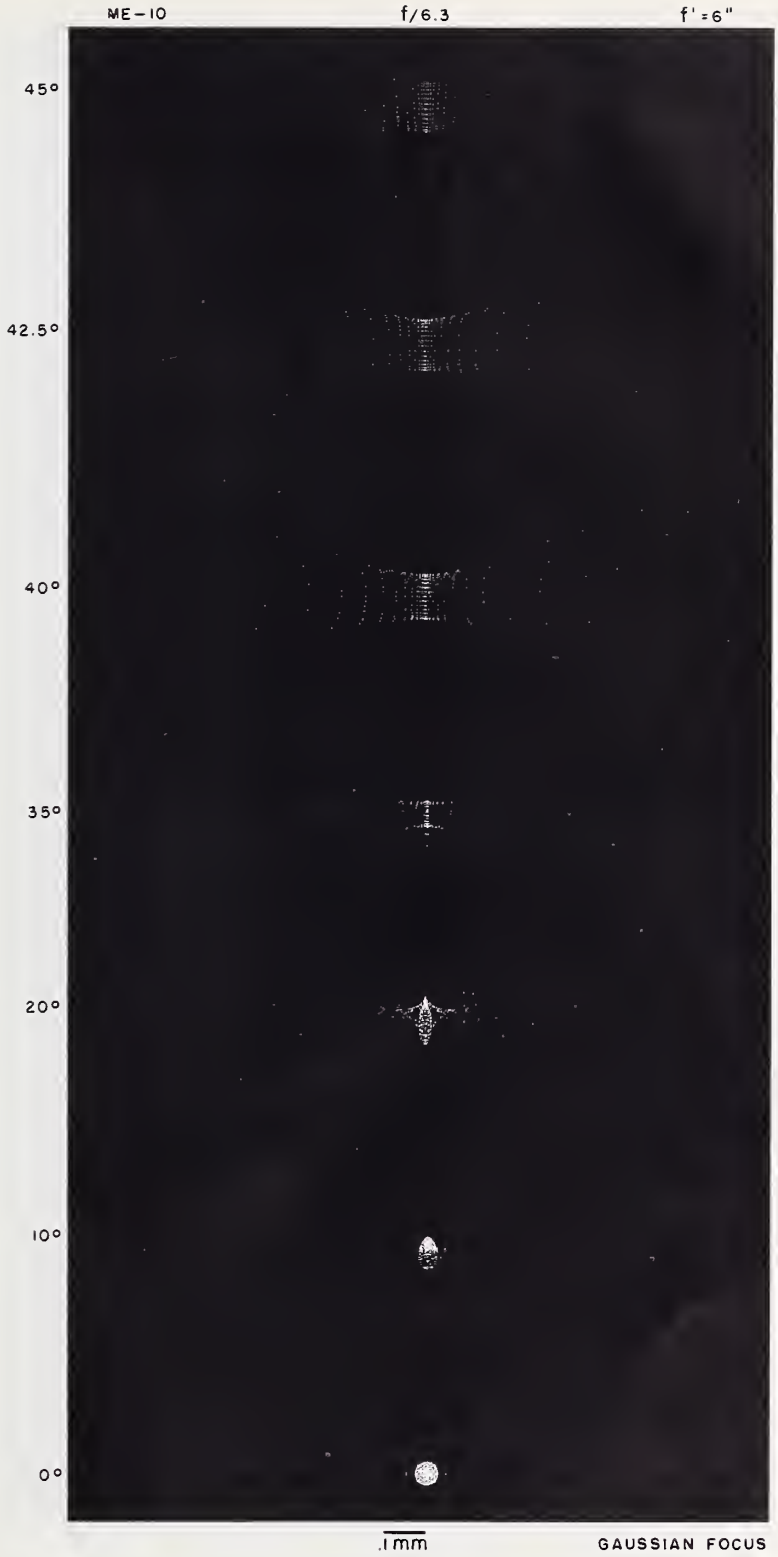

FIGURE 28c.

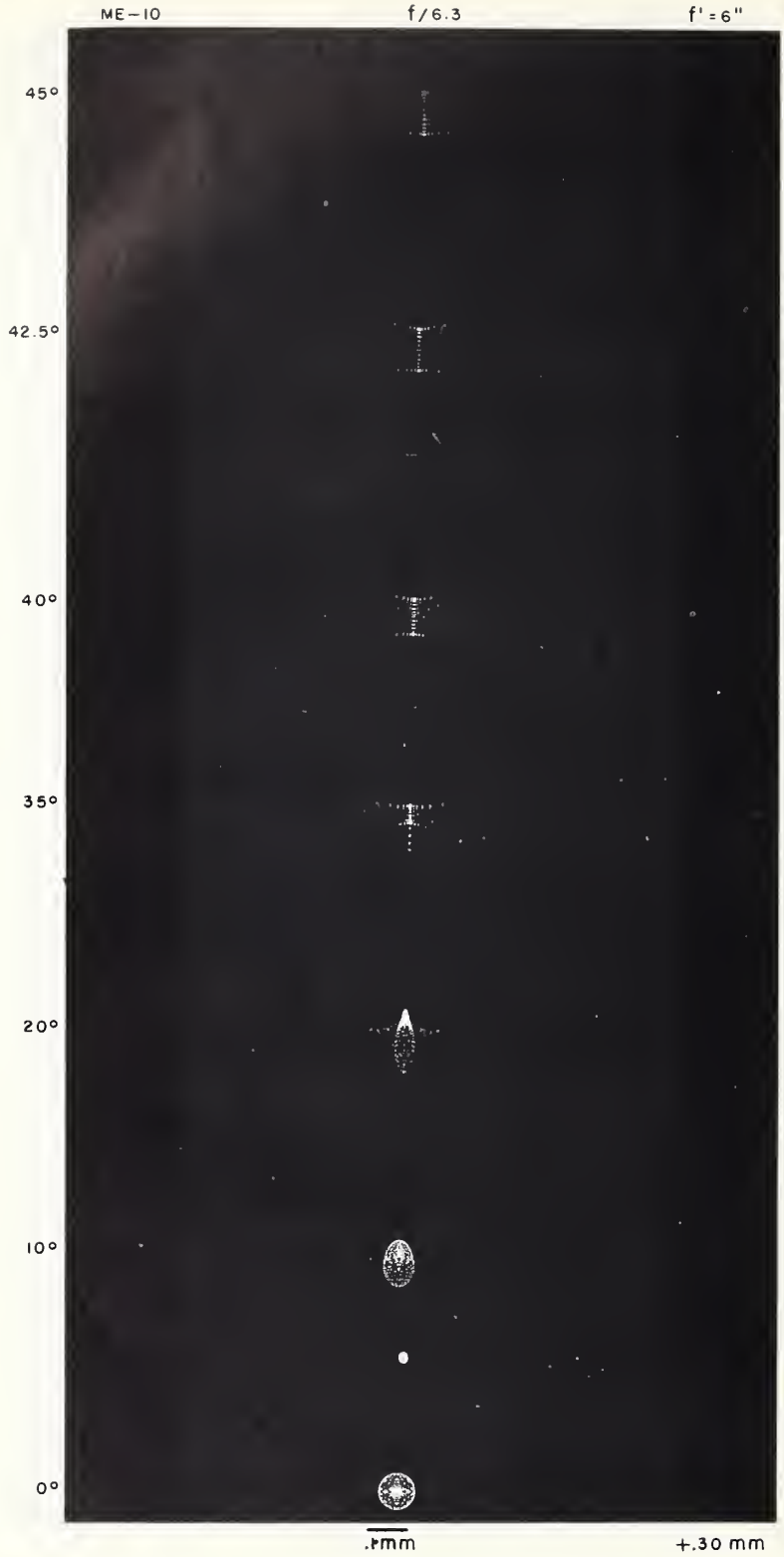

FIGURE 28d.

CO–1—12 in. *f*/4, 9×9 in. format

This lens (see figures 29a–29d) is similar to a Biotar and the general pattern of the image-points is representative of that type of lens. The spot diagrams show a large weak flare of light around each of the central cores, particularly for the 12, 20, and 25° obliquities. For these angles, 9, 25, and 20 percent, respectively, of the points computed were too widely spaced to be included in the spot diagrams, and the thinnest part of the flares had to be omitted. These flares cause a loss of contrast, especially for low-contrast objects, but this loss will not be reflected in the resolution figures since the cores are fairly small. Thus this lens furnishes an example of a case in which resolution figures are an incomplete criterion of overall quality of imagery.

Distortion is held to within 0.1 percent over the entire field. It was noted in the report on this lens that the chromatic aberration was checked and found to be within tolerance. The depth of focus appears to be fairly large.

CO–1—12 in. *f*/4 aerial camera lens for a 9×9 in. format

	Radius	Separations	Outside diameters	Clear apertures	Glass	Index	Abbe No.
	in.	*in.*	*in.*	*in.*			
1	+3.0457	0.7228	3.800	3.720	DBC–9	1.651	55.8
2	+7.0008			3.538			
		.3736					
3	+6.6272	.4819	3.550	3.300	DF–1	1.605	38.0
4	+2.1264		2.500	2.500			
		.2772					
5	+3.6732	.3252	2.800	2.500	DBC–9	1.651	55.8
6	+6.0539			2.620			
		.7228					
7	−8.5874	.2650	2.800	2.620	DBC–9	1.651	55.8
8	−4.4405			2.500			
		.3854					
9	−2.3961	.3614	2.500	2.500	DF–1	1.605	38.0
10	−10.0319		3.250	3.150			
		.3614					
11	−11.6256	.7228	3.700	3.370	DBC–9	1.651	55.8
12	−3.0457			3.580			

Stop position: 0.463 in. from sixth surface.
Opening: 2.265 in. at *f*/4.

Resolving power—CO–1

Field angle	Predicted resolving power in lines/mm†		Measured resolving power in lines/mm*	
	R	*T*	*R*	*T*
deg				
0	35	35	35.8	35.8
5			27.9	31.6
10			23.4	24.2
12	33	25		
15			15.2	22.1
20	31	23	13.2	18.8
25	25	15	14.2	15.4

†Predicted by measuring dimensions of spot diagram.
*Courtesy of the U.S. Air Force Reconnaissance Laboratory, Wright Field.

Distortion—CO–1

Field angle (nominal)	Tangent	Distortion	Distortion
deg		*in.*	%
12	0.21256	-15.7×10^{-5}	−0.0062
20	.36397	−171.1	−.0392
25	.46631	−557.9	−.0997

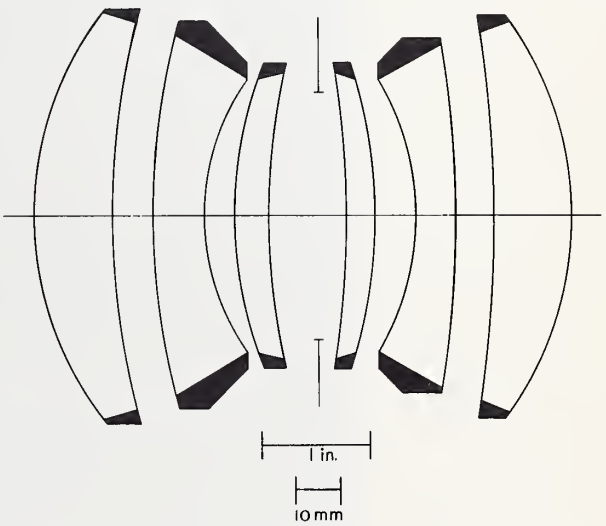

FIGURE 29a.

FIGURE 29b.

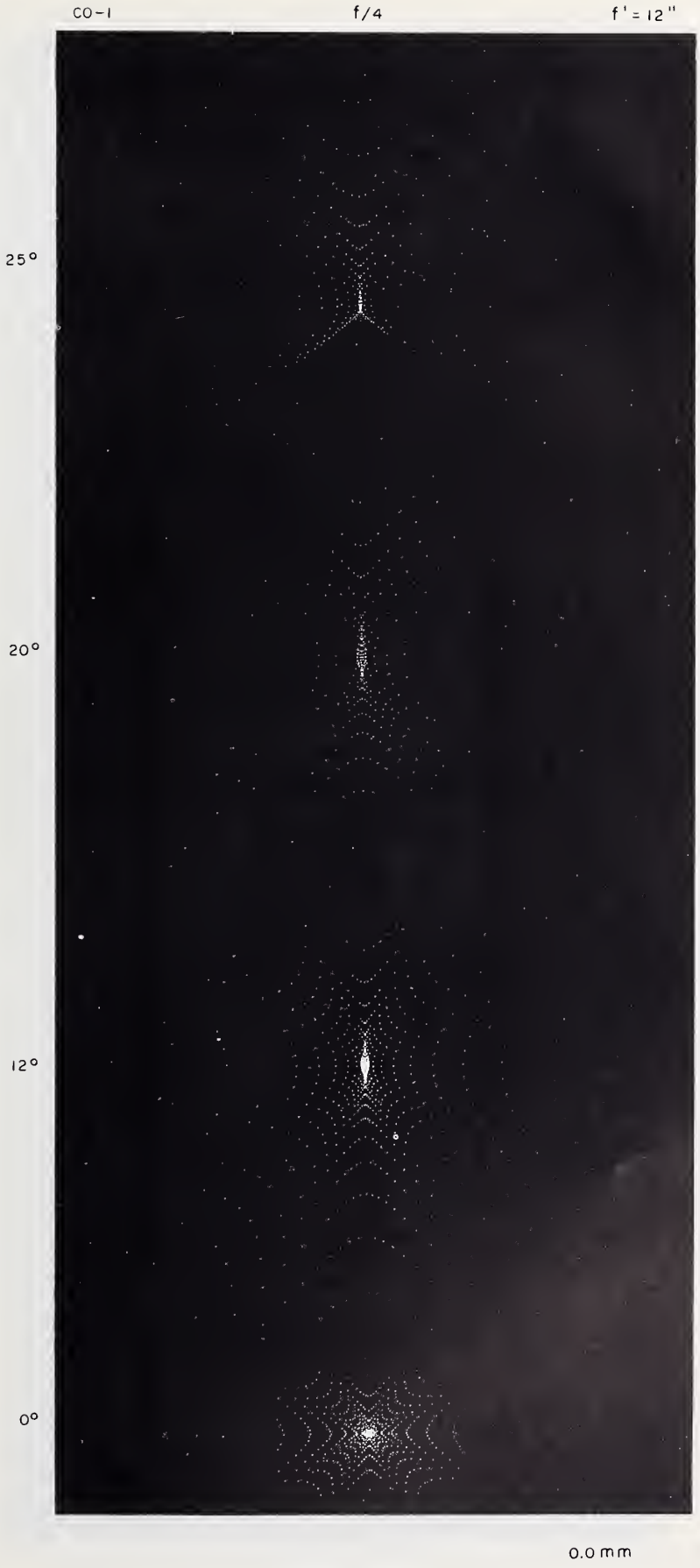

FIGURE 29c.

FIGURE 29d.

012AA045 40—12 in. *f*/4.5, 80° field

This design is unusual in that it covers a wide field and at the same time operates at a relatively low *f*-number. (See figures 30a–30g.) The position at −0.67 mm was chosen as the plane of best focus because of the dense cores produced here at both the 0 and 38° obliquities. Curvature of field will be noted from the fact that at 28° the best focus would definitely be farther from the lens. However, the general appearance of these spot diagrams is favorable because both the cores and the total areas of the image points depicted remain relatively small. The latter consideration is important for the resolution of low-contrast objects. The tables show that the number of rays transmitted drops off only slightly at the edge of the field and that distortion is held to within 0.4 percent.

The Conrady sum graphs show the presence of considerable chromatic aberration. However, most of the lateral color occurs quite near the edge of the field.

012AA045 40—12 in. *f*/4.5 aerial camera lens for an 80° field

	Radius	Separation	Clear aperture	Glass	Index	Abbe No.
	mm	*mm*	*mm*			
1	+339.01		324			
		10		BK-7	1.51625	64.0
2	+182.72		277			
		48.5				
3	+568.59		276			
		10		BK-7	1.51625	64.0
4	+214.32		247			
		141.44				
5	+183.58		168			
		12		EK-110	1.69680	56.15
6	+149.09		157			
		48.39		SF-15	1.69874	30.1
7	+123.19		124			
		42.83		EK-448	1.88040	
8	+80.36		96			
		60.6		EK-110	1.69680	56.15
9	∞		71.8			
		20				
10	∞		71.8			
		60.6		EK-110	1.69680	56.15
11	−80.36		92			
		42.83		EK-448	1.88040	
12	−123.19		116			
		12		SF-15	1.69874	30.1
13	−220.66		129			
		48.39		EK-110	1.69680	56.15
14	−183.58		158			
		97.42				
15	−180.48		206			
		10		BK-7	1.51625	64.0
16	−518.14		230			
		45.21				
17	−154.91		235			
		10		BK-7	1.51625	64.0
18	−297.35		277			

Stop position: 10 mm from ninth surface.
Opening: 70.8 mm at *f*/4.5.

Relative entrance pupil area (012AA045 40)

Field angle	No. transmitted rays	% of 0°
deg		
0	996	100.0
16	996	100.0
28	1008	101.2
34	946	95.0
38	828	83.1

Distortion and lateral color (012AA045 40)

Field angle (nominal)	Tangent	Distortion	Distortion	H_F-H_C
deg		*in.*	%	*in.*
16	0.28675	$+59.1\times10^{-5}$	0.017	-91.9×10^{-5}
28	.53171	+703.2	.111	+32.6
34	.67451	+1926.7	.240	+266.5
38	.78129	+3608.8	.388	+547.5

Predicted resolving power (012AA045 40)

Field angle	Predicted resolving power in lines/mm	
	High contrast	Low contrast
deg		
0	36	22
16	14	13
28	8	7
34	12	9
38	24	17

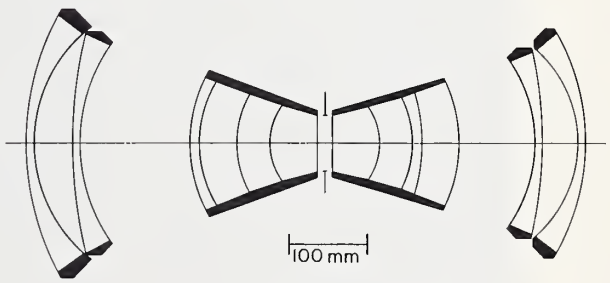

FIGURE 30a.

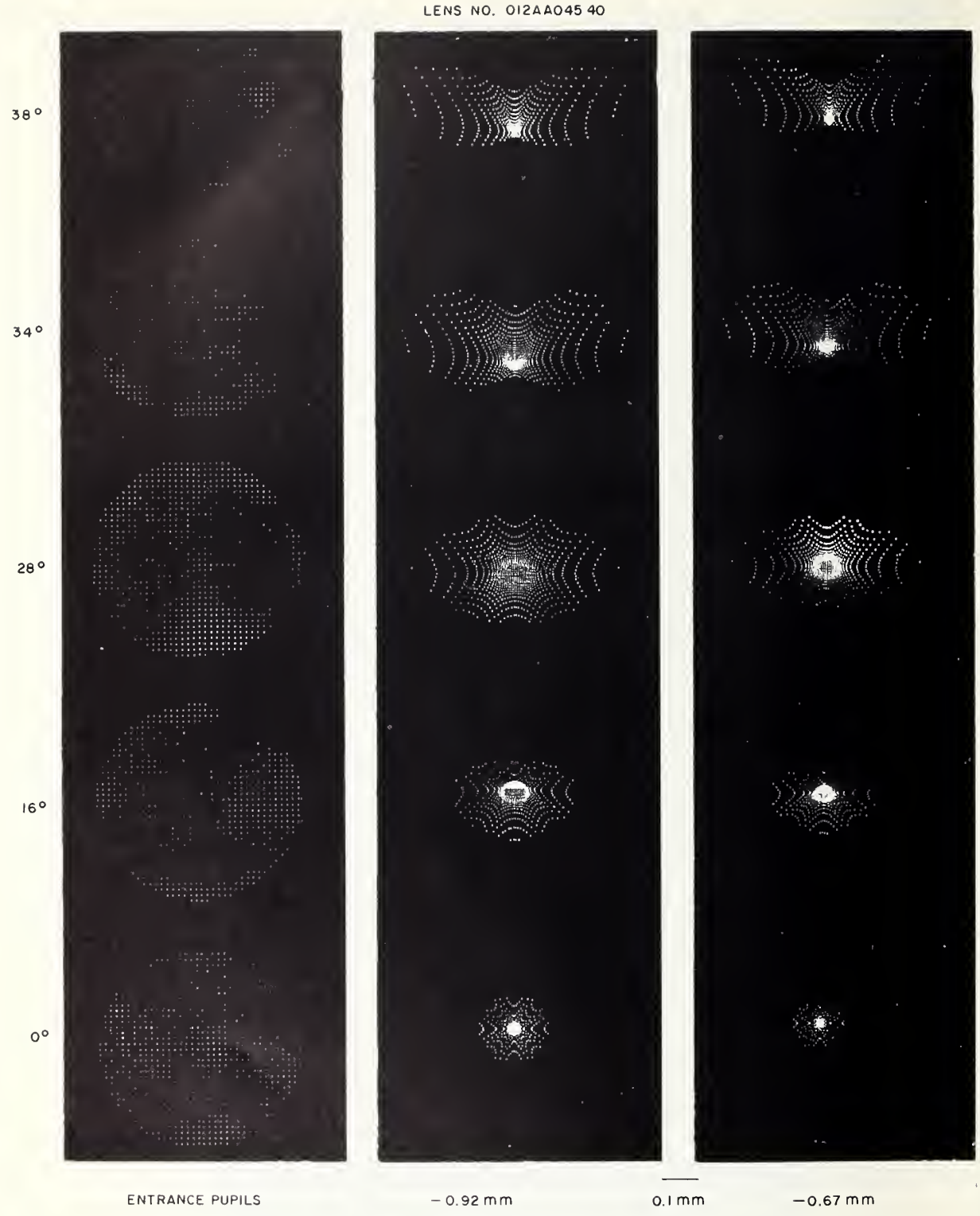

FIGURE 30b, c, d.

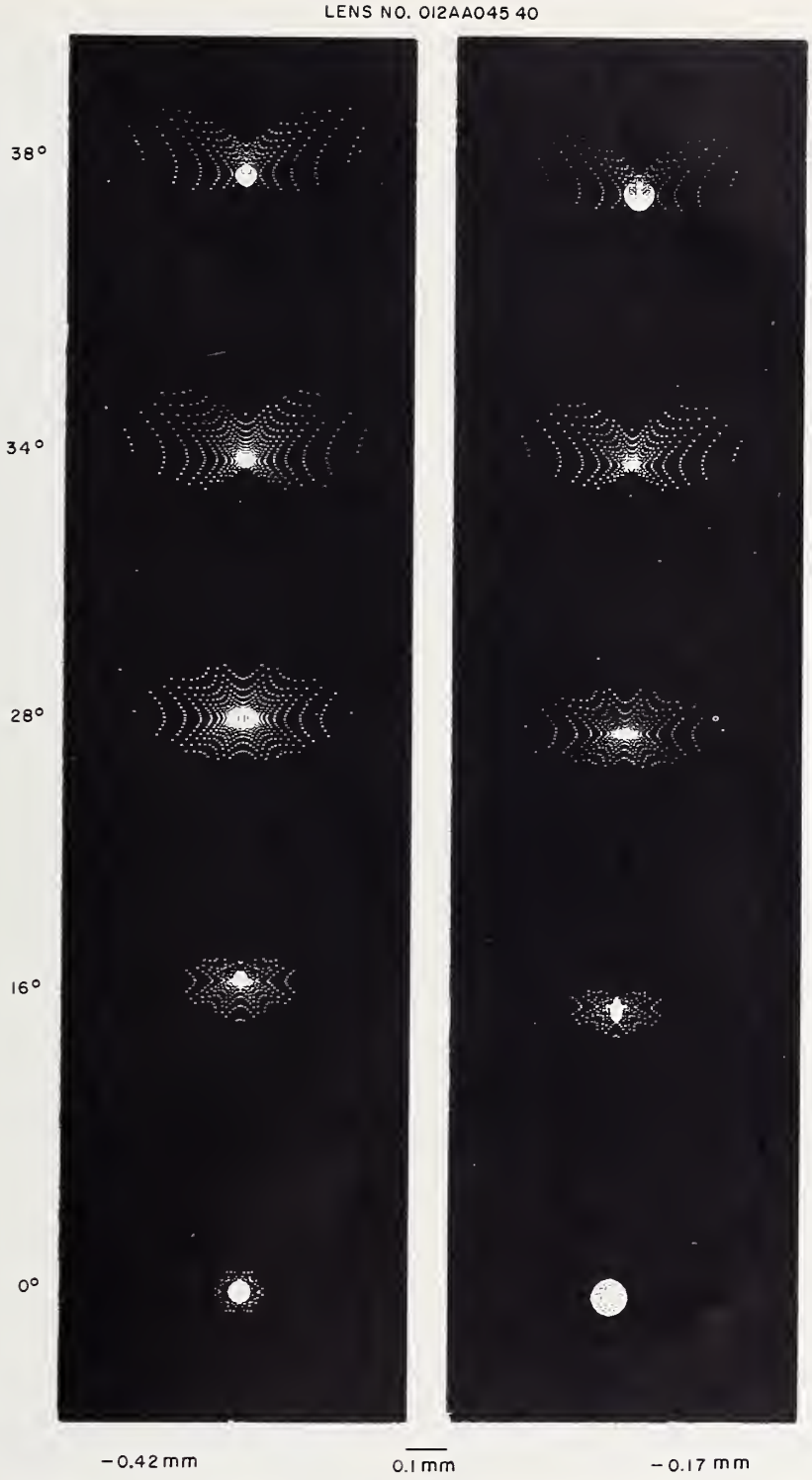

FIGURE 30e, f.

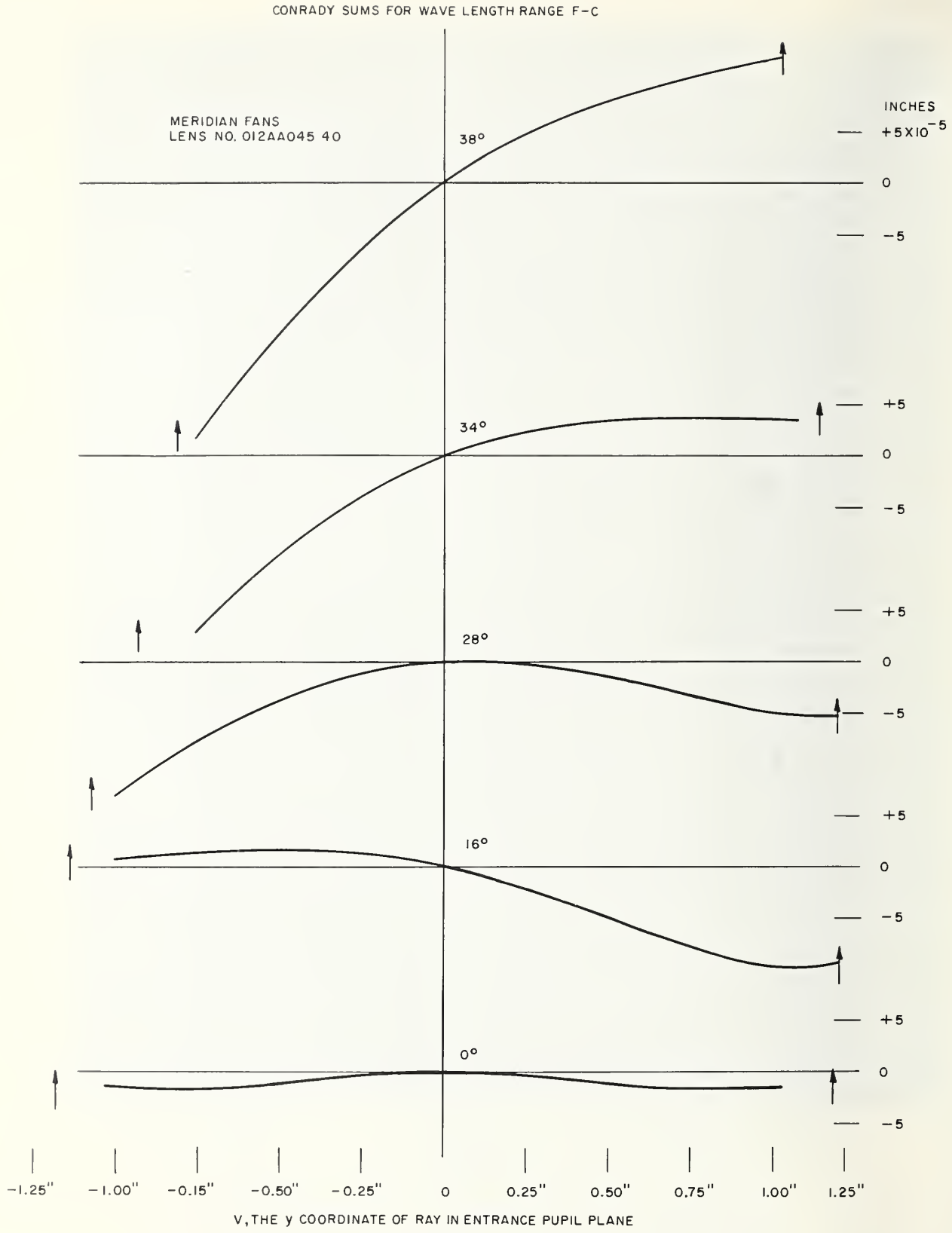
CONRADY SUMS FOR WAVE LENGTH RANGE F-C
MERIDIAN FANS
LENS NO. 012AA045 40
INCHES
+5X10⁻⁵
38°
34°
28°
16°
0°
+5
0
-5
-1.25"
-1.00"
-0.15"
-0.50"
-0.25"
0
0.25"
0.50"
0.75"
1.00"
1.25"
V, THE y COORDINATE OF RAY IN ENTRANCE PUPIL PLANE

FIGURE 30g.

024AA060 23—24 in. *f*/6, 46° field

The design drawing of this lens shows that it features great economy of means in its design. (See figures 31a–31f.) From the spot diagrams and the figures on resolving power given here, it appears that the quality of imagery depicted compares favorably at 0° with somewhat more elaborate lenses designed for similar uses. However, the off-axis image quality at the plane of best focus (−1.19 mm) falls off noticeably, particularly at 16°. The inward curvature of the field at the 10° and 16° obliquities does not indicate that a different choice of focal plane would produce a significant improvement of imagery. The 0° bundle would be upset by any sizable shift from the plane at −1.19 mm in this case.

The correction of distortion is impressive in this lens, remaining under 0.05 percent out to 20°. The Conrady sum graphs show the presence of both types of chromatic aberration, consisting, at 20°, largely of overcorrected lateral color. The positive slope of the 20° curve indicates that the blue image height is greater than that of the red.

024AA060 23—24 in. aerial camera lens for 46° field

	Radius	Separation	Glass	Index	Abbe No.
	in.	*in.*			
1	+6.028	0.8	611572	1.611	57.2
2	−69.14	.9			
3	−11.37	.23	580410	1.580	41.0
4	+5.442	1.5			
5	−21.05	.23	529516	1.529	51.6
6	+5.333	1.07	611572	1.611	57.2
7	−7.581				

Stop position: 0.836 in. from fourth surface.
Opening: 3.44 in. at *f*/6.

Relative entrance pupil area (024AA060 23)

Field angle	No. transmitted rays	Percent of 0°
deg		
0	698	100.0
10	672	96.1
16	586	84.0
20	504	72.2

Distortion and lateral color (024AA060 23)

Field angle (nominal)	Tangent	Distortion		H_F-H_C
deg		*in.*	*%*	*in.*
10	0.17633	+25.8×10⁻⁵	0.006	+31.3×10⁻⁵
16	.28675	+136.3	.020	+100.0
20	.36397	+400.1	.045	+213.6

Resolving power (024AA060 23)

Field angle	Predicted resolving power in lines/mm		Measured resolving power in lines/mm*
	High contrast	Low contrast	Lowest resolution—radial or tangential
deg			
0	41	20	28.0±2.5
5			18.5±1.3
10	14	10	17.9±1.8
15			16.4±1.3
16	7	7	
20	8	4	16.2±1.6
22.5			12.4±2.1

*Courtesy of the U.S. Air Force Reconnaissance Laboratory, Wright Field. The mean of 30 measurement's labeled "Lowest Resolution, radial or tangential."
±Probable error.

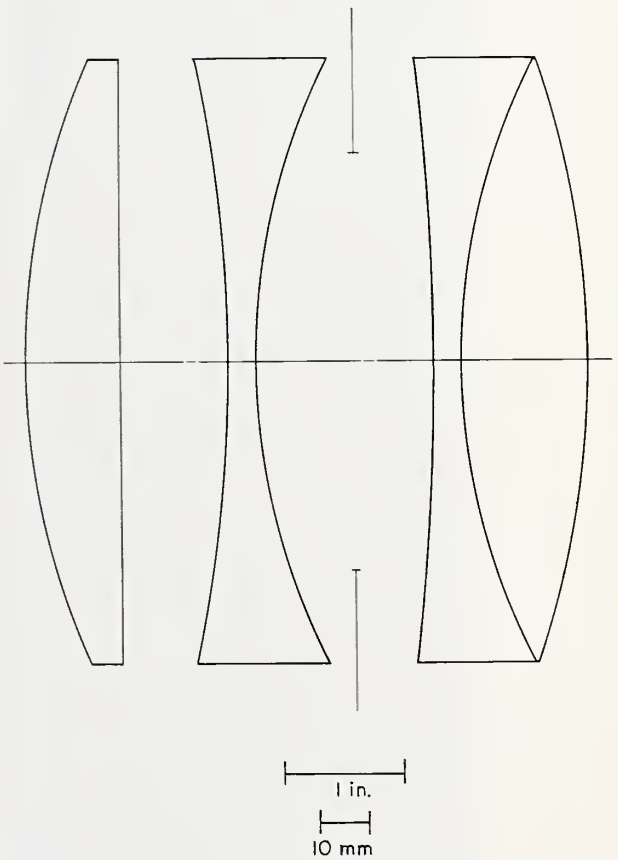

FIGURE 31a.

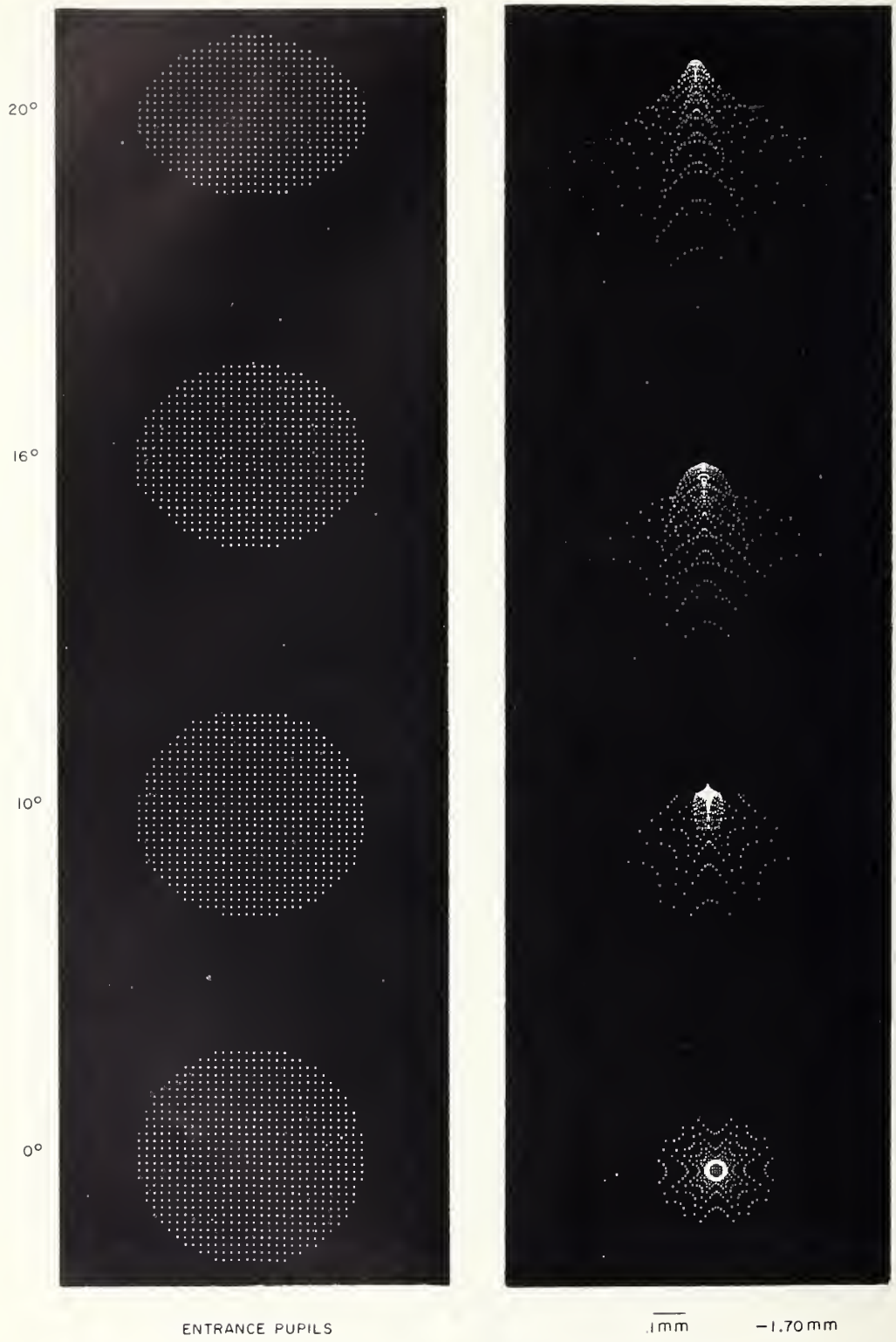

FIGURE 31b, c.

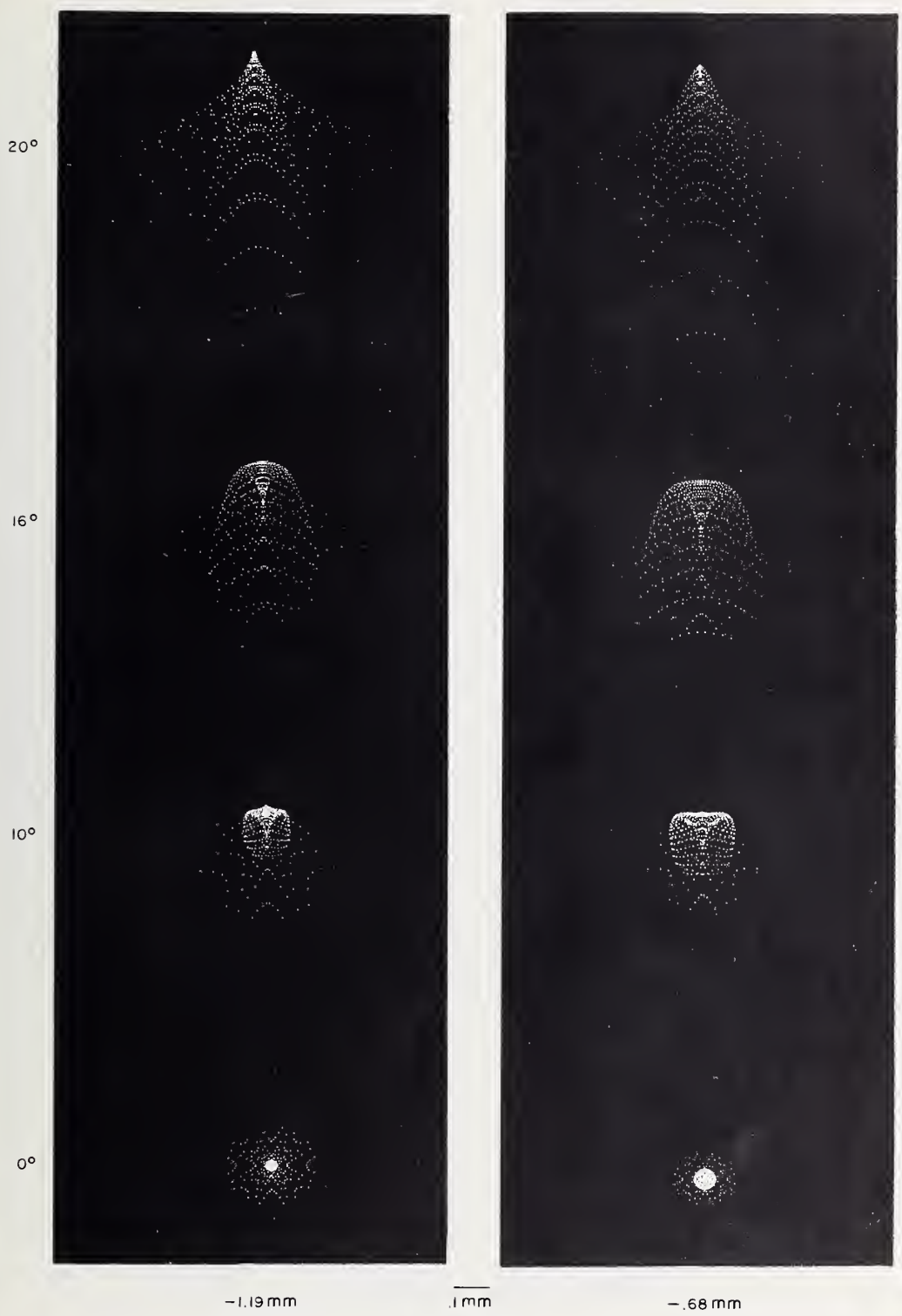

FIGURE 31d, e.

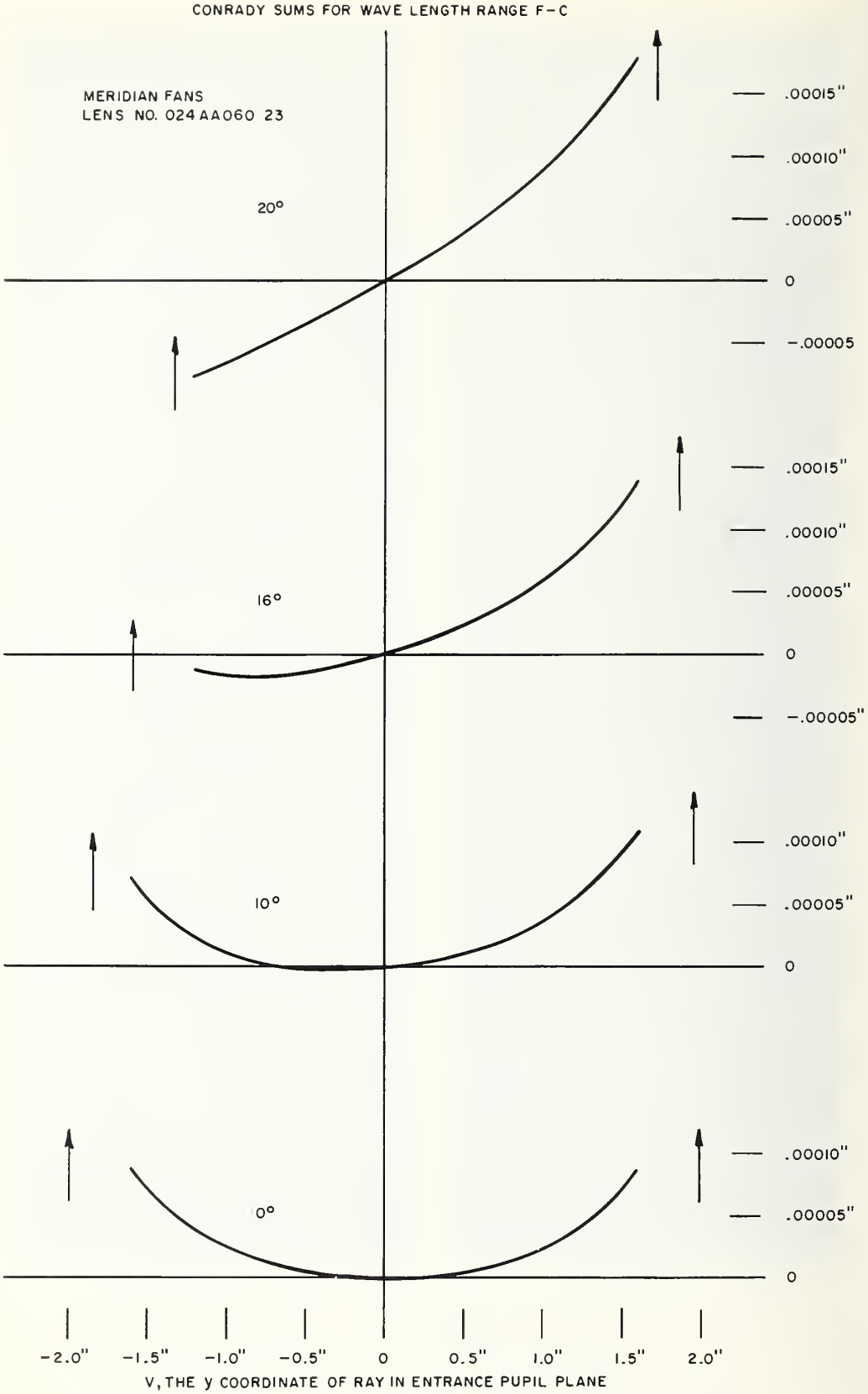
CONRADY SUMS FOR WAVE LENGTH RANGE F–C
MERIDIAN FANS
LENS NO. 024 AA060 23
20°
16°
10°
0°
.00015"
.00010"
.00005"
0
–.00005
.00015"
.00010"
.00005"
0
–.00005"
.00010"
.00005"
0
.00010"
.00005"
0
–2.0"
–1.5"
–1.0"
–0.5"
0
0.5"
1.0"
1.5"
2.0"
V, THE y COORDINATE OF RAY IN ENTRANCE PUPIL PLANE

FIGURE 31f.

024BB060 23—24 in. $f/6$, 9×18 in. format

For this lens (see figures 32a–32g), the best of the image planes shown in the spot diagrams appears to be that at −0.68 mm, and the resolving power estimates for 10, 16, and 20° are for that focal position. However, at 0°, the best plane is definitely between the two planes at −0.68 mm and −0.17 mm, and the size of the image at this obliquity is particularly dependent on the image plane position. Thus, the required adjustment was computed for each ray of the 0° spot diagram, and the resolving power estimates at 0° are given for a plane at −0.425 mm. The off-axis imagery did not appear sufficiently sensitive to small focal shifts to require such a special computation, since estimates were needed only for the geometric mean of radial and tangential resolving powers. For the off-axis obliquities, the spot diagrams indicate a small amount of astigmatism, which may be observed in the small dark lines forming the cores of the images. These lines are roughly vertical at the inward focal planes and gradually change to become horizontal with increasing back focal distance. Judging from the appearance of the spot diagrams at the −0.68 mm plane, the image quality appears reasonably good out to about 16°, and then the points begin to spread out somewhat more in the 20° diagram, although the greater symmetry which is apparent in the 20° diagram might well tend to compensate for this spreading of the points.

Illumination holds up rather well over the field in this lens. Distortion appears well corrected for ordinary applications. The Conrady sum graphs indicate an excellent correction of chromatic aberration.

024BB060 23—24 in. $f/6$ aerial camera lens for a 9×18 in. format

	Radius	Separations	Outside diameters	Clear aperture	Glass	Index	Abbe No.
	in.	*in.*	*in.*	*in.*			
1	+6.000	1.20	5.375		DBC-9	1.651	55.8
2	+32.000	.30		5.000			
3	+24.000	.80	4.875		LF-2	1.580	41.0
4	+4.283	.40	4.320	4.04			
5	+7.000	.80	4.661		DBC-2	1.617	54.9
6	+10.235	1.40	3.660	3.46			
7	−10.800	.80	3.340	3.10	DBC-2	1.617	54.9
8	−7.000	.30	3.781				
9	−4.603	.80	4.200	3.650	LF-1	1.573	42.5
10	+200.0	.20	4.681				
11	+200.0	1.25	5.219	5.018	DBC-9	1.651	55.8
12	−6.156			5.018			

Stop position 0.6 in. from sixth surface.
Opening: 3.094 in. at $f/6$.

Relative entrance pupil area (024BB060 23)

Field angle	No. transmitted rays	Percent of 0°
deg		
0	678	100.0
10	650	95.9
16	570	84.1
20	468	69.0

Distortion and lateral color (024BB060 23)

Field angle (nominal)	Tangent	Distortion	Distortion	H_F-H_C
deg		*in.*	*%*	*in.*
10	0.17633	$+164.8\times10^{-5}$	0.039	-20.1×10^{-5}
16	.28675	+722.9	.105	−15.5
20	.36397	+1498.8	.171	+1.2

Resolving power (024BB060 23)

Field angle	Predicted resolving power in lines/mm		Measured resolving power* in lines/mm		
	High contrast	Low contrast	R	T	$\sqrt{RT}$
deg					
0	44	24	36	36	36
5			36	36	36
10	24	13	25	31	28
15			22	24	23
16	20	7			
20	9	5	38	25	31
25			17	19	18

*Courtesy of the U.S. Air Force Reconnaissance Laboratory, Wright Field.

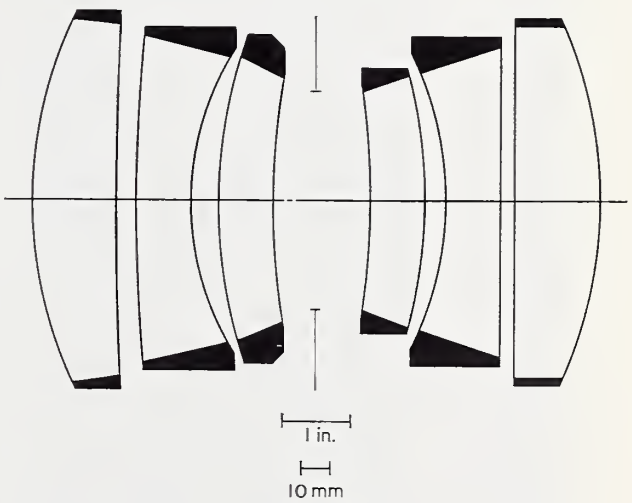

FIGURE 32a.

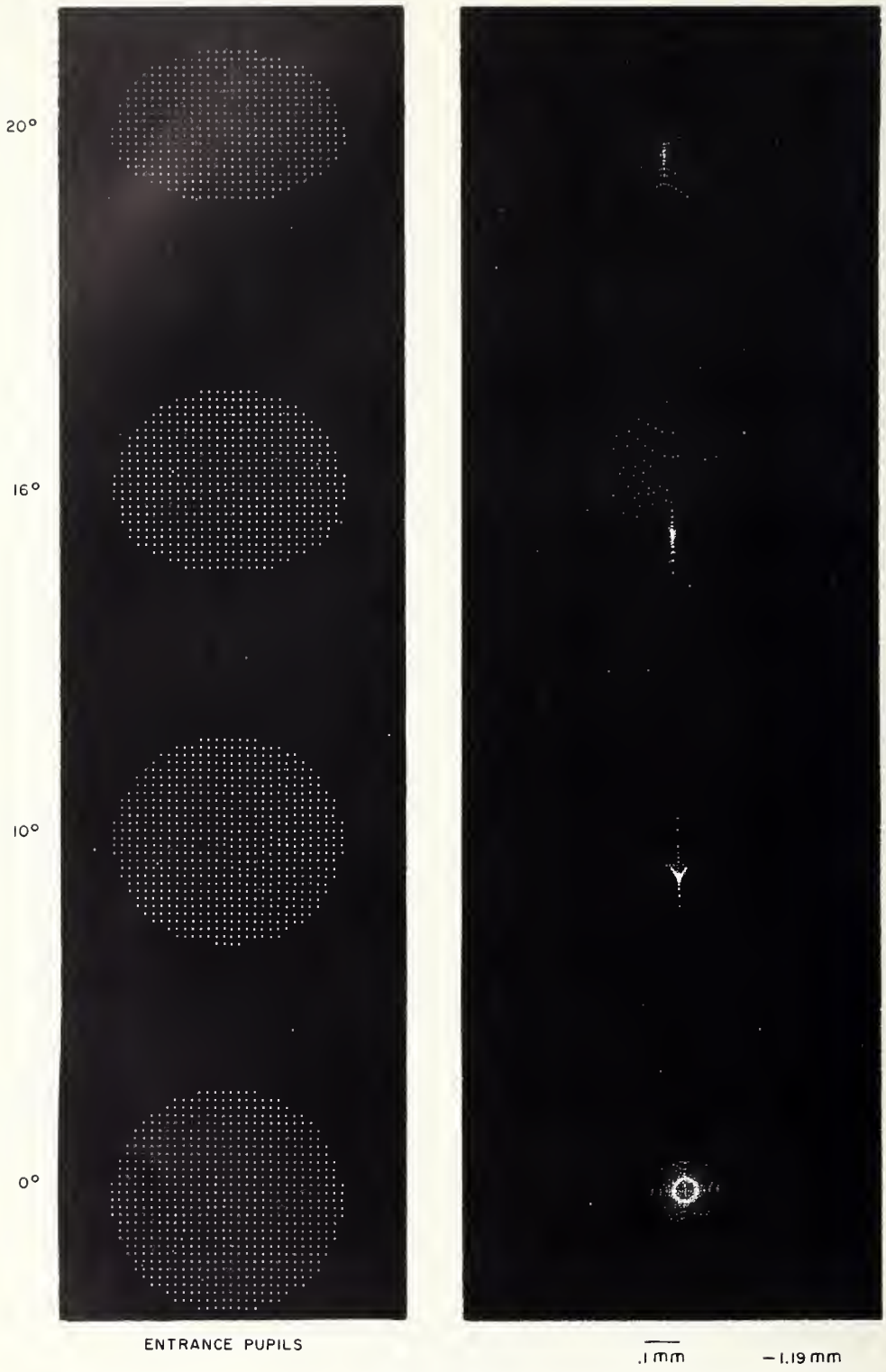

FIGURE 32b, c.

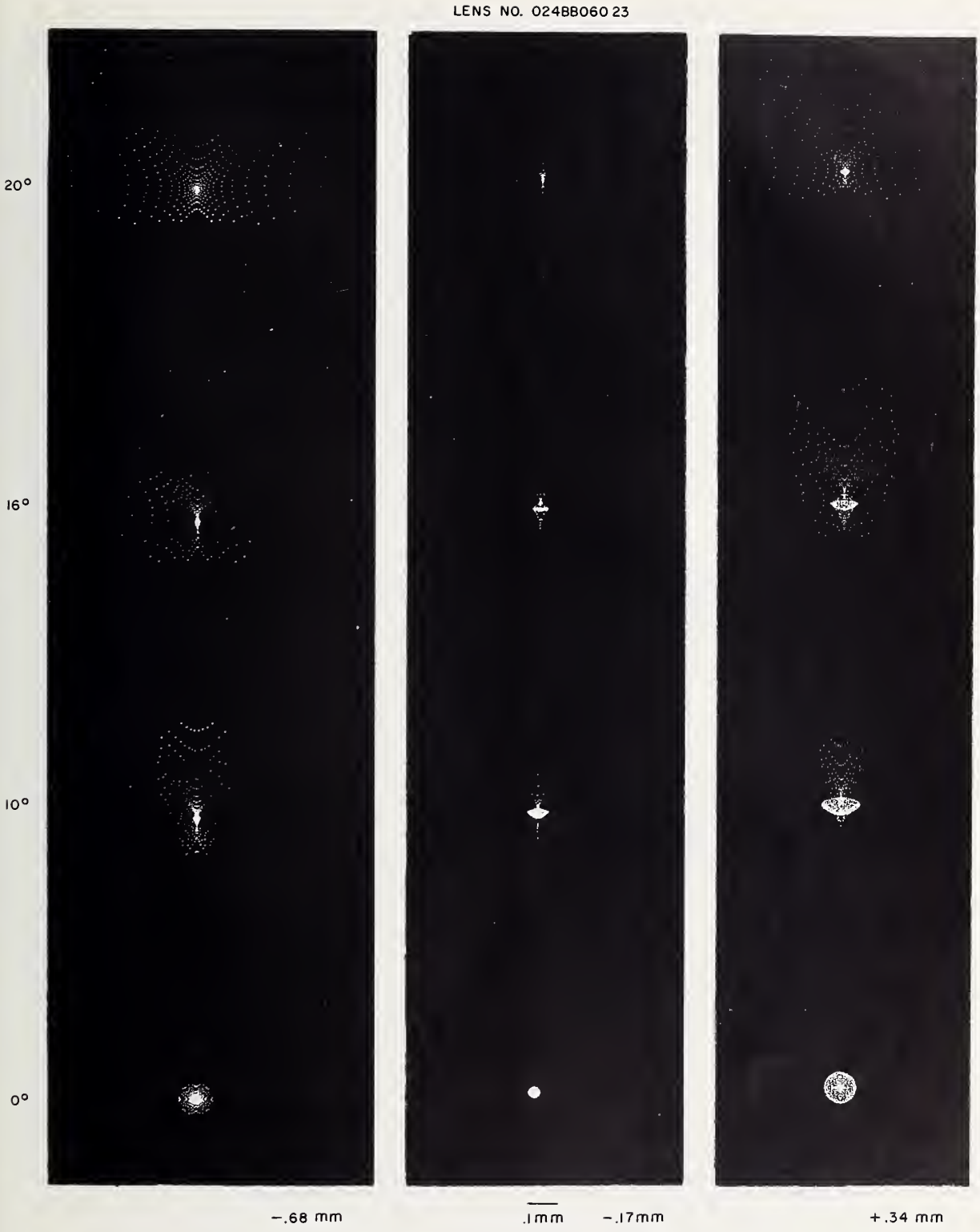

FIGURE 32d, e, f.

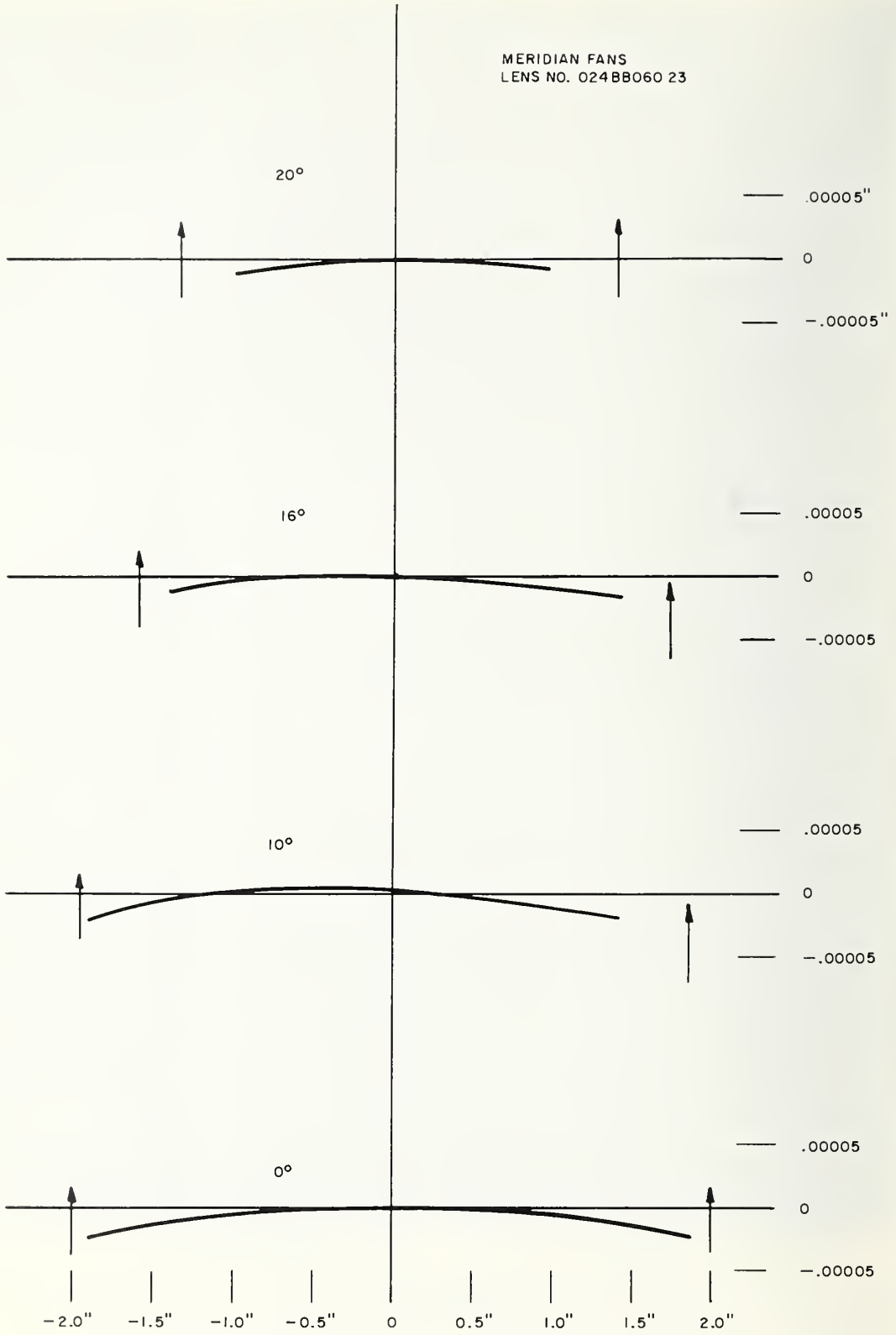
MERIDIAN FANS
LENS NO. 024BB060 23
20°
.00005"
0
−.00005"
16°
.00005
0
−.00005
10°
.00005
0
−.00005
0°
.00005
0
−.00005
−2.0"
−1.5"
−1.0"
−0.5"
0
0.5"
1.0"
1.5"
2.0"
V, THE y COORDINATE OF RAY IN ENTRANCE PUPIL PLANE

FIGURE 32g.

024CC060 23—24 in. *f*/6, 46° field

These spot diagrams indicate a slight inward curvature of field at 10 and 16°. (See figures 33a–33g.) The best focus was taken to be at −0.68 mm and the resolution estimates given here were computed at that plane. (Estimates were also made for the plane at −1.19 mm as a check, but the small increase in resolution obtained at 10 and 16° was far outweighed by a larger loss of resolution at 0°.) The imagery depicted at −0.68 mm looks particularly favorable out to about 16°. It is clear that the image quality will not be quite up to the same level closer to the edge of the field at obliquities of 20° or more.

Illumination appears a little better than average in this case, and distortion seems well corrected for ordinary applications. The longitudinal color correction is good, while the lateral color is undercorrected, as shown by the Conrady sum graphs. This indicates that the blue image height is less than that of the red at the higher obliquities.

024CC060 23—24 in. *f*/6 aerial camera lens for a 46° field

	Radius	Separation	Outside diameter	Clear aperture	Glass	Index	Abbe No.
	in.	*in.*	*in.*	*in.*			
1	+5.099			4.790			
		1.166	5.000		DBF671-520	1.66770	52.0
2	−27.173			4.390			
		.059					
3	−23.747			4.320			
		.413	4.750		BF605-434	1.60390	43.4
4	+3.818			3.570			
		.291					
5	+5.364			3.480			
		.486	3.750		DBC589-610	1.59020	61.0
6	+7.595			3.370			
		1.263					
7	−10.120			3.270			
		.923	3.750		DBC589-610	1.59020	61.0
8	−6.482			3.540			
		.400					
9	−4.608			3.660			
		.413	4.750		BF605-434	1.60390	43.4
10	+27.586			4.200			
		.077					
11	+27.586			4.260			
		1.226	5.000		DBF671-520	1.66770	52.0
12	−6.144			4.650			
		20.666					

Stop position: 0.560 in. from sixth surface.
Opening: 3.305 in. at *f*/6.

Relative entrance pupil area (024CC060 23)

Field angle	No. transmitted rays	Percent of 0°
deg		
0	698	100.0
10	654	93.7
16	594	85.1
20	522	74.8

Distortion and lateral color (024CC060 23)

Field angle (nominal)	Tangent	Distortion	Distortion	H_F-H_C
deg		*in.*	%	*in.*
10	0.17633	-172.2×10^{-5}	−0.041	-62.7×10^{-5}
16	.28675	−787.3	−.114	−107.8
20	.36397	−1708.9	−.196	−145.7

Resolving power (024CC060 23)

Field angle	Predicted resolving power in lines/mm		Measured resolving power* in lines/mm		
	High contrast	Low contrast	R	T	$\sqrt{RT}$
deg					
0	32	21	42.0	42.0	42.0
5			41.7	37.2	39.4
10	26	16	26.2	26.2	26.2
15			25.2	22.4	23.8
16	21	13			
20	15	8	18.5	18.5	18.5

*Courtesy of the U.S. Air Force Reconnaissance Laboratory, Wright Field.

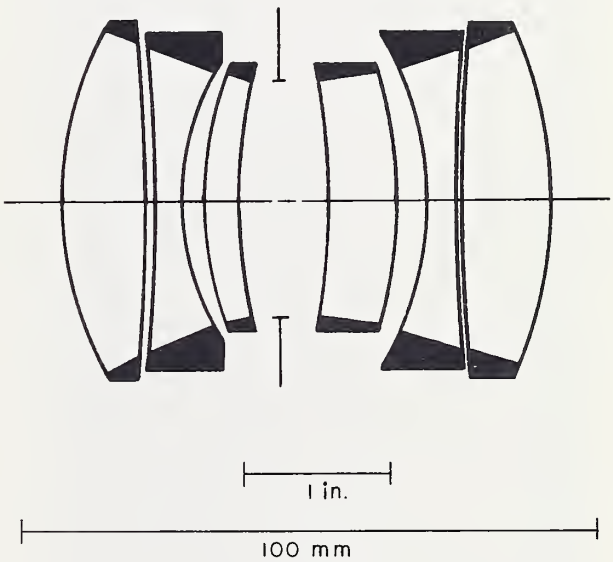

FIGURE 33a.

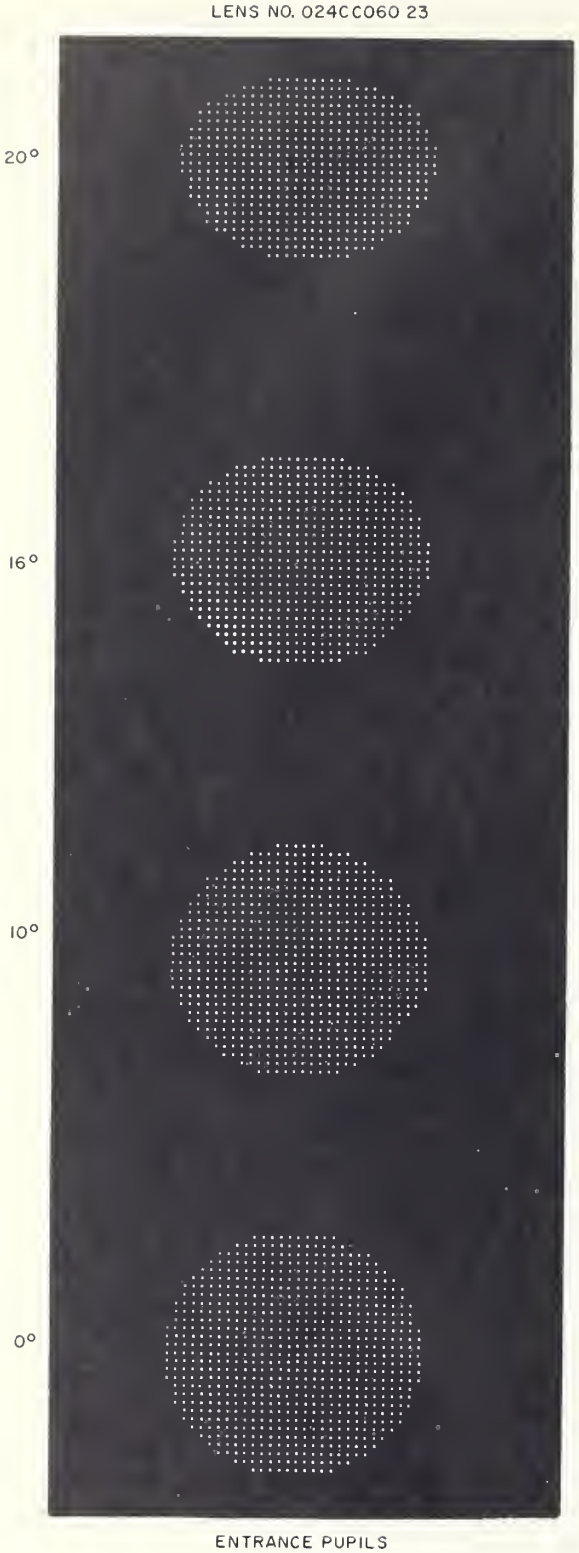

FIGURE 33b.

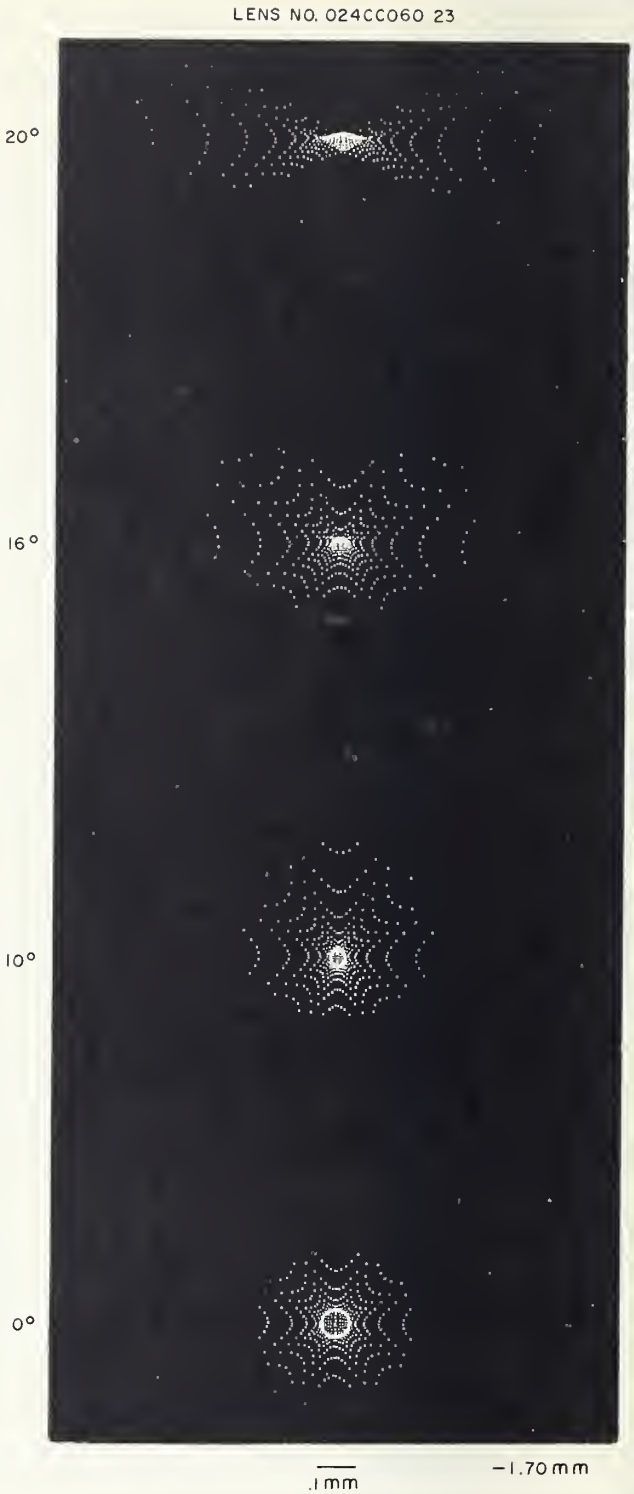

FIGURE 33c.

FIGURE 33d.

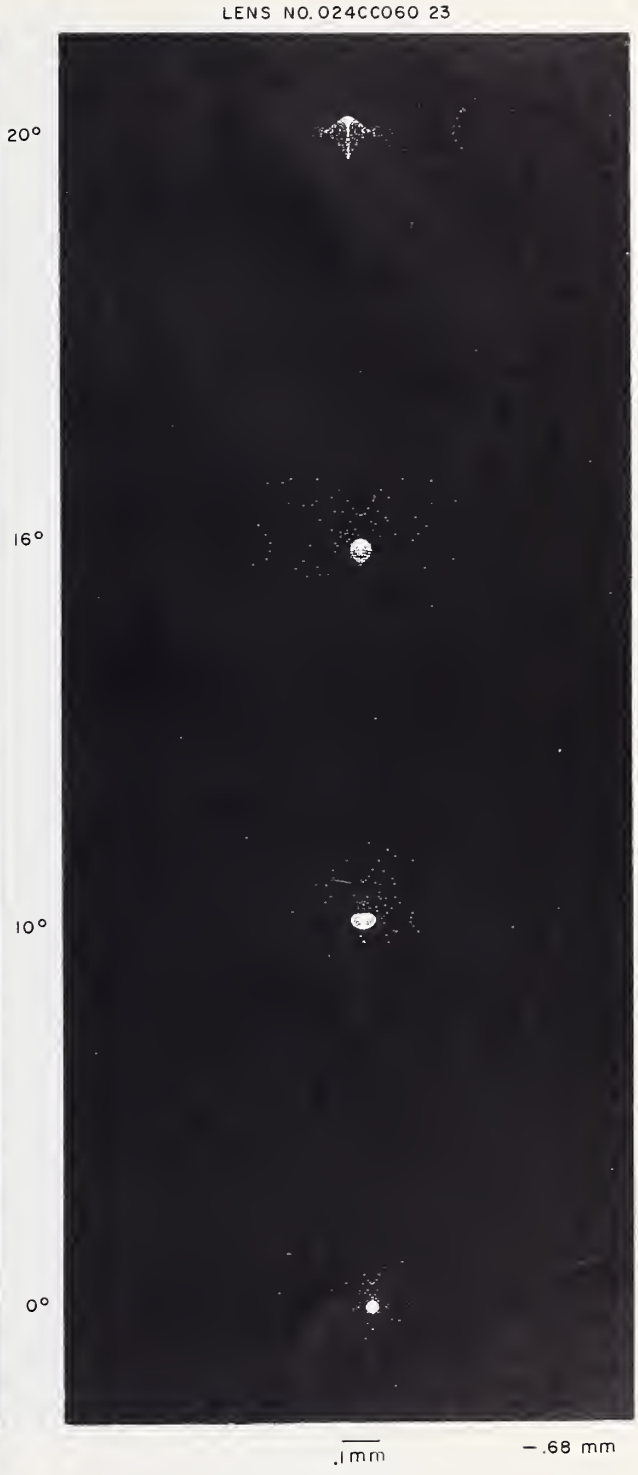

FIGURE 33e.

769-553 O—65——7

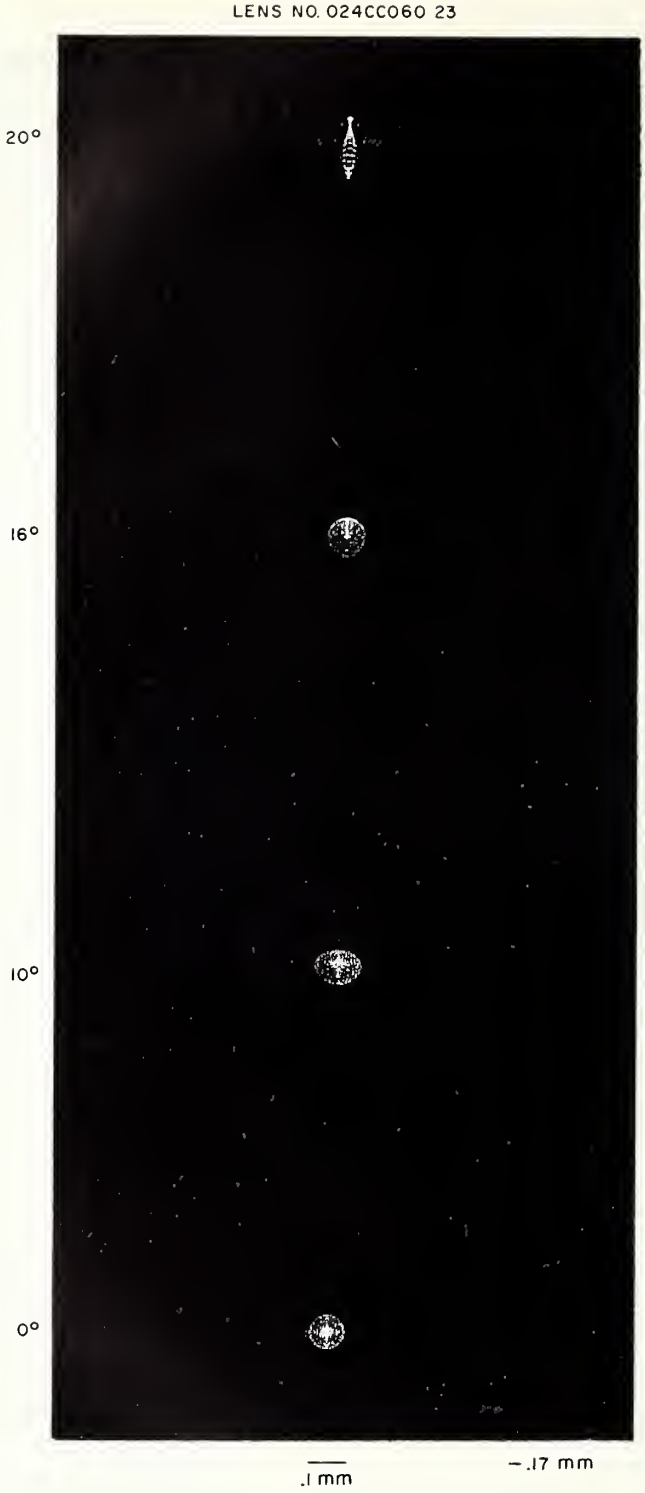

FIGURE 33f.

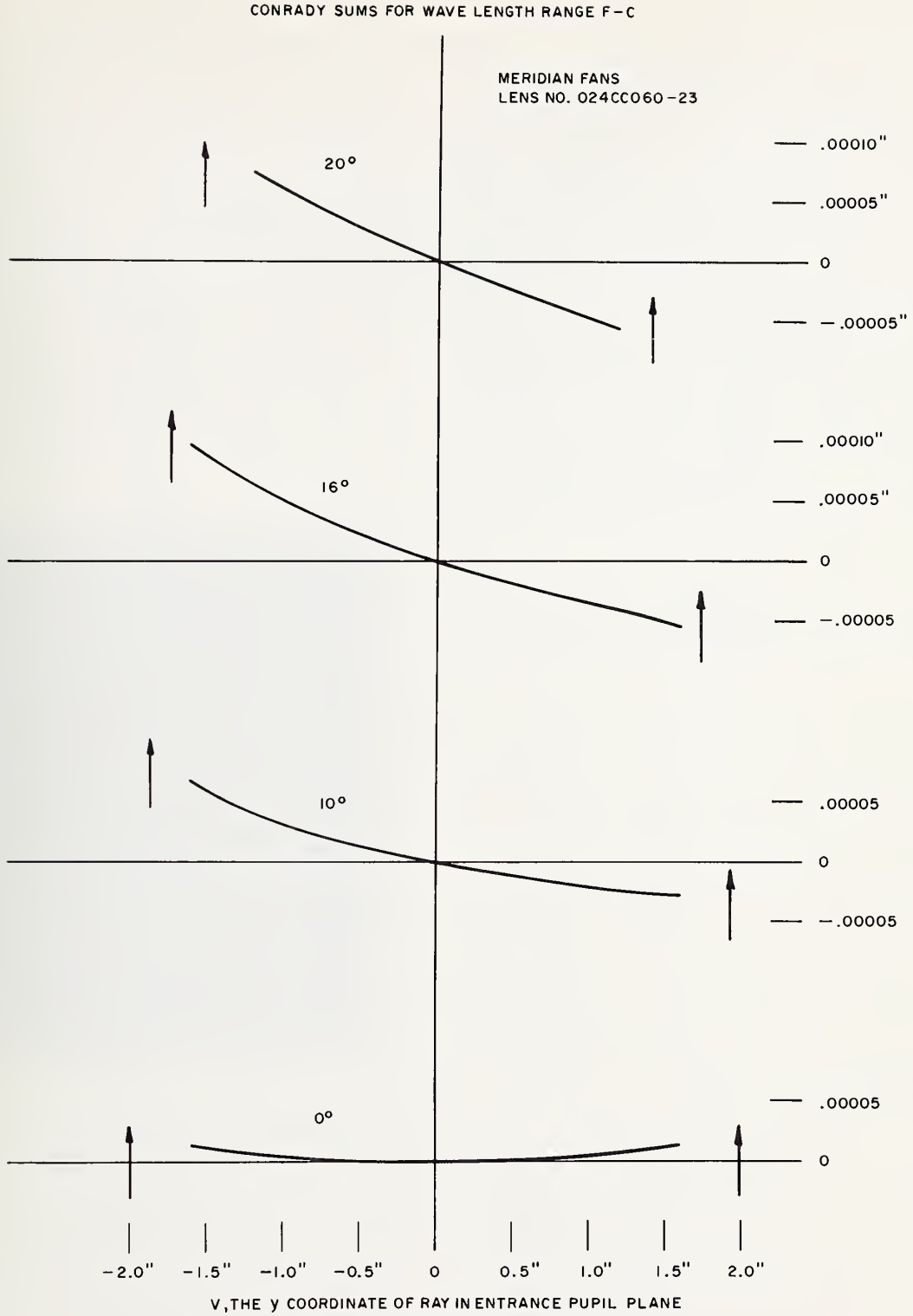
CONRADY SUMS FOR WAVE LENGTH RANGE F-C
MERIDIAN FANS
LENS NO. 024CC060-23
20°
16°
10°
0°
.00010"
.00005"
0
-.00005"
.00010"
.00005"
0
-.00005
.00005
0
-.00005
.00005
0
-2.0"
-1.5"
-1.0"
-0.5"
0
0.5"
1.0"
1.5"
2.0"
V, THE y COORDINATE OF RAY IN ENTRANCE PUPIL PLANE

FIGURE 33g.

ALPHA—36 in. *f*/3.7, 9×18 in. format

This lens is characterized by a remarkably flat field. (See figures 34a–34c.) Both the appearance of the spot diagrams and the figures on resolving power indicate that the small and solid image core observed at 0° is to a large extent retained over very nearly the entire field. The increased flare observable toward the edge of the field scarcely affects the resolution, but may be expected to reduce the performance somewhat in terms of contrast. The figures on predicted resolving power are given for the best of the three focal planes depicted here, that is, at −0.23 mm. The position of best overall focus can be estimated a little more accurately from the results depicted. Thus, the imagery may be judged to be slightly better for all angles except 15° at about −0.18 mm.

Illumination, as judged by estimates of the relative number of rays transmitted, was found to be at a satisfactory level over the entire field. Distortion rose slowly with increasing field angle to a maximum value of 0.18 percent at 15°.

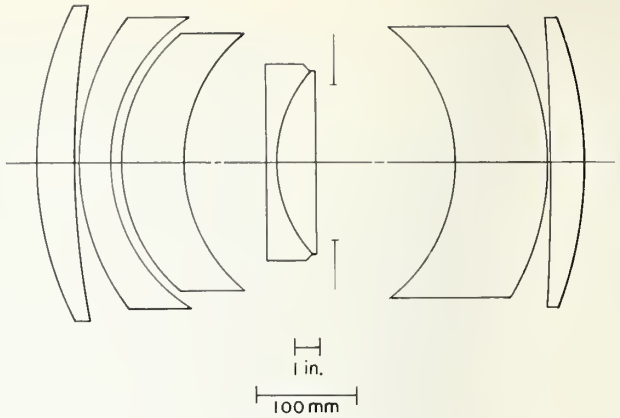

FIGURE 34a.

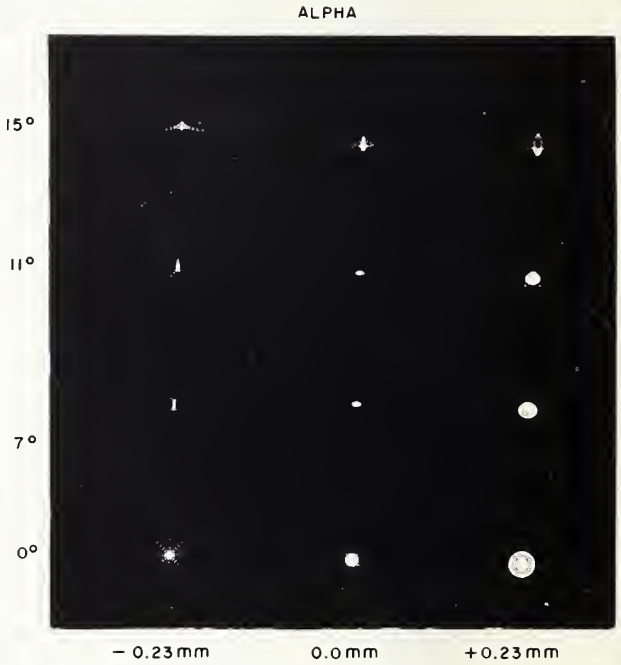

FIGURE 34b.

ALPHA −36 in. *f*/3.7 aerial camera lens for a 9×18 in. format

	Radius	Separation	Outside diameter	Glass	Index	Abbe No.
	in.	*in.*	*in.*			
1	+13.646	1.529	12.5	SK–4	1.61272	58.6
2	+32.889	.146				
3	+9.395	1.274	11.5	F–4	1.61659	36.6
4	+6.742	.437				
5	+6.609	2.507	10.125	SK–4	1.61272	58.6
6	+6.483	3.277				
7	+291.26	.437	7.75	F–4	1.61659	36.6
8	+5.354	1.529	7.25	SK–4	1.61272	58.6
9	∞	5.643				
10	−6.742	3.732	10.75	F–4	1.61659	36.6
11	−10.104	.146				
12	−91.02	1.384	11.5	SK–4	1.61272	58.6
13	−15.830	20.7				

Stop position: 0.729 in. from ninth surface.
Opening: 6.135 in. at *f*/3.7.

Resolving power—ALPHA

Field angle	Predicted resolving power*		Lowest measured resolving power**
	R	*T*	
deg			
0	34	34	30
5			30
7	41	19	
10			25
11	41	19	
12.5			25
15	41	21	20

*Predicted by measuring dimensions of spot diagrams.
**Courtesy of the U.S. Air Force Reconnaissance Laboratory, Wright Field.

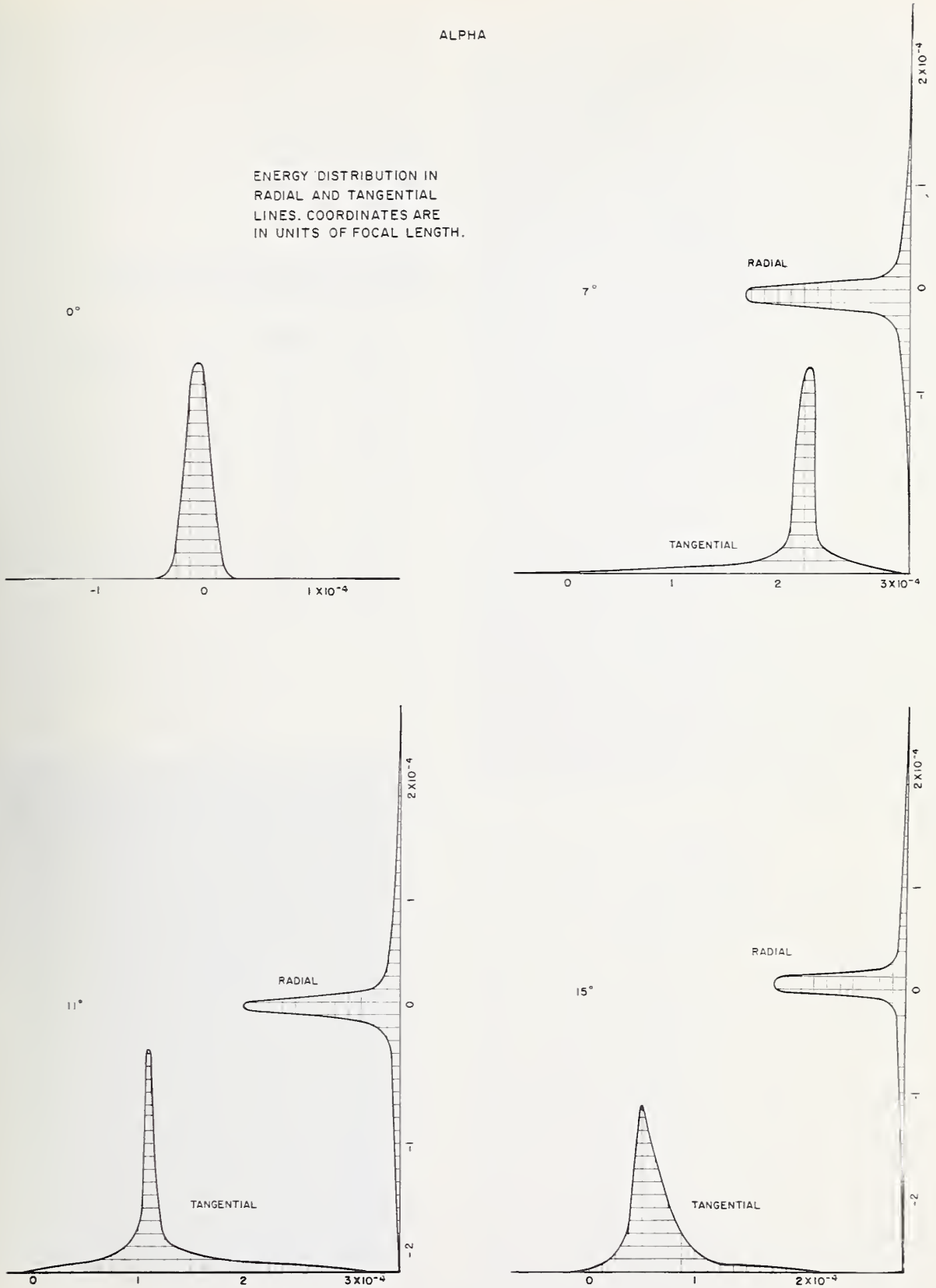

FIGURE 34c. *Alpha—Energy distribution in radial and tangential lines.*

Coordinates are in units of focal length. Curves shown are for the Gaussian focal plane.

BETA—36 in. *f*/4, 9×18 in. format

The spot diagrams for this lens (see figures 35a–35c) indicate that the image quality of the 15° bundle definitely will be less favorable than those obtained at 0, 7, and 11°. The chief reason for this effect is a pronounced curvature of field that places the best focus for only the 15° bundle on the plane located at +0.46 mm. Of the three focal planes depicted here, the one at −0.46 mm shows the best overall imagery and was used to obtain the figures on predicted resolving power. The imagery at this plane appears good at the lower obliquities, despite the loss in resolving power toward the edge of the field. By inspecting the complete set of spot diagrams, it is possible to judge, a little more accurately than it was known prior to these results, where the best focal plane is located. In this case, it appears that for a plane at about −0.37 mm the resolving power at 0° would be somewhat higher than the estimate given for the plane at −0.46 mm. At the same time, it appears that the off-axis imagery would be only slightly affected by such a shift of focal position.

Illumination appears to be adequate in this lens, as judged by estimates of the relative number of rays transmitted at the different obliquities. Distortion was negative at all field angles and rose slowly in magnitude to a value of −0.42 percent at 15°. This correction is considered good for all purposes except precision mapping. Both lateral and longitudinal color were found to be quite well corrected in this lens, which was designed for a wavelength range from 6563 to 9000 Å. However, this evaluation of the chromatic aberration is subject to a small uncertainty. The refractive index of SK–4 at 9000 Å had to be estimated, and the exact value is not known.

BETA—36 in. *f*/4 aerial camera lens for a 9×18 inch format

	Radii	Separations	Outside diameter	Clear apertures	Glass	Index*
	in.	*in.*	*in.*	*in.*		
1	20.00	1.152	9.2	9.0	SK4	1.60694
2	720.00	.036		8.87		
3	11.901	2.160	8.8	8.65	SK4	1.60694
4	−360.0	.036		8.05		
5	∞	.576	8.5	8.05	LLF-1	1.54064
6	13.433	1.969		7.45		
7	−43.552	.684	7.05	6.85	SF12	1.63728
8	11.327	2.700		6.65		
9	−11.753	.576	7.37	6.75	LLF-1	1.54064
10	36.00	.072		7.1		
11	36.00	2.160	7.7	7.1	SK-4	1.60694
12	−12.945	.540		7.5		
13	33.256	1.080	8.5	8.3	BK-7	1.51098
14	−27.744			8.3		

*N_4'.

Resolving power—BETA

Field angle	Predicted resolving power*		Measured resolving power**	
	R	*T*	*R*	*T*
deg				
0	25	25	39	35
5			29	28
7	14	10		
8			24	24
11	19	6		
11.5			21	21
13.5			25	25
15	3	11		
15.5			6	12

*Predicted by measuring dimensions of spot diagrams.
**Courtesy U.S. Air Force Reconnaissance Laboratory.

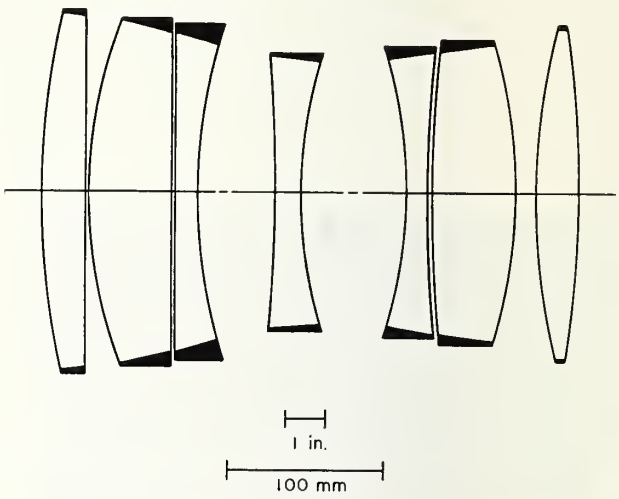

FIGURE 35a.

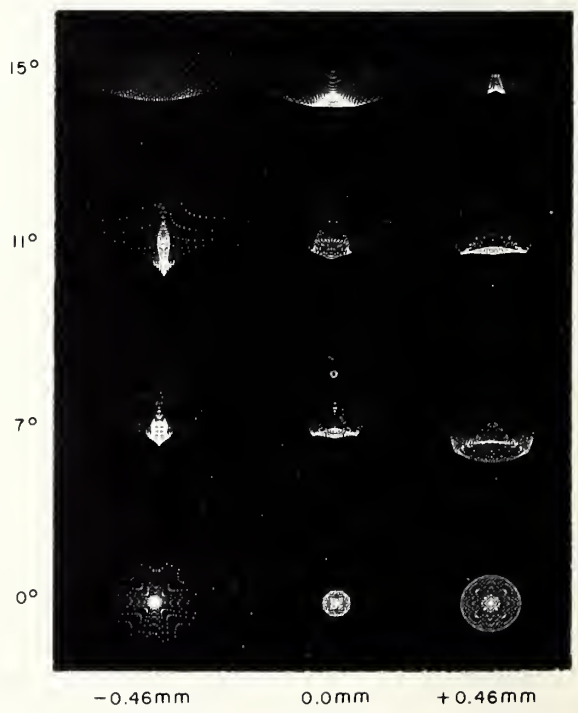

FIGURE 35b.

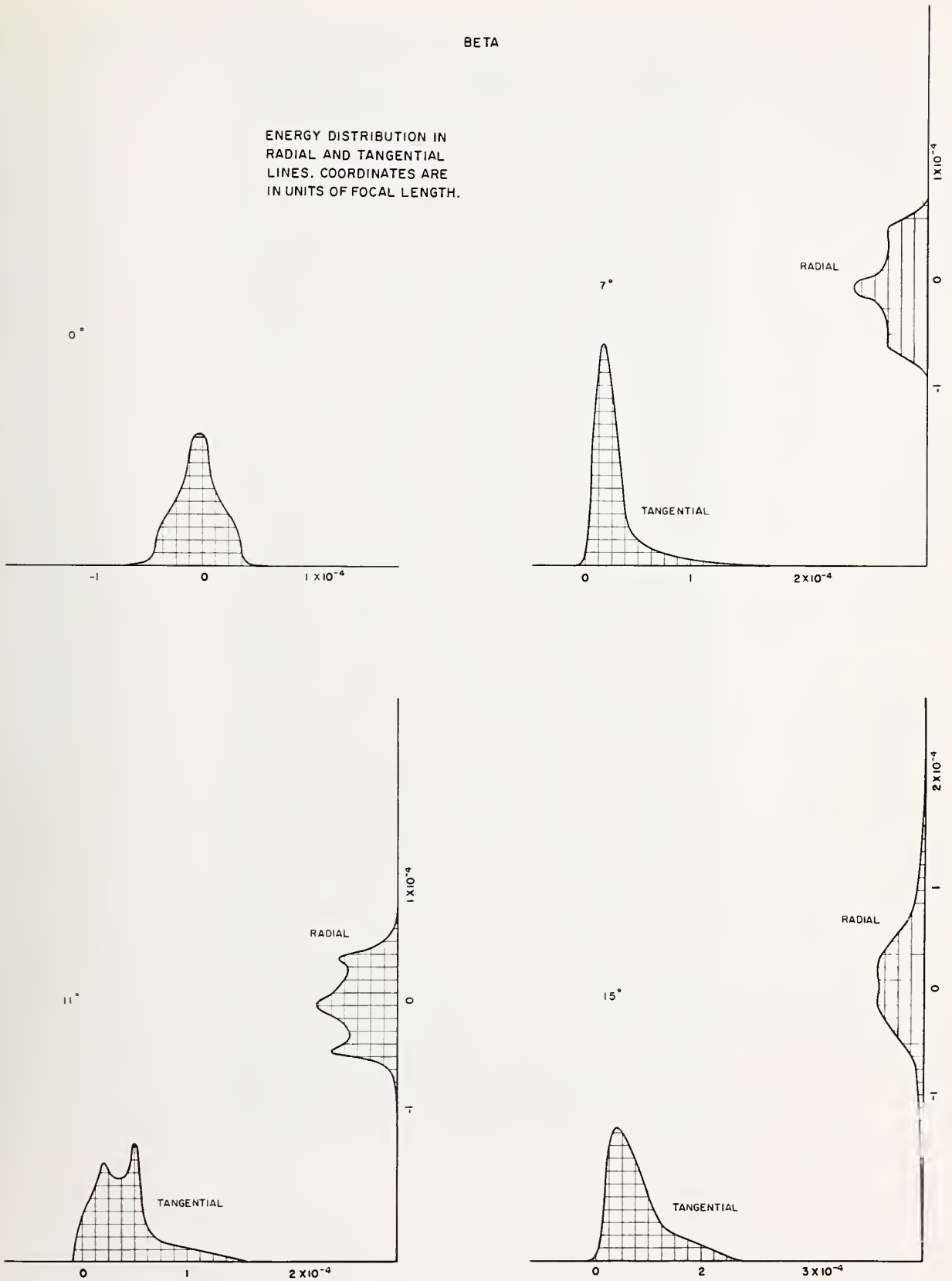

FIGURE 35c. *Beta—Energy distribution in radial and tangential lines.*
Coordinates are in units of focal length. Curves shown are for the Gaussian focal plane.

CO–3—48 in. *f*/4.5, 9×18 in. format

This lens (see figures 36a–36d) was designed to have a maximum half-field coverage of 11.9°. The analysis was extended out to 15° to include the same angles that were used in analyzing another similar 48 in. lens. For this particular lens, however, the imagery at the edge of the field will be much closer to that depicted at 11° than at 15°. At the best focal plane, near −0.55 mm, the spot diagrams show dense cores at 0 and 11° with the core tending to spread over a larger area for intermediate angles near 7°. The core at 0° appears dense because only a small percentage of the total rays traced are involved in forming the thin flare observed here.

Illumination over the field for this lens was found to be sufficient. Distortion is positive over the entire field and rises to a value of 1.75 percent at 11.9°. This lens was corrected for color over the wavelength range from 6563 to 9000 Å. The correction obtained was found to be very good, particularly with respect to lateral color. This evaluation of the chromatic correction is subject to a small uncertainty, however. The refractive index of SK–4 at 9000 Å had to be estimated, and the exact value is not known.

CO–3—48 in. *f*/4.5 I. R. night lens for a 9×18 in. format

	Radius	Separation	Outside diameter	Clear aperture	Glass	Index*	Abbe No.
	in.	*in.*	*in.*	*in.*			
1	+17.910	1.440	10.95	10.70	BK–7	1.51098	64.0
2	+842.11	—.048—		10.60			
3	+12.655	2.160	10.40	10.20	SK–4	1.60594	58.6
4	−32.086	—.048—		9.80			
5	−32.330	.672	10.00	9.80	SF–12	1.63728	33.8
6	+21.838	—2.784—		9.00			
7	+41.631	.672	7.70	7.60	LF–5	1.57260	40.8
8	+8.4498	—2.784—		7.10			
9	−16.128	.672	7.20	6.85	SF–12	1.63728	33.8
10	−51.447	—1.968—		7.00			
11	+82.759	1.440	8.60	8.00	SF–12	1.63728	33.8
12	−20.961	—31.10—		8.40			

Stop position: 5.6 mm (0.220 in.) behind seventh surface.
Opening: 187.2 mm (7.370 in.) at *f*/4.5.

*Index=N_A'.

Resolving power—CO–3

Field angle	Predicted resolving power in lines/mm	
	R	*T*
deg		
0	18	18
7	10	10
11	18	16
15	6	4

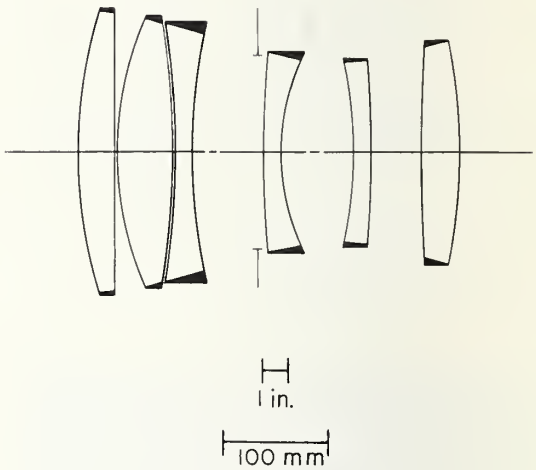

FIGURE 36a.

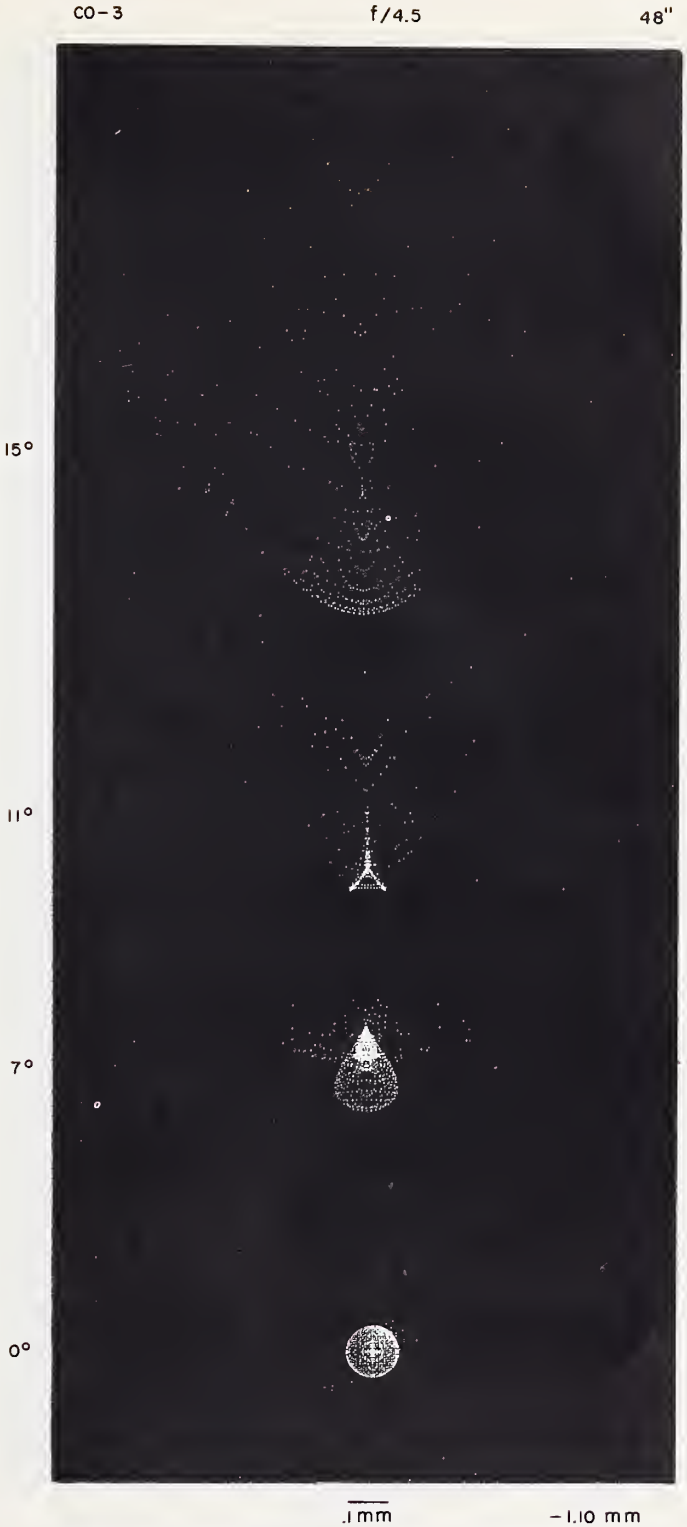

FIGURE 36b.

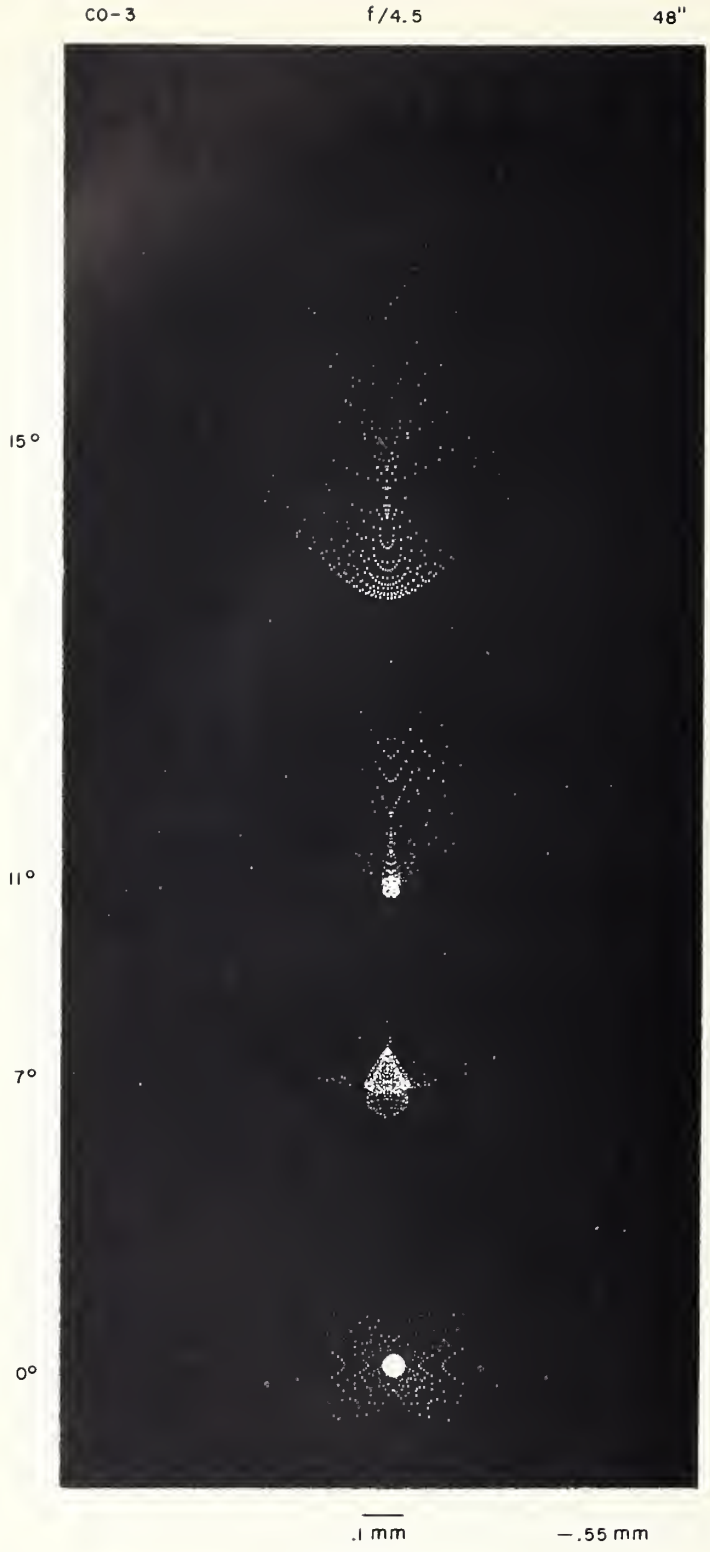

FIGURE 36c.

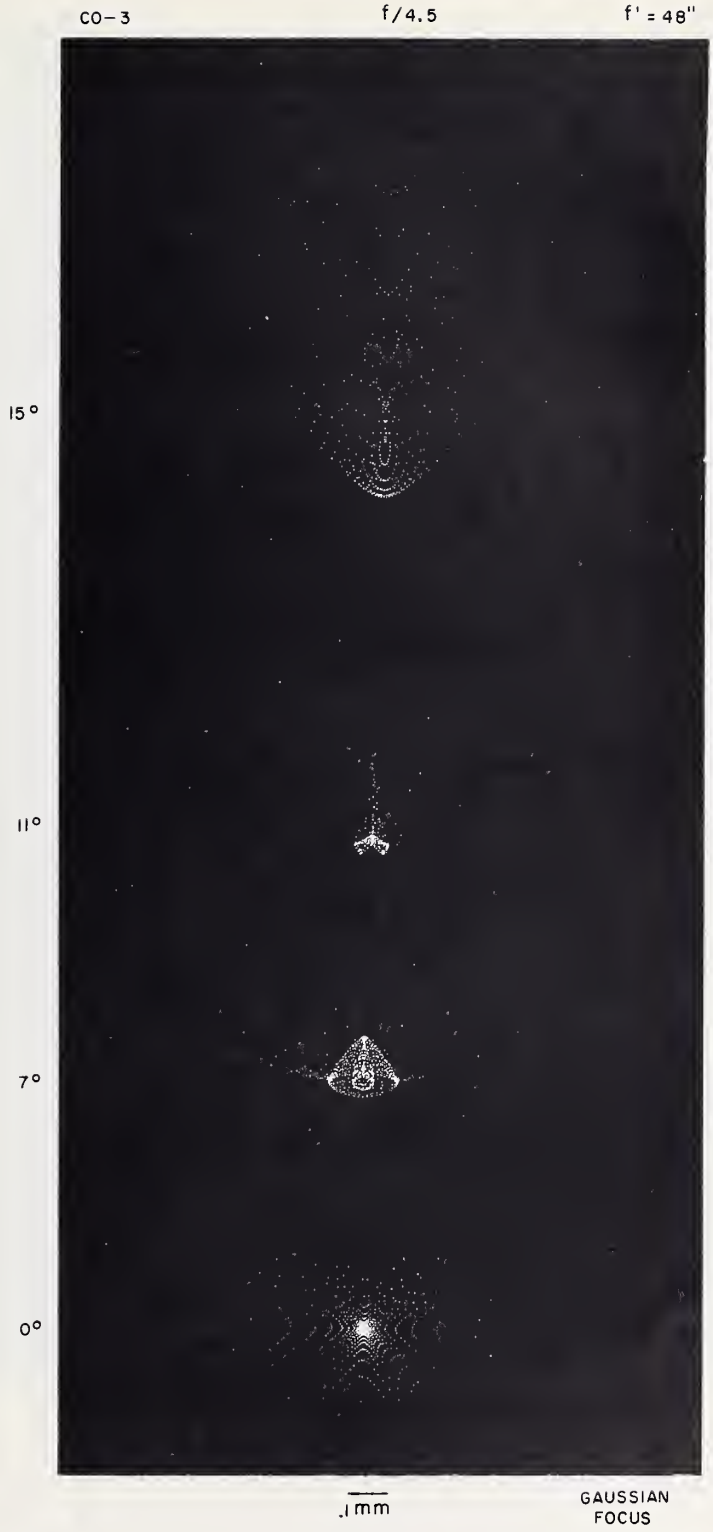

FIGURE 36d.

BA–4—48 in. *f*/4.5, 18×18 in. format

For this lens (see figures 37a–37e), the plane of best focus is farther from the lens than the Gaussian focus and is close to the plane depicted at +0.36 mm. The central cores of the spot diagrams appear to have a stronger than average concentration of points, with the exception of the diagram at 15°, where a larger percentage of the light is spread out to form flare. However, the total areas covered by these diagrams remain quite small, which should help in maintaining the resolution of low-contrast objects. The light-gathering ability of this lens was indicated at the time it was analyzed by arrows marking the vignetting on graphs of meridian and sagittal fans of rays. These arrows indicated that the entrance pupil at 15° is of about the same width and roughly half the height of that at 0°. This gradual narrowing to a cat's-eye shape is quite typical, and the implied loss of illumination at the edge of the field does not appear to be excessive.

Distortion is held to within 0.07 percent over the entire field and is negative at 15°. This lens was designed to operate over an unusual wavelength range: 6563 to 9000 Å. At the latter wavelength, the refractive index of SK–4 had to be estimated and the exact value is not known. Assuming that this estimate is substantially correct, the analysis indicated good correction of lateral color and a definite residual of undercorrected longitudinal color. This residual, if actually present, appears to be correctable through a minor modification, however.

BA–4—48 in. *f*/4.5 I.R. night lens for a 18×18 in. format

	Radius	Separation	Outside diameter	Clear aperture	Glass	Index*	Abbe No.
	in.	*in.*	*in.*	*in.*			
1	+17.385	1.679	12.400	12.000	SK–4	1.61272	58.6
2	+40.442			11.675			
		.148					
3	+11.737	1.232	11.500	11.200	F–15	1.60565	37.9
4	+5.799	3.204	9.900	9.801	SK–16	1.62041	60.3
5	+8.454			8.732			
		10.845					
6	−9.301	2.958	9.650	8.405	SK–16	1.62041	60.3
7	−6.345	1.371	11.400	9.552	F–15	1.60565	37.9
8	−13.827			11.043			
		.148					
9	+410.78	1.725	12.400	11.692	F–15	1.60565	37.9
10	−30.095			12.000			
		30.395					

Stop position: 6.774 in. from fifth surface.
Opening 7.100 in. at *f*/4.5.
*N_d given in table. Spot diagram calculations used N_A'.

Resolving power—BA–4

Field angle	Predicted resolving power in lines/mm*		Measured resolving power in lines/mm**	
	R	*T*	*R*	*T*
deg				
0	25	25	31	35
5			37	33
7	25	20		
10			22	16
11	25	25		
12.5			21	14
15	17	25		

*Using dimensions of spot diagrams.
**Courtesy of U.S. Air Force Reconnaissanse Laboratory, Wright Field.

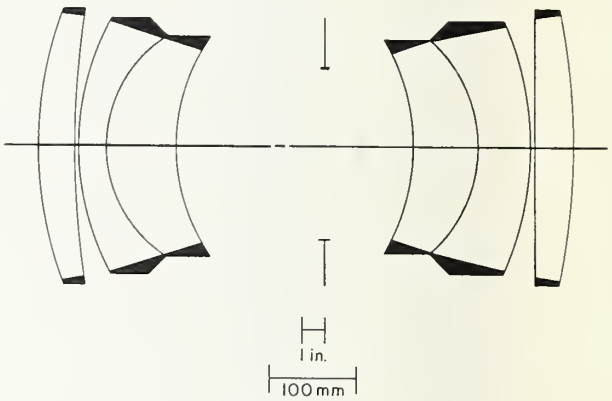

FIGURE 37a.

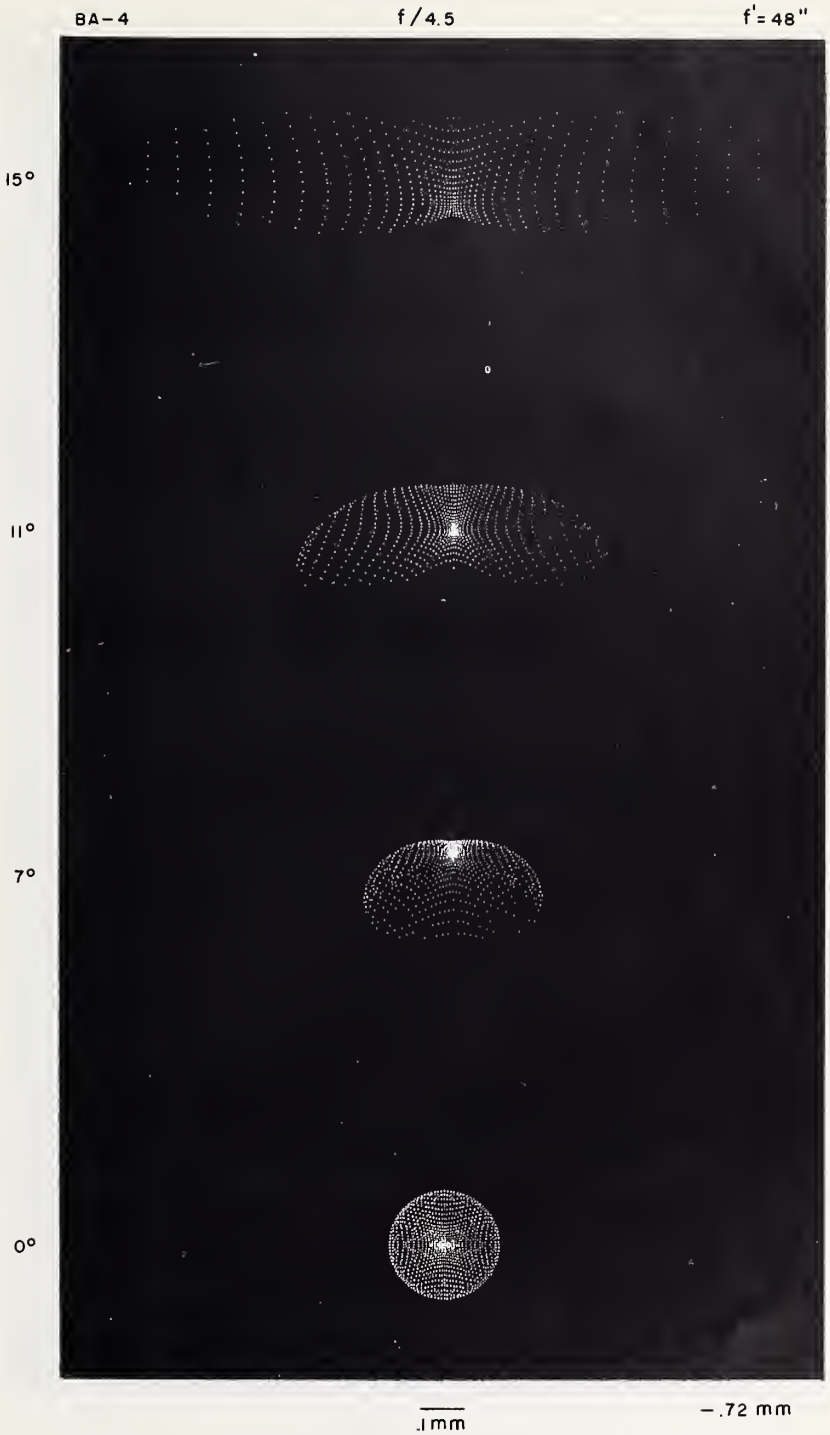

FIGURE 37b.

FIGURE 37c.

FIGURE 37d.

FIGURE 37e.

U.S. GOVERNMENT PRINTING OFFICE : 1965 O—769-533

U.S. DEPARTMENT OF COMMERCE
WASHINGTON, D.C. 20230

OFFICIAL BUSINESS

POSTAGE AND FEES PAID
U.S. DEPARTMENT OF COMMERCE